Modulating Metal-Semiconductor Schottky effect with electrostatic doping : Au-InSe as a case study

Yimin Zhang

Sorbonne Université

Institut de Minéralogie, de Physique des Matériaux et de Cosmochimie

ÉCOLE DOCTORALE 397 - Physique et Chimie des Materiaux

Thèse de doctorat

présentée par

Yimin ZHANG

Modulating Metal-Semiconductor Schottky effect with electrostatic doping : Au-InSe as a case study

---

dirigée par Abhay Shukla
co-encadrée par Johan Biscaras

Soutenue le 28 juin 2024 devant le jury composé de :

M[me] Nedjma Bendiab	Université Grenoble Alpes	Rapportrice
M. Alberto Zobelli	Université Paris Saclay	Rapporteur
M. Massimiliano Marangolo	Université Sorbonne	Président du jury
M. Abhay Shukla	Université Sorbonne	Directeur
M. Johan Biscaras	Université Sorbonne	Co-encadrant

Institut de minéralogie, de physique
des matériaux et de cosmochimie
4 place Jussieu
75005 Paris

Acknowledgement

At the end of my PhD journey, I feel like everything is nicer. It seems I have put on "graduation goggles" to life at this ending time, making me softer and more gentle. However, when it comes to writing my acknowledgments, I want to express my gratitude based on an objective perspective, not just through these graduation goggles. Otherwise, it would be like, "everything is nice and I thank everybody who appeared in my life ; without you, I wouldn't be me today, thank you, goodbye."

No, I know I will revisit this thesis many times in the future, and I hope that when the future me or my next generation read this part, we can learn something valuable and new.

The first people I need to thank is myself. I made all the decisions and I take myself here today. As a physicist (read Hawking since a kid), I really respect time, because I have to let it pass by and let it control me. I cherish time, so I not only completed a program at INSEAD business school during my PhD but also finished my PhD six months ahead of the contract.

Another reason I finished my PhD earlier is that, after three years, I still had no published papers. This pain I can't forget. As a hedge against further sunk costs, I gave up the paper publishing thing and decided to complete my PhD ahead of time. By gaining extra time, I hope to explore more opportunities, make more decisions, and increase my tolerance for mistakes. This creates a positive feedback loop. Yes, at this time, from 26-28 years old, I am a typical ENTJ (MBTI personality type).

Next, I need to thank my supervisors : Abhay Shukla and Johan Biscaras. I appreciate their guidance in revising my thesis, setting research goals, developing experiments, finding the logic to construct a PhD thesis, and their help in the preparation of the defense. However, I do not appreciate the life obstacles that I faced during my PhD. For a long period, I blamed **MYSELF** for not handling these challenges efficiently and not being able to come to work happily every day. But these obstacles should not even have occurred in the first place. As a foreigner, I should have received more support with various French procedures, especially since I was working for the institution. Ultimately, **myself** was the last person to blame for these difficulties. During that challenging time, I felt like the only one suffering and blamed myself for not achieving a balance between work and life, which led to depression.

But now, I understand, and I want the future me to remember : I am not the only one responsible for the life obstacles if they are not caused by me. I should not blame myself or try to deal with everything alone. There should be people who have the responsibility to help.

Next, I would like to thank all the people who cared about me and helped me overcome these obstacles during my PhD. These include Mme Cynthia Travert (the Prevention Assistant of IMPMC), Arnaud Duverger and Laurane Fogret (the representatives of non-permanent members of IMPMC), Mme Nadine Witkowski (Director of ED 397), Mme

Amélie Juhin and Mme Pauline Rovillain (CSI jury members), Mme Natalia Hristic (who assisted with my accommodation and *titre de séjour*), and Mme Pauline Sellier (my French teacher who taught me from A1 to B1). Asking for help from these people was a good choice, and I appreciate you helping me within your duty. I have never expected anyone to stand in my shoes and really care about my daily life, but all the conversations with these people made me feel cared for.

I also need to thank my colleagues and friends, who are numerous and have played a significant role in my journey. My colleagues from the corridor have been kind and supportive, often helping to lift my spirits. My friends, both from Sorbonne University and INSEAD Business School, respect me, support me, and give me valuable advice. I remember when I sent a WhatsApp message about a complaint, my friend sent me back an email with a detailed solution plan. I remember my friend went to a French government department with me on a early morning and said they would help me at any time. All my friends have helped me navigate life obstacles and provided much-needed emotional support.

As an extroverted person, my energy comes from my external environment. Therefore, I deeply appreciate all the friendships I have formed. These connections have been crucial in sustaining me through this journey.

I would like to extend my gratitude to the jury members during my PhD defense : Mme Nedjma Bendiab, M. Alberto Zobelli, and M. Massimiliano Marangolo. I thoroughly enjoyed the defense process and appreciated all the perspectives you shared. Thank you for making it a memorable and enriching experience.

I am also grateful to the China Scholarship Council for their support. Their assistance has been instrumental during my PhD, and I remain committed to becoming a valuable contributor to society.

Additionally, I want to thank the engineers from INSP's cleanroom for their help with the machinery during sample preparation. Your expertise and support were invaluable to my research.

I would like to thank IMPMC and ED397 for the academic opportunities and experiences they provided. Through presenting my work and creating posters, I made new friends and gained valuable knowledge. Additionally, I attended a summer school on 2D materials and won first prize for my presentation on "Twisted Graphene Bilayer and Magic Angle." Initially, I knew little about the magic angle of graphene. During the summer school, I learned about it from a professor and exchanged ideas with other experts. I stayed up one night studying this topic and preparing my presentation, which ultimately won first prize. I also attended a conference at Cambridge University, which was enriching. I learned extensively about topics ranging from InSe to industry, and from TMDs to chips. This experience also helped me broaden my professional network.

Attending summer schools and conferences is truly an enriching experience. I wish I could have had more opportunities like these during my PhD. One of my friends from the LKB laboratory attended different summer schools every year and one or two different conferences each semester in different countries. I was quite jealous of that. Of course, he had a more fulfilling PhD experience than me, worked more happily than me, and could learn things faster than me. Also, he went with his colleagues which can enhance teamwork while I went alone because my lab is small and doesn't have a team. Even so, I won the first prize, made lots of new friends, and I deeply appreciated and enjoyed my only summer school and conference experience during my PhD.

Everything I have expressed gratitude for above represents the golden moments of this PhD journey. I want my future self to remember these times and learn how to create more

of them :

— Efficiently seeking help when obstacles arise, rather than struggling alone.
— Continuously investing in myself.
— Maintaining the right perspective and enjoying intellectual debates.
— Participating in more high-caliber events.

Abstract

Modulating Metal-Semiconductor Schottky effect with electrostatic doping: Au-InSe as a case study

English version

This thesis presents an in-depth analysis of the Schottky Barrier Height (SBH) in metal/indium selenide (InSe) contacts and explores the modifications to contact characteristics through electrostatic doping within a Schottky diode framework. The study begins by investigating the influence of doping on SBH in metal/InSe junctions using gold (Au), aluminum (Al), and silver (Ag) as contact metals. It was found that Au contacts did not form ideal Schottky barriers, showing signs of resistive leakage, while Al and Ag contacts demonstrated quasi-linear behavior with significant resistances and stability issues, respectively.

Further exploration revealed that varying metal contacts or using asymmetric configurations had minimal impact on improving the I-V characteristics, which were predominantly resistive and slightly non-linear. This behavior suggests non-ideal interface conditions, potentially due to defects and metal-induced gap states. The two-way parallel diodes model was effective in fitting I-V curves, reflecting the complexities at the metal-semiconductor interface and allowing for the extraction of key parameters, such as the non-saturating current behavior at elevated voltages.

A notable observation across different metal contacts is the consistent SBH of around 0.5 eV, indicating a Fermi level pinning phenomenon that overrides individual metal characteristics. Despite attempts at electrostatic doping, only minor changes in SBH were observed, underscoring the challenges posed by Fermi level pinning by metal-induced gap states, particularly with Au contacts.

The research progresses to optimizing electronic interfaces for Schottky diodes by targeting ohmic behavior through selective doping and device geometry, which confines electrostatic space charge doping. This involves a significant Fermi level shift, essential for depinning at targeted junctions to achieve ohmic contacts. The culmination of this work is demonstrated in devices that exhibit true Schottky rectifying behavior, highlighted by a substantial increase in current due to doping-induced mechanisms, although leading to rapid device failure under extreme conditions.

Overall, the thesis advances the understanding of SBH in metal/InSe junctions and contributes novel approaches to achieving optimized Schottky diodes through precise control of doping and device architecture.

Keywords

[Schottky, InSe, Diode]

Version française

Cette thèse présente une analyse approfondie de la hauteur de la barrière Schottky (SBH) dans les contacts métal/séléniure d'indium (InSe) et explore les modifications des caractéristiques des contacts par dopage électrostatique dans un cadre de diode Schottky. L'étude commence par étudier l'influence du dopage sur la SBH dans les jonctions métal/InSe utilisant l'or (Au), l'aluminium (Al) et l'argent (Ag) comme métaux de contact. Il a été constaté que les contacts Au ne formaient pas des barrières Schottky idéales, montrant des signes de fuite résistive, tandis que les contacts Al et Ag démontraient un comportement quasi-linéaire avec respectivement des problèmes de résistance et de stabilité importants.

Une exploration plus approfondie a révélé que la variation des contacts métalliques ou l'utilisation de configurations asymétriques avaient un impact minimal sur l'amélioration des caractéristiques IV, qui étaient principalement résistives et légèrement non linéaires. Ce comportement suggère des conditions d'interface non idéales, potentiellement dues à des défauts et à des états induits dans la bande interdite par le métal. Le modèle de diodes parallèles bidirectionnelles s'est avéré efficace pour ajuster les courbes IV, reflétant les complexités de l'interface métal-semi-conducteur et permettant l'extraction de paramètres clés, tels que le comportement de non saturation du courant à des tensions élevées.

Une observation notable sur différents contacts métalliques est le SBH constant d'environ 0,5 eV, indiquant un phénomène de blocage au niveau de Fermi qui remplace les caractéristiques métalliques individuelles. Malgré les tentatives de dopage électrostatique, seuls des changements mineurs dans le SBH ont été observés, soulignant les défis posés par le blocage du niveau de Fermi par les états induits par le métal, en particulier avec les contacts Au.

La recherche progresse vers l'optimisation des interfaces électroniques pour les diodes Schottky en ciblant le comportement ohmique grâce au dopage sélectif et à la géométrie du dispositif, qui limite le dopage de charge d'espace électrostatique. Cela implique un changement de niveau de Fermi significatif, essentiel pour le déblocage du niveau de Fermi aux jonctions ciblées afin d'obtenir des contacts ohmiques. Le point culminant de ce travail est démontré dans des dispositifs qui présentent un véritable comportement de redressement Schottky, mis en évidence par une augmentation substantielle du courant due aux mécanismes induits par le dopage, bien que conduisant à une défaillance rapide du dispositif dans des conditions extrêmes.

Dans l'ensemble, la thèse fait progresser la compréhension du SBH dans les jonctions métal/InSe et propose de nouvelles approches pour obtenir des diodes Schottky optimisées grâce à un contrôle précis du dopage et de l'architecture des dispositifs.

Mots-clés

[Schottky, InSe, Diode]

Long résumé en français

Chapitre 1. Introduction

Ce travail a été initié dans le contexte de la recherche actuelle sur les matériaux 2D, qui atteint un stade où les applications et les dispositifs sont mis en évidence, parallèlement à l'intérêt toujours renouvelé pour les aspects fondamentaux. Les dispositifs en matériaux 2D présentent quelques défis majeurs [**?**]. Le premier de ces défis est la nécessité de fabriquer des plaquettes monocristallines de grande surface à partir de matériaux 2D ultraminces à une ou quelques couches. La présence d'impuretés ou d'inhomogénéités dans les approches ascendantes telles que les techniques de dépôt chimique en phase vapeur ou les techniques de dépôt physique en phase vapeur a souvent constitué un obstacle. Cependant, un effort long et soutenu commence enfin à porter ses fruits avec quelques succès récents dans ce domaine [**?**]. Un autre défi est que la plupart des matériaux 2D sont sensibles et peuvent être pollués ou altérés de manière irréversible par l'exposition ambiante [**?**]. Il est clair que la fabrication et l'utilisation sous vide ne constituent pas une alternative industrielle viable. L'effet d'une telle contamination doit être efficacement caractérisé et d'éventuelles stratégies de lutte doivent être trouvées, par exemple une encapsulation efficace [**?**]. La contamination peut également résulter des techniques de lithographie en salle blanche et ce problème doit également être abordé.

Enfin, un problème simple mais fondamental subsiste. Tous les dispositifs, qu'ils soient électroniques ou optoélectroniques, ont besoin d'être mis en contact avec des contacts métalliques pour l'extraction ou l'injection de charges. Étant donné que l'écrasante majorité des dispositifs en matériaux 2D utilisent des semi-conducteurs, un contact métal-semiconducteur entre en jeu. Deux défis fondamentaux se présentent [**?**]. Premièrement, ces contacts doivent être établis de manière à ne pas endommager le matériau lui-même. Ceci est particulièrement critique pour les matériaux à couche unique et un peu moins pour les matériaux à plusieurs couches où la détérioration de la couche supérieure ne compromet pas nécessairement le dispositif. Ces dommages peuvent provenir de produits chimiques utilisés pour la lithographie, mais aussi de l'impact physique d'atomes métalliques déposés à haute température, ou de la diffusion d'atomes métalliques dans ou entre les couches de matériau 2D, brouillant ainsi l'interface métal-semiconducteur [**?**]. Cette interface métal-semiconducteur est la fameuse jonction Schottky, présentée dans tous les manuels de physique de la matière condensée [**?**] et également utilisée dans des dispositifs [**?**]. En bref, cette jonction, qui est idéalement une jonction de redressement, résulte du transfert de charge et de la charge d'espace et de la courbure de bande qui en résultent lorsqu'une jonction métal-semiconducteur propre et nette est formée.

Comme le montre la Figure 3.1, une barrière de redressement est formée dans la mesure où, pour un semi-conducteur dopé n, le côté métal est l'anode et le côté semi-conducteur est la cathode. Le courant circule ohmiquement du métal au semi-conducteur, mais doit traverser une barrière entre le semi-conducteur et le métal. La hauteur de cette barrière

pour un semi-conducteur de type n est la différence entre la fonction de travail du métal (différence entre le niveau du vide et le niveau de Fermi du métal) et l'affinité électronique du semi-conducteur (différence entre le niveau du vide et le bord de la bande de conduction du semi-conducteur) et est obtenue à partir de la condition qu'à l'équilibre thermique, les niveaux de Fermi des deux matériaux doivent être alignés.

Il est bien connu que les niveaux de Fermi des semi-conducteurs peuvent être modifiés de manière substantielle (changements de l'ordre de 1eV) par le dopage, généralement par l'introduction d'atomes d'impureté. De même, les fonctions de travail des métaux courants diffèrent également par des énergies de l'ordre de l'eV. À titre d'exemple, nous considérons les fonctions de travail de Au (5.1 eV), Ag (4.7 eV) et Al (4.1 eV). Nous devrions donc nous attendre à ce que les barrières Schottky soient modulables dans cette gamme d'énergie d'un eV ou plus, soit en changeant de métal, soit en modulant le niveau de Fermi du semi-conducteur en changeant le dopage. Cependant, il est bien connu depuis plusieurs décennies que dans les jonctions Schottky semi-conducteurs-métal conventionnelles, le changement de la hauteur de la barrière Schottky (SHB) est en fait presque dix fois plus petit, limité à quelques dizaines d'eV [**?**]. Des résultats similaires sont observés dans les jonctions Schottky 2D matériau-métal [**?**]. Les raisons de cette divergence sont également bien connues. Dès 1965, Volker Heine [**?**] a donné une explication simple liée à l'épinglage du niveau de Fermi dans le semi-conducteur. Il a montré qu'à l'interface métal-semiconducteur d'un semi-conducteur massif, une "densité même d'une fraction d'un état de surface par atome de surface par eV est tout à fait suffisante pour absorber toute charge supplémentaire nécessaire dans la bande des états de surface sans que le niveau de Fermi dans cette bande ne se déplace beaucoup". Ainsi, l'EF à la surface du semi-conducteur est effectivement fixé à une valeur fixe. Il s'agit de la première référence que nous connaissons dans la littérature au sujet de la "fixation" du niveau de Fermi. Heine a également déclaré que les états de surface localisés dans la bande interdite ne peuvent pas exister (à moins qu'une restructuration de la surface ne soit envisagée). Les états dans l'intervalle peuvent donc exister en cas de défauts ou d'impuretés (les niveaux donneur ou accepteur bien connus dans les semi-conducteurs), mais aussi en leur absence, à la jonction, en raison de la queue de la fonction d'onde métallique dans le semi-conducteur, que l'on peut estimer à un nm [**?**] et qui est inversement proportionnelle à la taille de l'intervalle. Cela signifie que pour un échantillon à quelques couches, la queue pénètre au moins une couche entière de l'échantillon et rend le pincement de la surface de Fermi plus efficace que dans un échantillon en vrac. Ces états associés à la queue ont également été appelés Metal Induced Gap States ou MIGS, par opposition aux Defect Induced Gap States ou DIGS. Le défi pour tout dispositif avec une interface métal - semi-conducteur est donc de contrôler le SHB (par exemple pour établir un contact ohmique). Comme nous le verrons dans cette thèse, cela peut être tenté en adaptant le métal à l'InSe ou en essayant de modifier le niveau de Fermi de l'InSe. Ces deux méthodes devront cependant contrer les effets de l'épinglage du niveau de Fermi. L'état actuel de l'art dans les matériaux 2D a été amplement décrit dans quelques articles de synthèse récents [**?**] [**?**] [**?**].

Notre objectif dans cette thèse est de moduler le Schottky Barrier Height (SBH) d'une jonction InSe - métal afin de réaliser une diode Schottky InSe - métal à quelques couches. Le choix de l'InSe est motivé par le fait qu'il s'agit d'un matériau 2D facilement exfoliable et qu'il appartient à la famille des monochalcogénures dont les bandes interdites s'étendent du proche IR au proche UV (InSe $\approx$ 1.2 eV, GaSe $\approx$ 2 eV, GaS $\approx$ 3 eV). Ces matériaux présentent une bande interdite directe au-dessus d'une épaisseur d'environ 5 couches (4 nm) et une bande interdite indirecte en dessous de cette épaisseur. Enfin, si le GaSe et le GaS sont sensibles à la contamination ambiante, l'InSe y résiste pendant quelques jours [**?**].

Ces propriétés en font un bon matériau prototype pour cet exercice.

En outre, nous proposons d'utiliser trois contacts métalliques couramment utilisés, Au, Ag et Al, afin de trouver une configuration et une géométrie appropriées. Pour ce faire, nous fabriquons et caractérisons des échantillons de quelques couches et des dispositifs (voir chapitre 2).

Dans le chapitre 3, nous fabriquons des dispositifs planaires avec des configurations symétriques (métal 1 - quelques couches d'InSe - métal 1) et asymétriques (métal 1 - quelques couches d'InSe - métal 2) pour tester la variation éventuelle du SBH avec le métal. Nous testons également l'effet du dopage électrostatique de la charge d'espace sur la variation du SBH dans ces dispositifs planaires.

Dans le chapitre 4, à la lumière des résultats du chapitre 3, nous testons une nouvelle géométrie où Au est le métal et où un seul contact Au - InSe est dopé pour le rendre ohmique. Nous constatons que cela n'est possible que dans le cas où, vraisemblablement, le niveau de Fermi est désépinglé par une séquence de dopage spécifique. Cela donne lieu à une diode Schottky de haute puissance.

Dans le chapitre 5, nous concluons et discutons de certaines perspectives découlant de ce travail. Les résultats peuvent ouvrir de nouvelles voies pour l'amélioration des dispositifs électroniques basés sur les matériaux 2D et pour l'optimisation des performances des diodes Schottky.

Chapitre 2. Techniques expérimentales

Dans ce chapitre, nous présentons les techniques expérimentales utilisées dans ce travail. Celles-ci comprennent la fabrication et la caractérisation d'échantillons ou de dispositifs, ainsi que des mesures électriques avec les dispositifs. Des techniques standard pour les dispositifs et les matériaux 2D sont utilisées ainsi que des techniques qui ont été développées spécifiquement dans notre laboratoire, telles que le collage anodique pour la fabrication d'échantillons et le dopage par charge d'espace pour le dopage électrostatique des échantillons.

Pour la fabrication d'échantillons et de dispositifs, nous utilisons le collage anodique pour la fabrication d'échantillons de quelques couches et des techniques standard de transfert à sec pour la superposition d'échantillons de quelques couches (mica sur InSe). Pour la fabrication de dispositifs, nous utilisons des masques au pochoir et l'évaporation de métal pour établir des contacts métal - semi-conducteur.

Pour la caractérisation des échantillons, nous utilisons la microscopie, la spectroscopie Raman et la photoluminescence.

Pour les mesures des dispositifs, nous utilisons des instruments standard pour mesurer les caractéristiques I-V et notre propre technique de dopage par charge d'espace pour le dopage électrostatique.

Le collage anodique est une technique sophistiquée développée pour le collage des substrats en verre dans la microfabrication et la production de systèmes microélectromécaniques (MEMS). Dans notre laboratoire, nous avons étendu cette technique à plusieurs semiconducteurs 2D, tels que GaS, GaSe, InSe, MoS_2, et WTe_2, pour la fabrication d'échantillons de quelques couches sur des substrats en verre. Cette méthode, qui fonctionne à haute température, combinée à un champ électrique, permet de créer une liaison forte et hermétique sans nécessiter de couches intermédiaires telles que des adhésifs.

Le principe qui sous-tend la liaison anodique implique la migration d'ions Na^+ activés par l'énergie thermique à des températures élevées, généralement comprises entre 180°C et 450°C. Lorsqu'une tension négative, généralement comprise entre quelques centaines et quelques milliers de volts, est appliquée sur la face arrière du substrat, les ions Na^+ migrent vers celui-ci et s'accumulent à la cathode. Cette migration laisse derrière elle des ions oxygène statiques, créant une charge d'espace négative à la surface du verre et une charge positive correspondante dans la plaquette. Ce phénomène se traduit par un champ électrostatique élevé à l'interface, liant le matériau au verre.

Pour la caractérisation de l'échantillon, nous utilisons la microscopie optique et la microscopie à force atomique au niveau macroscopique et microscopique respectivement. La spectroscopie Raman et la photoluminescence sont utilisées pour étudier la qualité cristalline de l'échantillon. Les propriétés spectroscopiques Raman de l'InSe sont influencées de manière significative par le polytype et l'épaisseur de la couche. Les différents polytypes d'InSe présentent des décalages Raman uniques, des pics spécifiques étant caractéristiques de certains polytypes. Par exemple, les polytypes ϵ et γ, que l'on trouve généralement dans l'InSe à quelques couches, présentent un pic distinctif autour de $196\,\mathrm{cm}^{-1}$. Dans l'analyse comparative des spectres Raman pour des échantillons d'InSe de 10 nm et d'InSe en vrac obtenus par la méthode de liaison anodique, comme le montre la figure 2.12, le pic A_{1g} net et intense dans les deux échantillons indique la bonne qualité cristalline du matériau après la méthode de liaison anodique. Les positions des pics A_{1g} et E^1_{2g} sont caractéristiques du polytype de phase β, mis en évidence par l'absence du pic $A_1(\Gamma^1_1)$ à $196\,\mathrm{cm}^{-1}$.

Dans la fabrication de nos dispositifs, nous utilisons l'évaporation de métal avec un masque d'ombre ou de pochoir, un processus de dépôt physique en phase vapeur (PVD)

qui est plus adapté que les méthodes lithographiques aux matériaux sensibles à l'environnement tels que l'InSe. Il implique la condensation du métal vaporisé sur le substrat pour former un film mince, sans avoir recours à des produits chimiques susceptibles de réagir avec l'InSe. Cette méthode réduit le risque de dommages chimiques à la surface de l'InSe, préservant ainsi son caractère intrinsèque.

Les mesures électriques du dispositif semi-conducteur InSe de cette thèse sont effectuées à l'aide de l'installation décrite à la figure 2.23. Le dispositif est monté dans un cryostat, qui sert également de chambre à vide. Cette conception facilite un contrôle précis de la température, essentiel pour recuire l'échantillon ou pour effectuer un dopage par charge d'espace en chauffant l'échantillon à des températures spécifiques. Le vide dans la chambre peut être maintenu à une pression inférieure à 10^{-6} mbar. La régulation de la température, qui va de la température ambiante à 420 K, est assurée par un chauffage résistif, ce qui garantit la stabilité et la précision des mesures.

Chapitre 3 : Dispositifs planaires symétriques et asymétriques en InSe

Lorsqu'un métal ayant une fonction de travail Φ_M entre en contact avec un semi-conducteur ayant une fonction de travail différente Φ_S, un transfert de charge se produit jusqu'à ce que l'équilibre soit atteint, alignant leurs niveaux de Fermi respectifs. Ce transfert entraîne la formation d'une couche de déplétion à l'interface du semi-conducteur, caractérisée par une absence de porteurs de charge libres. Cette couche est désignée comme la région de charge d'espace en raison de son accumulation caractéristique de charges immobiles. Cette couche est cruciale pour l'établissement d'une jonction de redressement Schottky.

Dans les scénarios où $\Phi_M < \Phi_S$, il y a injection d'électrons du métal vers le semi-conducteur, ce qui conduit à une jonction ohmique sans couche de déplétion. Inversement, le contact entre un métal et un semi-conducteur de type n avec $\Phi_M > \Phi_S$ entraîne la formation d'une couche de déplétion, d'un champ électrique et d'un potentiel intégré (Φ_i) à la jonction, ce qui entrave la diffusion des charges, comme le montre la figure 3.1.

La barrière de Schottky et son importance

La barrière de Schottky (Φ_B) apparaît comme une discontinuité dans les états d'énergie autorisés à l'interface métal/semiconducteur, servant de barrière contre le flux d'électrons. La relation Schottky-Mott exprime Φ_B en termes de fonction de travail du métal (Φ_M) et d'affinité des électrons du semi-conducteur (X) :

$$\Phi_B = \Phi_M - X$$

Une barrière similaire existe pour le flux de trous dans les jonctions métal/semi-conducteur de type p :

$$\Phi_B = E_g - |\Phi_M - X|$$

La somme des hauteurs de la barrière de Schottky (SBH) pour les électrons et les trous est censée être égale à la bande interdite du semi-conducteur (E_g). La hauteur de la barrière Schottky est une caractéristique essentielle des jonctions de redressement M/S, car elle influence leurs caractéristiques de redressement. Un SBH plus important est généralement obtenu avec des métaux à fonction de travail élevée sur des semi-conducteurs de type n, ou avec des métaux à fonction de travail faible sur des semi-conducteurs de type p. Cependant, les données expérimentales suggèrent que les relations Schottky-Mott ne sont valables que qualitativement, le SBH étant souvent presque indépendant de la fonction de travail du métal.

Le modèle Schottky-Mott traditionnel, un cadre établi dans la physique des semi-conducteurs, tente d'élucider la hauteur de la barrière Schottky (SBH) en fonction de la fonction de travail du métal (Φ_M) et de l'affinité électronique du semi-conducteur (X). Ce modèle a toutefois été constamment remis en question par les résultats expérimentaux, en particulier lorsqu'on tient compte du rôle des états de surface aux jonctions métal/semiconducteur (M/S). Les travaux fondamentaux de J. Bardeen en 1947 ont introduit le concept d'états de surface, également connus sous le nom d'états de Shockley-Tamm [7]. Ces états sont des états électroniques localisés à la surface du semi-conducteur, émergeant de facteurs tels que des liaisons covalentes incomplètes, la présence d'atomes étrangers et des défauts cristallins. La théorie de Bardeen proposait que ces états de surface, dont les énergies se situent dans la bande interdite du semi-conducteur (voir figure 3.2), puissent affecter

de manière significative la distribution des charges à l'interface M/S. Cette découverte a marqué un changement fondamental par rapport à l'époque où les semi-conducteurs étaient considérés comme des matériaux de base. Cette idée a marqué un changement fondamental par rapport au modèle Schottky-Mott, qui supposait une relation directe entre la fonction de travail du métal et le SBH, en négligeant la nature dynamique des états de surface.

Contacts métal-InSe

L'interaction entre le InSe, caractérisé par une affinité électronique d'environ 4.6 eV, et des métaux tels que l'or (Au), l'argent (Ag) et l'aluminium (Al) présente un paysage complexe pour la formation de jonctions Schottky et de contacts ohmiques. L'exposition atmosphérique peut également modifier les propriétés de surface de ces métaux, ce qui complique encore leur interaction avec l'InSe. En partant de la règle de Schottky-Mott discutée précédemment, les métaux comme Au, avec une fonction de travail d'environ 5.1 eV, ont tendance à former des jonctions Schottky avec l'InSe, conduisant à une hauteur de barrière d'environ 0.5 eV. Inversement, les métaux dont les fonctions de travail sont plus proches ou inférieures à l'affinité électronique de l'InSe, tels que Ag (4.3eV) et Al (4.2eV), peuvent faciliter la formation de contacts ohmiques ou de barrières Schottky minimales, en fonction des spécificités de leur interaction. Cet alignement permet un transfert d'électrons plus efficace, caractérisé par une relation linéaire courant-tension. Dans ce travail, nous avons donc choisi d'utiliser les trois métaux différents Au, Al et Ag pour fabriquer nos dispositifs, Au donnant probablement des contacts Schottky et les deux autres étant plus Ohmiques. Par conséquent, la création de dispositifs avec des métaux symétriques ou asymétriques comme contacts devrait permettre de former différents dispositifs de type diode avec leurs propres caractéristiques, et permettre l'étude de leur comportement sous un dopage de charge d'espace élevé.

Modèles analytiques pour l'extraction de paramètres à partir des ajustements des caractéristiques I-V

La formulation pour l'ajustement des courbes courant-tension (I-V) est dérivée de l'équation classique de la diode, modifiée pour incorporer les caractéristiques uniques des dispositifs, en particulier les contacts asymétriques impliquant Al-Ag, Au-Ag et Au-Al. L'équation de la diode sert de modèle mathématique définissant les caractéristiques I-V d'une diode. Cependant, pour un dispositif symétrique ou asymétrique avec une barrière Schottky aux deux interfaces métal/semiconducteur, le modèle précédent ne peut pas représenter l'ensemble de la caractéristique (I-V), même si l'on peut tenter de modéliser chaque polarité indépendamment. Au lieu de cela, nous pouvons créer un nouveau modèle comprenant deux diodes Schottky, disposées dans une configuration dos à dos avec une résistance série intermédiaire (figure 3.8). Ce modèle est plus général que les dispositifs symétriques Au/Au. Enfin, en raison des effets de la fuite résistive dans les contacts métal/semiconducteur, qui s'écartent du comportement idéal traditionnellement attendu dans les contacts Schottky, nous introduisons un dernier modèle modifié pour tenir compte de ces effets dans les dispositifs symétriques ou quasi-symétriques, comme le montre la figure 3.12. La caractéristique I(V) de ce modèle est assez simple à calculer car les courants dans les deux branches s'additionnent. Nous pouvons donc calculer le courant dans chaque branche à chaque V comme décrit précédemment pour la diode et la résistance en série, avec une en sens inverse, et additionner les résultats. Dans le cas le plus général, cela conduit à six paramètres indépendants, ce qui peut donner une large gamme de compor-

tements. Il est important de noter qu'il n'y a pas de saturation du courant à haute tension dans ce modèle.

Conclusions

Pour l'analyse détaillée des mesures et des adaptations aux différents dispositifs, le lecteur peut consulter directement le chapitre 3. Nous reproduisons ici les conclusions de cette étude. Plusieurs conclusions qualitatives et quantitatives peuvent être tirées du travail présenté dans ce chapitre. Comme nous le verrons, elles orienteront le travail présenté dans le chapitre suivant et conduiront au résultat principal de cette thèse, à savoir la modulation de la hauteur de la barrière Schottky et la fabrication expérimentale d'une diode Schottky métal - InSe - métal à l'aide d'un dopage électrostatique. Les mesures effectuées sur nos dispositifs nous ont permis de constater que le fait de changer les contacts métalliques ou d'utiliser des contacts métalliques asymétriques au lieu de symétriques ne modifie pas substantiellement les caractéristiques I-V. Celles-ci restent très résistives et faiblement résistives. Celles-ci restent très résistives et légèrement non linéaires. Le comportement de diode Schottky n'est jamais observé même si, d'après les estimations idéales du SBH, le contact Au peut être supposé Schottky et les contacts Ag et Al peuvent être supposés ohmiques. La raison probable en est la nature non idéale de l'interface qui peut résulter de défauts et d'impuretés (états de lacune induits par des défauts ou dopage par des impuretés), de liaisons pendantes à partir des bords de la couche et d'états de lacune induits par le métal à partir des queues des fonctions d'onde métalliques qui peuvent pénétrer dans le semi-conducteur. Un autre problème typique des matériaux a été observé dans le cas de l'interface Ag - InSe où l'on observe une inter-diffusion substantielle de l'Ag dans l'InSe. Cela modifie probablement considérablement les propriétés de l'InSe, comme le montrent les courants beaucoup plus élevés dans les dispositifs dotés de contacts en Ag. Ces interfaces non idéales ont conduit à l'utilisation d'un modèle qui tient compte de l'interface métal-semiconducteur complexe pour ajuster les courbes I-V mesurées de nos dispositifs. Ainsi, chaque contact métal-semiconducteur est considéré comme un contact Schottky et un canal résistif supplémentaire est introduit parallèlement au canal Schottky. Avec ce modèle de diode parallèle à deux voies, nous parvenons à ajuster nos courbes mesurées et à extraire certains paramètres quantitatifs. En particulier, nous expliquons efficacement le comportement non saturant du courant à une tension plus élevée dans les courbes I-V mesurées.

Une question intéressante que nous avons soulevée au début de ce chapitre concerne la hauteur de la barrière Schottky et la possibilité de la moduler. Comme nous l'avons montré à l'aide d'une étude bibliographique, quel que soit le contact métallique, la Schottky Barrier Height (SBH) dans un dispositif métal-InSe est toujours estimée à environ 0.5 eV. Cela indique clairement que le SBH est déterminé par l'épinglage du niveau de Fermi plutôt que par la différence entre le niveau de Fermi du métal et l'affinité électronique de l'InSe. Les expériences de dopage sur nos dispositifs asymétriques apportent une preuve supplémentaire de l'immobilisation du niveau de Fermi. Celles-ci n'ont pu modifier le SBH que de $0.02-0.07$ eV alors que le niveau de Fermi dans nos échantillons d'InSe a été mesuré à environ 0.3 eV en dessous du minimum de la bande de conduction.

Enfin, trois conclusions peuvent être formulées pour notre objectif de fabriquer une diode Schottky à partir d'une interface métal-InSe :

1. Sur les trois métaux (Au, Ag, et Al) que nous avons essayés, seul Au est suffisamment stable pour servir de contact métallique avec InSe. L'interface Au-InSe présente également le comportement le plus semblable à celui de Schottky. Cepen-

dant, nous ne pouvons pas espérer modifier l'une des interfaces Au-InSe avec un dopage de charge d'espace, dans un dispositif avec deux contacts Au. Les deux interfaces seront modifiées de la même manière en raison du dopage.

2. La modification du SBH par le dopage de charge d'espace est minime. Pour rendre un contact Au-InSe ohmique ou presque ohmique, il faut déplacer le niveau de Fermi d'environ 0.3 eV. Cependant, le dopage de la charge d'espace ne réussit qu'à apporter des changements qui, selon nos estimations, sont d'un ordre de grandeur inférieur. La raison probable en est la fixation du niveau de Fermi à des états dans le vide qui pourraient être des MIGS induits par le contact Au.
3. Pour fabriquer une diode Schottky avec un dispositif Au-InSe-Au, nous devons résoudre le problème du blocage de la surface de Fermi afin que le dopage de la charge d'espace puisse être efficace pour modifier le SBH. Nous devons également être en mesure de doper un seul des deux contacts Au-InSe pour le rendre ohmique et obtenir ainsi une diode Schottky.

Chapitre 4. Diode à gradins verticaux en InSe

Dans le dernier chapitre, nous avons tiré quelques conclusions concernant les jonctions métal-InSe et la manière dont leurs caractéristiques peuvent être modifiées :

1. Le modèle qui décrit le plus précisément le comportement mesuré dans nos dispositifs planaires est celui qui inclut un chemin de "fuite" ohmique, c'est-à-dire des diodes Schottky dos à dos avec un chemin résistif parallèle. Cela suppose une jonction "non idéale".
2. Quel que soit le métal utilisé (Au, Ag ou Al), la caractéristique I-V de la jonction métal-InSe est similaire. Cela nous amène à conclure que le SBH est, dans un certain sens, indépendant du métal utilisé. Nous concluons également que le SBH change peu ($\approx 0.01\,\text{eV}$) lors du dopage électrostatique. Cela implique que le niveau de Fermi est fixé à des états dans la fente, qui sont probablement des états de fente induits par le métal (MIGS).
3. Un dispositif de redressement Schottky doit avoir un contact ohmique et un contact Schottky. Puisque nous voulons induire un contact ohmique par le dopage électrostatique de l'InSe, nous devons nous assurer que :
   — Seul l'InSe correspondant à une jonction est dopé alors que l'autre ne l'est pas et reste une barrière Schottky métal-InSe. Ceci peut être réalisé en choisissant une géométrie "en escalier" spécifique pour le dispositif. En effet, le dopage électrostatique des charges d'espace à travers le substrat opère sur une certaine épaisseur (longueur de Debye) liée aux propriétés d'écran diélectrique du semi-conducteur à doper. Cette longueur a été calculée pour MoS_2 [**?**] à environ 2 nm. Pour InSe avec une constante diélectrique plus faible, nous pouvons donner une limite supérieure de quelques nm. Cela signifie que l'épaisseur des quelques couches d'InSe où nous souhaitons induire une transition dopée électrostatiquement vers une haute conductance ne doit pas dépasser quelques couches. Nous choisissons une épaisseur de $\approx 5\,\text{nm}$, ce qui correspond à 6-7 couches. De même, l'épaisseur de l'InSe à la jonction où nous ne voulons pas que le dopage électrostatique ait un effet doit être bien supérieure à cette valeur et nous choisissons environ $\approx 20\,\text{nm}$ ou environ 30 couches.
   — Pour obtenir un chemin de courant à travers les deux jonctions, nous devons nous assurer que le courant passe verticalement à travers la jonction InSe mince (en bas de l'échantillon) et à travers l'InSe épais (en haut de l'échantillon), comme le montre la figure 4.1.
   — Enfin, nous devons nous assurer que le dopage électrostatique par charge d'espace de l'InSe induit effectivement un changement significatif du niveau de Fermi dans le semi-conducteur sous le contact mince, de sorte que nous obtenons une jonction ohmique. En bref, nous devons dé-pincer le niveau de Fermi ici.

Nous avons effectué plusieurs mesures avec de tels dispositifs en induisant un dopage électrostatique sur le contact mince. Comme notre InSe est intrinsèquement dopé n avec un niveau de Fermi proche de la bande de conduction et que nous souhaitons améliorer la conductivité pour atteindre la bande de conduction, nous commençons par mesurer nos dispositifs avec un dopage n à travers la charge d'espace dans le substrat. Comme le montre la figure 4.5, la caractéristique I-V mesurée est essentiellement la même que celle mesurée au chapitre 3, c'est-à-dire sans rectification de type Schottky ni saturation. Avec un dopage n plus important, le dispositif devient moins résistant, comme prévu, mais il n'y a pas de changement dans le comportement. L'analyse avec le modèle "2-way Parallel Diode" et "1-Diode + Resistor" nous indique que le niveau de Fermi de l'InSe change peu

(à l'ordre de quelques centièmes d'électronvolt) en fonction du dopage et pas suffisamment pour induire un contact ohmique. Ce comportement a été observé à plusieurs reprises dans trois ou quatre autres dispositifs. Notre conclusion est que l'épinglage du niveau de Fermi au MIGS au stade initial, comme on l'a déjà vu dans les dispositifs du chapitre 3, empêche le contact de devenir ohmique, même après un dopage substantiel.

La question se pose alors de l'épinglage du niveau de Fermi pour obtenir un mouvement du niveau de Fermi et un contact ohmique à la fine jonction InSe. Nous nous inspirons de l'observation récurrente selon laquelle une barrière d'oxyde entre le semi-conducteur et le métal est un inhibiteur efficace du MIGS dans le semi-conducteur et empêche le pincement du niveau de Fermi tout en permettant l'injection de charge par effet tunnel [**?**] [**?**]. Le raisonnement derrière cette observation est que la barrière d'oxyde réduit ou annule l'extension de la queue de la fonction d'onde du métal dans le semi-conducteur en raison de la plus grande bande interdite et de la plus petite constante diélectrique. Bien que nous n'introduisions pas de couche d'oxyde à cette jonction, nous pouvons effectivement chercher à réduire la pénétration de la fonction d'onde du métal dans le semi-conducteur et la génération de MIGS, en dopant d'abord le semi-conducteur. En effet, la conductivité est considérablement réduite et la pénétration de la queue de la fonction d'onde dans le semi-conducteur devrait l'être également.

Dans les deux cas, à un certain niveau de dopage, un comportement de redressement apparaît. Il s'agit de la première observation de ce type dans tous nos dispositifs :

- Ce comportement apparaît rapidement sur trois ou quatre cycles I-V au fur et à mesure du dopage.
- Le courant passe rapidement de quelques centaines de nA à quelques dizaines de microampères, soit deux ordres de grandeur.
- L'augmentation du courant chauffe localement le dispositif, ce qui augmente instantanément la concentration de charge, à la fois par l'augmentation du dopage de la charge d'espace (augmentation de la mobilité des ions dans le verre en raison de la température plus élevée) et par l'augmentation de la charge libre induite par la température dans l'InSe. Comme il s'agit d'une boucle de rétroaction positive, elle conduit à la défaillance du dispositif, comme nous le verrons plus loin.
- L'augmentation de la température est clairement visible par l'hystérésis pendant les boucles I-V.
- Il est si rapide que, dans nos deux appareils, il a provoqué une défaillance de l'appareil par brûlure, comme le montrent les photos.
- Le courant élevé peut être attribué à deux facteurs : nous atteignons un véritable comportement de redressement Schottky, ce qui signifie un courant élevé dans le sens de la polarisation directe. La géométrie verticale signifie que la section transversale du dispositif est environ 1000 fois plus élevée que celle d'un dispositif plan. Comme la direction du courant est verticale, c'est la section horizontale ou la surface du dispositif qui agit comme section efficace plutôt que la section verticale.

Nous avons donc, pour la première fois, réussi à dépinner le niveau de Fermi dans un semi-conducteur avec un dopage électrostatique de charge d'espace.

Nous avons réussi à construire un dispositif où un véritable comportement de redressement Schottky est obtenu en modulant le niveau de Fermi dans le semi-conducteur sur une jonction d'un dispositif métal - semi-conducteur - métal de manière à créer une jonction ohmique.

Chapitre 5. Conclusion et perspectives

Dans cette thèse, un travail d'investigation approfondi a été mené pour élucider la hauteur de la barrière de Schottky (SBH) sur les contacts métal/séléniure d'indium (InSe) et les changements subséquents apportés par le dopage électrostatique, avec un accent sur la modification des caractéristiques de contact dans un cadre de diode Schottky. L'entreprise a commencé par une étude concentrée sur les implications du dopage sur le SBH au sein des jonctions métal/InSe. Un ensemble de dispositifs, incorporant InSe en conjonction avec trois métaux différents - or (Au), aluminium (Al) et argent (Ag) - ont été fabriqués et examinés. Par comparaison et analyse, le modèle de diodes parallèles à deux voies a été conclu comme le plus pertinent pour les dispositifs échantillons considérés dans ce corps de travail. Ce modèle s'est avéré instrumental pour délimiter la corrélation entre les caractéristiques courant-tension (I-V) des dispositifs et les paramètres du modèle d'ajustement.

En approfondissant, il a été constaté que les contacts Au sur InSe n'ont pas réussi à former une barrière Schottky idéale. Au lieu de cela, les caractéristiques I-V ont révélé des signes de fuite résistive, laissant présager la présence de canaux conducteurs alternatifs divergeant du modèle Schottky traditionnel. Parallèlement, les contacts Al ont montré un comportement de contact quasi linéaire mais se distinguaient par leur résistance considérablement élevée. De même, les contacts Ag ont affiché un comportement quasi linéaire, mais leur utilité a été compromise en raison de la tendance de l'Ag à infiltrer le InSe, compromettant potentiellement la stabilité et l'efficacité du contact au fil du temps.

L'évidence empirique suggère que la modification des contacts métalliques ou l'emploi de configurations métalliques asymétriques a peu fait pour décaler de manière significative les caractéristiques I-V. Les résultats I-V étaient invariablement très résistifs et présentaient une légère non-linéarité, s'écartant du comportement attendu de la diode Schottky. Cette divergence est potentiellement attribuable à la nature non idéale de l'interface, possiblement due à des états de gap induits par des défauts, un dopage d'impureté, des liaisons pendantes des bords des couches et des états de gap induits par le métal.

La revue de littérature a souligné une observation à travers différents contacts métalliques : la SBH dans les dispositifs métal-InSe avoisinait les 0.5 eV. Cette constance suggère un phénomène de pincement du niveau de Fermi qui prévaut sur la variance du niveau de Fermi du métal et l'affinité électronique du InSe. Les expériences de dopage menées sur des dispositifs asymétriques ont corroboré cela, manifestant seulement de légers ajustements dans le SBH (variant de 0.02 à 0.07 eV), malgré le niveau de Fermi dans les échantillons de InSe mesuré à environ 0.3 eV en dessous du minimum de la bande de conduction dans un dispositif avec des contacts Au doubles [**?**].

Dans la quête de développement d'interfaces électroniques optimales entre les contacts métalliques et l'InSe, le chapitre 3 présente une analyse minutieuse des effets du dopage par charge d'espace sur la hauteur de la barrière de Schottky (SBH) dans les jonctions métal/InSe. Un effort critique de ce travail est l'établissement de conditions propices au comportement ohmique ou quasi-ohmique, particulièrement au contact Au-InSe. Pour réaliser de telles conditions, un déplacement requis du niveau de Fermi d'environ 0.3 eV a été identifié, ce qui présente des défis en raison de l'impact comparativement minimal du dopage par charge d'espace. Il est supposé que la persistance de ce défi découle du pincement du niveau de Fermi par les états de gap induits par le métal (MIGS) associés aux contacts Au.

Pour construire une diode Schottky fonctionnelle utilisant une configuration Au/InSe/Au, il devient impératif d'aborder le phénomène de pincement du niveau de Fermi. Une modification efficace de la SBH par le dopage par charge d'espace exige une approche stratégique,

qui comprend le dopage sélectif d'une seule interface des contacts Au-InSe pour favoriser un comportement ohmique. La réalisation d'une telle approche détient le potentiel de débloquer les pleines capacités des diodes Schottky.

Le modèle des diodes parallèles à deux voies émerge comme un cadre robuste pour capturer le comportement complexe au sein des dispositifs planaires à l'étude. Il souligne la nature "non-idéale" des jonctions et met en lumière une observation notable : la SBH semble présenter un degré d'indépendance par rapport au type de métal. De plus, la recherche délimite que le dopage électrostatique n'incite qu'une variation marginale de la SBH, pointant vers la prédilection du niveau de Fermi pour le pincement aux MIGS.

Pour la construction d'un dispositif de redressement Schottky, les conditions pour établir un contact ohmique par le dopage électrostatique de l'InSe impliquent :

1. Une spécificité de dopage, où seule la couche d'InSe à une jonction est dopée, tandis que la couche correspondante à la jonction opposée reste vierge, maintenant une barrière Schottky métal–InSe. Une telle spécificité peut être atteinte via une géométrie de dispositif en 'escalier', exploitant les propriétés d'écran diélectrique du semi-conducteur pour confiner le dopage par charge d'espace électrostatique à une certaine profondeur.
2. Le design du dispositif doit assurer un chemin de courant à travers les deux jonctions, avec un courant passant verticalement à travers la couche mince d'InSe au bas de l'échantillon et à travers l'InSe plus épais au sommet.
3. Le design et le dopage doivent corroborer un déplacement significatif du niveau de Fermi au sein du semi-conducteur sous le contact mince. Ce déplacement est crucial pour le dé-pincement du niveau de Fermi et la réalisation d'une jonction ohmique au site prévu.

Les perspectives obtenues du chapitre 4 signalent des avancées dans la conception et la fabrication des dispositifs Schottky InSe, où le contrôle précis des caractéristiques de contact est primordial. Le travail souligne l'interaction délicate entre le dopage, la géométrie du dispositif et les propriétés des matériaux dans la quête d'optimisation des composants électroniques. Dans les dispositifs du chapitre 4, une exploration des niveaux de dopage dans les dispositifs à semi-conducteurs a mis à jour des résultats concernant l'induction d'un comportement redresseur. Une augmentation profonde du courant, s'intensifiant de deux ordres de grandeur, a été observée à des seuils de dopage spécifiques. Cette augmentation considérable du courant entraîne un échauffement local dans le dispositif, conduisant à une augmentation rapide de la concentration de charge due à deux mécanismes principaux : un dopage de charge d'espace intensifié découlant d'une mobilité accrue des ions dans le verre à des températures plus élevées, et la génération de porteurs de charge libres au sein de l'indium sélénide (InSe) instiguée par l'élévation thermique.

L'occurrence de cette boucle de rétroaction positive, bien qu'indicative d'une activité accrue du dispositif, conduit inévitablement à la défaillance du dispositif. Cette issue préjudiciable est mise en évidence par la manifestation de l'hystérésis dans les mesures I-V et est en outre corroborée par les dommages physiques aux dispositifs. La nature instantanée de l'augmentation de la température, couplée à l'augmentation significative du courant, précipite une condition accablante que la structure du dispositif ne peut supporter, aboutissant à sa combustion.

Malgré ces défis, la recherche présentée dans ce chapitre marque une réalisation significative : l'atteinte d'un véritable comportement redresseur Schottky. Notamment, l'architecture verticale du dispositif contribue à une aire de section transversale qui est substantiellement plus grande—d'environ trois ordres de grandeur—comparée à celle d'une

configuration planaire. Cet attribut structurel implique que la section transversale horizontale, plutôt que la dimension verticale, assume le rôle de la zone de section efficace au sein de ces dispositifs.

Ce travail a réussi le dé-pincement du niveau de Fermi dans un semi-conducteur par l'application méthodique du dopage de charge d'espace électrostatique. La percée réside dans le développement d'un dispositif où un véritable comportement redresseur Schottky est actualisé. Ceci est réalisé en modulant adroitement le niveau de Fermi à l'une des jonctions métal-semi-conducteur, établissant ainsi une jonction ohmique. La création d'un tel dispositif présentant une méthode innovante pour adapter les propriétés électroniques des dispositifs métal-semi-conducteur-métal et démontrant la faisabilité de la manipulation du niveau de Fermi à travers des processus de dopage stratégiques.

Perspectives

1. Étudier le mécanisme de désépaississement. Il s'agit d'une proposition difficile car les MIGS devraient être très difficiles à observer par d'autres moyens que la modification des caractéristiques de l'appareil. Il n'y a aucun moyen de les observer par spectroscopie puisqu'ils ne sont pas liés à des sites de défauts. Même les sites défectueux ne produiront qu'un très faible niveau de signal. Cependant, un moyen de détection consiste à utiliser d'autres matériaux et à utiliser des matériaux dopés n et des matériaux dopés p qui nécessiteraient différents niveaux de dopage et différentes polarités pour annuler l'effet MIGS par désamorçage.
2. Un meilleur contrôle des paramètres de dopage et de chaleur et la prévention des défaillances du dispositif. La défaillance du dispositif est un problème à surmonter, mais il ne devrait pas être compliqué à résoudre. Le contrôle peut être réalisé par une simple modification du logiciel qui contrôle le dopage et la mesure I-V pour surveiller le courant et les niveaux d'hystérésis et interrompre les mesures en conséquence lorsque le comportement de redressement est atteint. Une résistance de limitation du courant en série constituera également une protection efficace.
3. L'extension immédiate à un matériau différent devrait concerner les TMDs et le MoS_2. Depuis que nous avons commencé à construire ces dispositifs, des améliorations considérables ont été apportées aux techniques de fabrication et de meilleurs dispositifs devraient être disponibles. Une extension intéressante consisterait à utiliser des matériaux de grande surface obtenus par dépôt chimique en phase vapeur (CVD) afin de voir l'effet des impuretés et des défauts sur le pincement du niveau de Fermi et d'évaluer l'intérêt pour les applications.

Contents

Introduction

This work was initiated in the context of current research in 2D materials reaching a stage where applications and devices are coming into focus. Devices of 2D materials present some major challenges [**?**]. The first such challenge is the need to make large area single crystal wafers of ultrathin single or few layer 2D materials. These have been often hampered by the presence of impurities or inhomogeneities in bottom-up approaches like CVD techniques or physical vapour deposition techniques. However, a long and sustained effort is finally beginning to pay dividends with some recent successes in this field [**?**]. Another challenge is that most 2D materials are sensitive and can be polluted or irreversibly altered by ambient exposure [**?**]. Clearly vacuum based fabrication and utilisation is not a viable industrial alternative. The effect of such contamination needs to be efficiently characterized and eventual counter strategies found, for example effective encapsulation [**?**]. Contamination can also result from cleanroom lithographic techniques and this problem too needs to be addressed.

Finally, a simple but fundamental problem remains. All devices, electronic or optoelectronic, need to be contacted with metallic contacts for extraction or injection of charge. Since the overwhelming majority of 2D material devices use semiconductors, a metal-semiconductor contact comes into play. Two basic challenges present themselves [**?**]. Firstly, these contacts need to established in a way such that the material itself is not damaged. This is particularly critical for single layer materials and a bit less so for few layer materials where damage to the top layer does not necessarily compromise the device. This damage may arise from chemicals used for lithography but also from the physical impact of metal atoms deposited at high temperature, or the diffusion of metallic atoms into or between the 2D material layers, blurring the clear metal-semiconductor interface [**?**]. This metal-semiconductor interface is the well-known Schottky junction, presented in all condensed matter physics textbooks and also used in devices. In short, this junction, which ideally is a rectifying junction, results from the charge transfer and resulting space charge and band bending that takes place when a clean and sharp metal-semiconductor junction is formed. As shown in the Figure 3.1 a rectifying barrier is formed in that, for an n-doped semiconductor, the metal side is the anode and the semiconductor side is the cathode. Current flows ohmically from metal to semiconductor but has to cross a barrier from semiconductor to metal. The height of this barrier for an n-type semiconductor is the difference between the metallic work function (difference between the vacuum level and the metal Fermi level) and the electron affinity of the semiconductor (difference between the vacuum level and the conduction band edge of the semiconductor) and is obtained from the condition that at thermal equilibrium the Fermi levels of the two materials have to be aligned.

It is well-known that semiconductor Fermi levels can be altered substantially (changes to the order of 1 eV) by doping, typically by introducing impurity atoms. Similarly, work functions of common metals also differ by energies in the eV range. As an example, we

consider the work functions of Au (5.1 eV), Ag (4.7 eV) and Al (4.1 eV). We should thus expect that Schottky barriers should vary in this energy range of an eV or more, either by changing the metal or by modulating the semiconductor Fermi level by changing the doping. However, it has been well known for many decades that in conventional semiconductor – metal Schottky junctions the change in Schottky Barrier Height (SBH) is actually almost ten times smaller, limited to a few tens of eV [**?**]. Similar results are seen in 2D material-metal Schottky junctions [**?**]. The reasons for this discrepancy are also well-known. As early as 1965, Volker Heine [**?**] gave a straightforward explanation related to Fermi-level pinning in the semiconductor. He showed that at the metal-semiconductor interface of a bulk semiconductor, a "density of even a fraction of a surface state per surface atom per eV is quite sufficient to absorb any required extra charge into the band of surface states without the Fermi level in this band moving very much. Thus E_F at the surface of the semiconductor is effectively pegged to some fixed value". This is the first reference that we know of in literature of the 'pinning' of the Fermi level. Heine also stated that surface states localized in the band gap cannot exist (unless some restructuring of the surface is considered). In-gap states then can exist in the case of defects or impurities (the well-known donor or acceptor levels in semiconductors), but also in their absence, at the junction due to the tail of the metallic wave function in the semiconductor which we can estimate to of the order of a nm [**?**], being inversely proportional to the gap size. This means that for a few-layer sample the tail penetrates at least one whole layer of the sample and makes the Fermi surface pinning more efficient than in a bulk sample. These states associated with the tail have also been called Metal Induced Gap States or MIGS, as opposed to Defect Induced Gap States or DIGS. The challenge then for any device with a metal – semiconductor interface is to control the SBH (for example to establish an ohmic contact). As we shall see in this thesis, this can be attempted by adapting the metal to InSe or by attempting to change the InSe Fermi level. Both methods however will have to counter the effects of Fermi level pinning. The current state of the art in 2D materials has been amply described in a few recent review articles [**?**] [**?**] [**?**]. Our aim in this thesis is to modulate the SBH of an InSe – metal junction so as to make a metal – few layer InSe – metal Schottky diode. The choice of InSe is made because it is a 2D material which can be easily exfoliated and belongs to the family of monochalcogenides with bandgaps spanning the range from near IR to near UV (InSe 1.2 eV, GaSe 2 eV, GaS 3eV). These materials have a direct bandgap above a thickness of about 5 layers (4 nm) and below this thickness they have an indirect bandgap. Finally, though GaSe and GaS are sensitive to ambient contamination, InSe is resistant over a few days [**?**]. These properties make it a good prototype material for this exercise. Furthermore, we propose to use three commonly used metal contacts, Au, Ag and Al to find a convenient configuration and geometry. To do this we fabricate and characterize few layer samples and devices (Chapter 2). In Chapter 3 we make planar devices with symmetric (metal 1 – few layer InSe – metal 1) as well as assymetric (metal 1 – few layer InSe – metal 2) configurations to test the eventual variation of the SBH with the metal. We also test the effect of electrostatic space charge doping on the variation of the SBH in these planar devices. In Chapter 4, in light of the results of Chapter 3, we test a new geometry where Au is the metal and only one Au – InSe contact is doped to render it ohmic. We find that this is possible only in the case where presumably the Fermi level is unpinned by a specific doping sequence. This gives rise to a high power Schottky diode. In Chapter 5 we conclude and discuss some prospectives arising from this work.

Chapter 1

2D Materials Introduction

This chapter serves as an introduction to two-dimensional (2D) materials, specifically focusing on indium selenide (InSe). It reviews prior research on InSe, followed by a detailed examination of Schottky devices that incorporate InSe, with an emphasis on Schottky barrier height.

1.1 Graphene, TMDs, Monochalcogenides

The discovery of graphene in 2004 by Geim and Novoselov marked the beginning of the modern field of two-dimensional (2D) materials [**?**], captivating the scientific community with their extraordinary properties and vast application potential. Graphene, a monolayer of carbon atoms arranged in a hexagonal lattice (as shown in Figure **??**), exhibits exceptional mechanical, electronic and quantum properties. This arrangement allows each carbon atom to form three covalent bonds, resulting in a structure where one p_z-electron per atom remains delocalized across the lattice [**?**], a key factor in graphene's outstanding electrical properties and efficiency in conducting electricity.

Graphene's distinctive electrical conductivity arises from its unique band structure, characterized by the meeting of conduction and valence bands at Dirac points(as shown in Figure **??**). This structure allows electrons to behave as massless particles with a linear dispersion, with high mobility of charge carriers and enabling the development of rapid electronic and photonic devices. In ideal scenarios: absence of impurities, defects, and in configurations where the width to length ratio is significantly high, graphene's charge transport at the Dirac point is mediated through evanescent waves, akin to tunneling phenomena, leading to a universal minimum conductivity value of $\sigma_{\text{Dirac}} = \frac{4e^2}{\pi h}$ [**?**].

Graphene's optical properties are also noteworthy, capable of absorbing a fixed portion of light across a broad spectrum with minimal layers. Its transmittance is governed by the fine structure constant $\alpha = \frac{e^2}{4\pi\epsilon_0 hc}$ [**?**], and can be approximated as $T = (1 - 0.5\pi\alpha)^2 \approx 1 - \pi\alpha \approx 0.977$ [**?**], highlighting graphene's suitability for transparent conductive coatings and advanced photonic devices.

The tunability of the Fermi energy (E_F) in graphene enables the manipulation of its electronic properties. The E_F in graphene can be adjusted through chemical doping by introducing external atoms or molecules like Potassium, Calcium, Ammonia, Oxygen, or various organic compounds, which alter its electron concentration by either donating or accepting electrons, thus shifting E_F. Alternatively, applying an electric field via gating induces an excess of carriers (electrons or holes), offering another method to modify E_F. This ability to control E_F allows for the precise modulation of carrier type and graphene's conductivity, offering advantages over traditional metal/semiconductor junctions, partic-

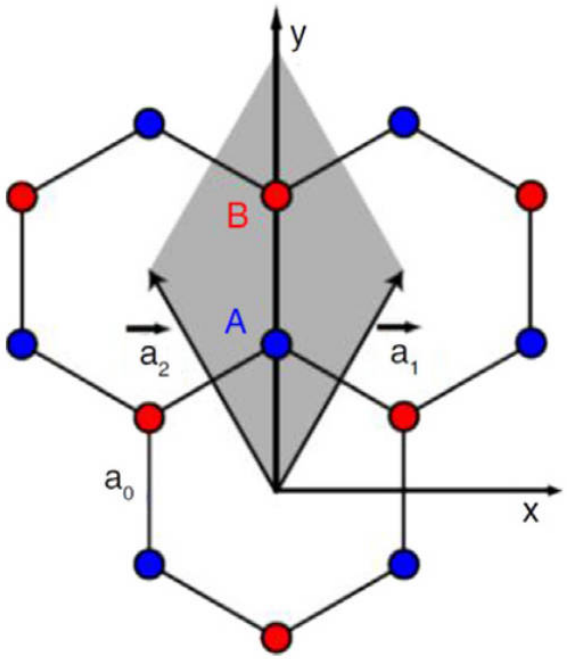

Figure 1.1 – Hexagonal honeycomb lattice of graphene. The blue and red circles indicate atoms belonging to different sub-lattices A and B; the lines between the circles indicate the chemical bonds. a_0 is the nearest-neighbor distance. $\vec{a}_1$ and $\vec{a}_2$ are primitive lattice vectors, and the gray cell is the unit cell [?].

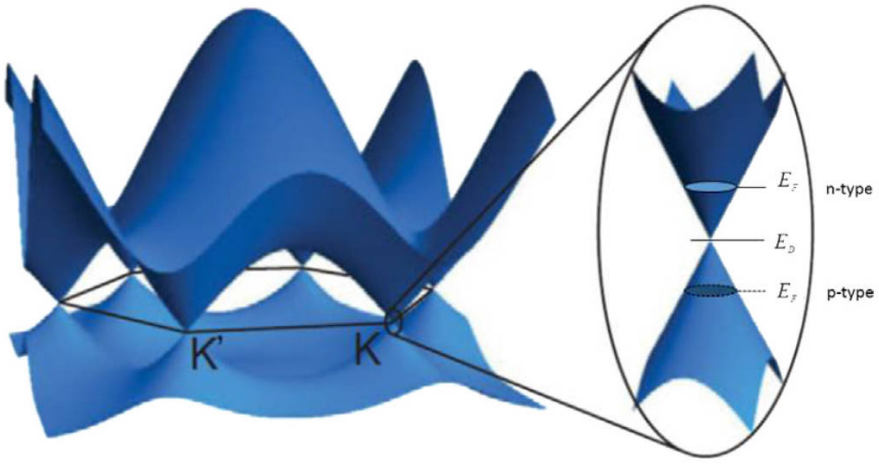

Figure 1.2 – Band structure of graphene showing the zero bandgap inequivalent Dirac points $\vec{K}$ and $\vec{K}'$. A Fermi level above (below) E_D corresponds to n (p)-type graphene [?].

ularly in graphene/semiconductor Schottky junctions by facilitating the adjustment of the Schottky barrier height and rectification properties for tailored electrical characteristics [?] [?].

The synthesis techniques for graphene have progressed from mechanical exfoliation to more sophisticated methods like chemical vapor deposition (CVD), facilitating large-scale production [?]. CVD techniques, particularly on copper substrates, have significantly

advanced graphene's application in diverse fields, from flexible electronics to composite materials. The advent of graphene has not only broadened the horizons of materials science but also set a benchmark for the exploration of other 2D materials such as Transition Metal Dichalcogenides (TMDs). These materials, with their considerable bandgap, contrast graphene's zero-bandgap nature, rendering them ideal for semiconductor applications. TMDs like MoS_2, WS_2, and $MoSe_2$ extend the scope of 2D materials, offering electronic properties that complement graphene and hold promise for the development of novel electronic and optoelectronic devices, thereby expanding the frontiers of nanotechnology and materials science.

2D TMDs, delineated by the general formula MX_2 where M represents a transition metal from groups IV–VII and X denotes a chalcogen (S, Se, or Te), form a multifaceted family of materials with over 40 distinct compounds. These compounds are distinguished by their unique structural composition, where strong intralayer bonding contrasts with weak interlayer van der Waals interactions, enabling the isolation of individual layers through various exfoliation or vapor deposition techniques. This structural peculiarity facilitates a significant transformation in their properties as the material transitions from bulk to monolayer form, primarily due to the two-dimensional confinement of charge carriers, thereby negating interactions in the z-direction. Such confinement endows single-layered TMD nanosheets with fundamentally different properties compared to their bulk analogues (as shown in Figure **??** : MoS_2 as an example), igniting interest for their potential in diverse applications such as catalysis, electronics, and photonics [**?**] [**?**].

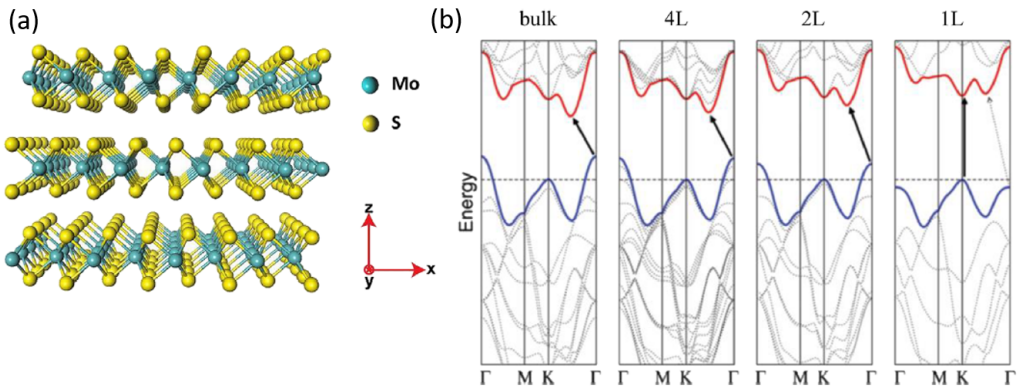

Figure 1.3 – (a) A schematic representation illustrates the structure of MoS_2, where two layers of sulfur (S) atoms (colored yellow) encapsulate a central layer of molybdenum (Mo) atoms (colored blue), forming a sandwich-like configuration [**?**]. (b) The calculated electronic band structures of MoS_2, ranging from bulk to monolayer forms, are depicted. Progressing from left to right, the images represent the bulk, tetralayer, bilayer, and monolayer configurations. Solid arrows within the figures highlight the lowest energy transitions. In the bulk form, MoS_2 is characterized by an indirect bandgap, where the valence band maximum (VBM) is located at the Γ-point of the Brillouin zone, and the conduction band minimum (CBM) is situated at a point of lower symmetry within the same zone. Conversely, in the monolayer form, MoS_2 exhibits a transition to a direct bandgap, with both VBM and CBM located at the K-point of the Brillouin zone [**?**].

Advancements in the synthesis and application of 2D TMDs have catalyzed extensive research aimed at elucidating their electronic and vibrational properties. Techniques such as CVD and chemical exfoliation have been optimized to fabricate high-quality, uniform

TMDs tailored for specific applications, ranging from fundamental condensed matter studies to practical implementations in catalysis and energy storage [**?**]. Notably, the synthesis of monolayer MoS_2 using CVD has shown significant potential in electronics due to its superior electrical properties [**?**], while mechanically exfoliated WS_2 has been applied in photonics, leveraging its distinctive optical characteristics [**?**]. This research trajectory has expanded to explore both mono- and multi-layered TMD nanosheets, distinguished by their unique physical, chemical, and electronic properties compared to their bulk forms. Techniques like mechanical cleavage and liquid phase exfoliation have enabled the synthesis of TMD nanosheets, laying the groundwork for creating functional hybrid nanostructures by integrating TMD nanosheets with various materials [**?**] [**?**] [**?**] [**?**], inspired by graphene-based composites. This approach has led to the development of novel materials, including MoS_2–reinforced metal organic frameworks for catalysis and WS_2–polymer composites for electronic applications, enhancing mechanical strength and electrical conductivity [**?**] [**?**]. Recent reviews highlight advancements in large-scale synthesis of 2D TMD nanosheets and their integration with advanced materials to fabricate functional composites for batteries, sensors, and biomedical devices [**?**]. Examples include the synthesis of $MoSe_2$ for the electrocatalytic hydrogen evolution reaction and TiS_2–based electrodes for lithium-ion batteries, demonstrating TMDs' broad potential in addressing critical technological challenges and their versatility in creating superior composites with enhanced properties [**?**] [**?**].

As research in TMDs has matured, demonstrating significant potential in electronics, photonics, and catalysis, the focus has increasingly shifted towards materials with even more unique and tunable properties. Monochalcogenides, compounds with the general formula MX where M is a metal and X is a chalcogen (S, Se, or Te), have emerged as a new class of 2D materials that promise to extend the frontier of material science even further. These materials share the layered structure characteristic of graphene and TMDs, with strong in-plane bonds and weak out-of-plane interactions, which facilitates the exfoliation into thin layers. Moreover, they offer a different set of bandgap energies and electronic properties, making them highly appealing for applications in novel electronic devices, optoelectronics, and energy storage systems. For instance, the direct bandgap in monolayer α-SnS and α-SnSe makes them excellent candidates for photovoltaic applications and photodetectors [**?**] [**?**], showcasing their potential to contribute to renewable energy technologies. Single-layer MX consist of four sublayers stacked in the sequence X-M-M-X, as illustrated in Figure **??** .

Recent theoretical studies have unveiled a stable class of single-layer group IV monochalcogenides YX ($Y = \mathrm{Si, Ge, Sn}$; $X = \mathrm{S, Se, Te}$), characterized as semiconductors with wide band gaps. These findings are complemented by research indicating that these materials undergo indirect-to-direct bandgap transitions under small mechanical strain, enhancing their appeal for nanoelectronics and optoelectronics. Furthermore, the application of large compressive strain to monolayers of GeX and SnX has demonstrated a transition from semiconductor to metal [**?**] [**?**] [**?**] [**?**], underscoring the capacity for electronic structure tuning. Despite these advancements, the chemical and physical mechanisms underpinning the observed structural and electronic properties of these 2D monolayers remain to be fully elucidated.

1.2 Group-III monochalcogenides

Parallel to the exploration of group IV monochalcogenides, group III metal chalcogenides (MX, where $M = \mathrm{B, Ga, Al, In}$; $X = \mathrm{O, S, Se, Te}$) have also garnered attention. Various MX systems, including InSe, GaS, GaSe, GaTe, have been experimentally real-

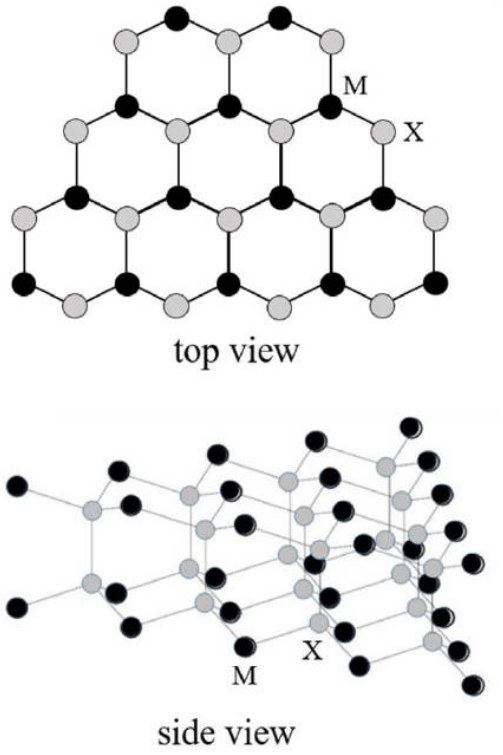

Figure 1.4 – Structural schematics of the top and side views of MX compounds. Black spheres represent chalcogen atoms (X= S, Se, Te), and gray spheres represent metal atoms (M) [**?**].

ized, with significant efforts devoted to uncovering their electronic and optical properties. Over the past decade, III–VI layered semiconductors such as GaSe, InSe, and GaS have established themselves as potential candidates for a myriad of applications, including field-effect transistors (FETs) and optoelectronic devices [**?**] [**?**] [**?**]. The intriguing properties of these materials are intricately linked to their structural characteristics, with the existence of various polytypes necessitating the identification of structural phases to fully exploit their potential. Single-layer GaS, GaSe, and InSe exhibit identical crystal structures, comprising four closely-packed monoatomic sheets arranged in an X - M - M - X sequence, where X represents S or Se, and M denotes In or Ga. These materials can adopt different polytypes through the stacking of single layers in distinct sequences. The most commonly described polytypes are β, γ, and ϵ, as illustrated in Figure **??**. Density functional theory calculations have been applied to study the structural and electronic properties of layered β-GaS, ϵ-GaSe, γ-InSe and GaTe compounds, the results are shown in Figure **??**.

Monolayer GaS and GaSe, in particular, have shown promise as photodetectors due to their strong absorption in the UV-visible spectrum [**?**] [**?**] [**?**] [**?**]. Theoretical studies suggest that single-layer GaS and GaSe could serve as effective photocatalysts for water splitting, based on the alignment of their band edge positions with the redox potential of water [**?**] [**?**]. Both experimental and theoretical research indicates that the band gap and optical properties of GaX can be tailored through mechanical deformation. Furthermore, the electronic properties of GaS/GaSe heterostructures can be modulated by strain, and

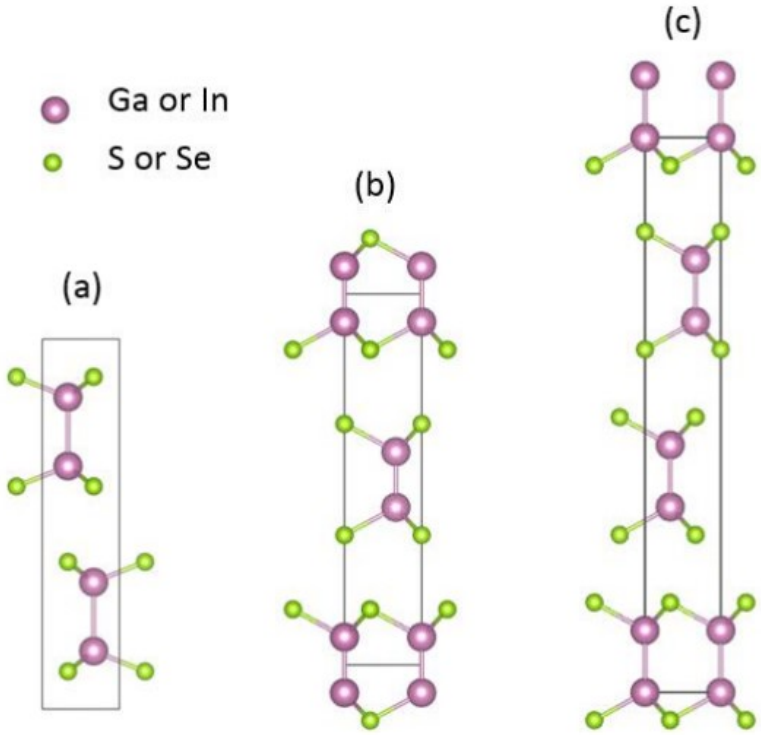

Figure 1.5 – Unit cells of three kinds of Polytypes in III-VI materials such as GaS, GaSe and InSe. (a) β polytype (b) ϵ polytype (c) γ polytype [?].

vertical stacking of single layers leads to electron and hole splitting [?] [?]. Interestingly, InSe exhibits a direct-to-indirect band gap transition as sample thickness decreases, a trend opposite to that observed in transition-metal dichalcogenides like MoS_2 [?]. This behavior suggests that few-layer InSe may offer distinct transport and photodetection performance compared to MoS_2, further expanding the potential applications of monochalcogenides in material science.

InSe, among the vast array of group-III monochalcogenides, has emerged as material of considerable promise, particularly due to its tunable bandgap in the few-layers regime – a result of pronounced quantum confinement effects [?] [?] [?]. This tunability, corroborated by both theoretical and experimental research, along with InSe's reported carrier mobility of up to $10^3\,cm^2\,V^{-1}\,s^{-1}$ at room temperature, sets it apart from other TMDs and black phosphorus (BP), underlining its superior performance [?] [?]. Furthermore, the allure of bulk InSe for photovoltaic applications [?] [?] lies in its direct bandgap, high solar energy conversion efficiency, and the capacity for controllable p-type and n-type doping, all while maintaining good chemical stability. The fabrication of 2D single-layer InSe-based field-effect devices, achieved through meticulous exfoliation and encapsulation in an inert atmosphere, showcases the significant progress in harnessing this material [?] [?].

Building on this foundation, the transition from bulk to monolayer InSe marks a shift from an direct gap to an indirect gap semiconductor [?] (as shown in Figure ??). Moreover, the pronounced suppression of electron-hole pair recombination in the 2D InSe monolayer, as confirmed experimentally, significantly boosts its potential in photocatalysis by facilitating enhanced charge separation and transport [?].

In summary, the 2D InSe-family group–III monochalcogenides' unique electronic and optical properties, combined with high carrier mobilities and structural versatility, position

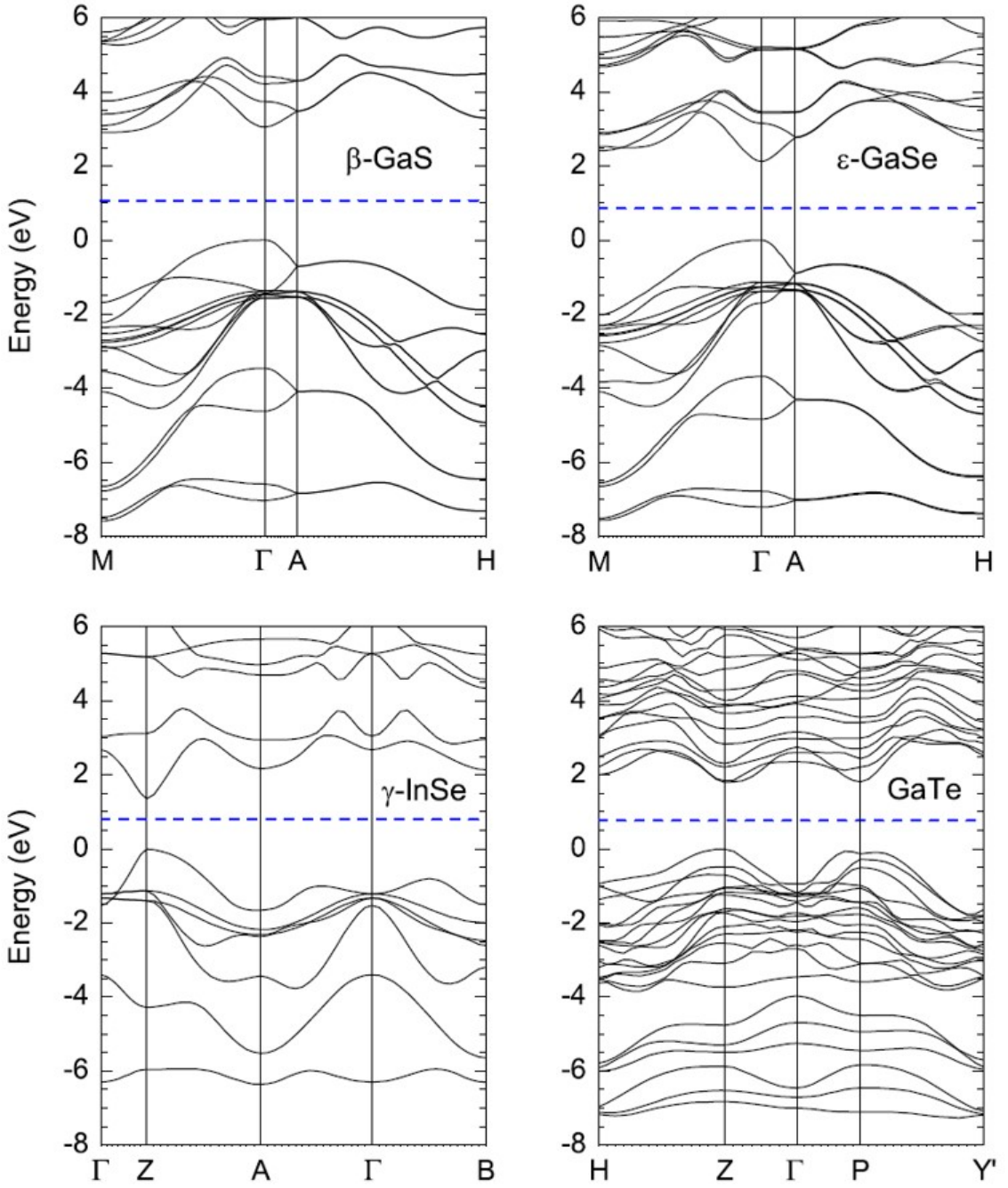

Figure 1.6 – Band structures of β-GaS, ϵ-GaSe, γ-InSe and GaTe compounds. The dashed lines indicate the location of CNL at low temperature. The valence band maximum is set at zero energy [**?**].

these materials as central players in the ongoing development of advanced nanodevices: from high-performance photodetectors and FETs to the applications in solar energy conversion and photocatalysis. GaS exhibits a bandgap of 3 eV and demonstrates extreme sensitivity to atmospheric pollution, where exposure for merely a few seconds is sufficient to degrade few-layer samples. GaSe, with a bandgap of 2.6 eV, also shows sensitivity to atmospheric conditions, but its few-layer samples can endure for a few hours before degradation. InSe however, stands out with its 1.2 eV bandgap, showcasing remarkable

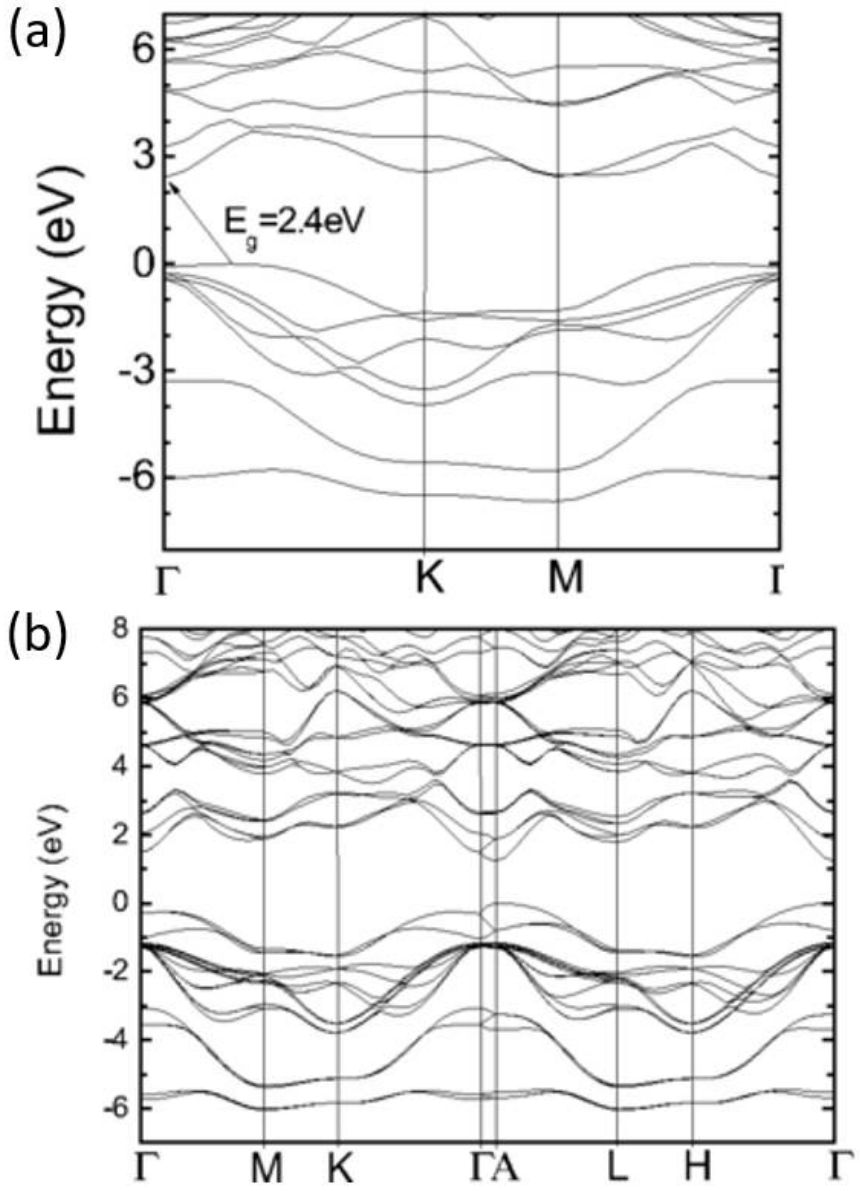

Figure 1.7 – Band structures of (a) monolayer (indirect band gap)and (b) bulk InSe (direct band gap)calculated using the screened exchange functional [**?**].

stability against atmospheric pollution, with few-layer samples remaining intact for several days. The InSe material family enables spanning the optical spectrum from infrared (IR) to ultraviolet (UV), presenting a versatile tool for optical applications. The choice to work with InSe in this thesis is motivated by its stability and small, tunable direct bandgap, which is significant for samples exceeding 5-6 layers, aligning with our research objectives.

1.3 Previous works on InSe

The synthesis of indium selenide (InSe) is crucial for the development of high-performance electronic devices. InSe can be synthesized using both top-down and bottom-up approaches, each offering unique advantages and suited to specific applications.

Top-down methods involve the exfoliation of bulk InSe into thinner layers. Mechanical exfoliation is a straightforward technique that repeatedly uses adhesive tape to peel off layers from bulk material, yielding high-quality InSe flakes. This process, while simple and low-cost, results in flakes of random sizes and thicknesses, which limits its scalability. Alternatively, liquid-phase exfoliation utilizes solvents and surfactants to exfoliate bulk InSe in a liquid medium, often followed by ultrasonication to disperse the material [**?**]. This method can produce size-sorted dispersions, allowing for the controlled deposition of flakes onto substrates, which is beneficial for applications like inkjet printing and photodetectors [**?**].

Bottom-up methods build the material layer by layer, offering better control over the thickness and uniformity of the resulting films. Physical vapor deposition (PVD) grows monolayer flakes directly on substrates, using InSe powder as the evaporation source [**?**]. However, controlling the flake thickness and uniformity is challenging. Van der Waals epitaxy, on the other hand, allows for the growth of well-oriented InSe flakes with precise thickness control by adjusting the growth conditions [**?**]. Pulsed laser deposition (PLD) is another bottom-up approach that deposits material onto a substrate using a high-energy pulsed laser, enabling the growth of large-area, highly crystalline InSe films with controlled thickness [**?**]. Finally, chemical vapor deposition (CVD) is a widely used method for synthesizing high-quality and uniform 2D layers. It utilizes gaseous precursors and a substrate, where the InSe layers form, offering reproducibility and scalability for industrial applications [**?**] [**?**].

Even though bottom up approaches allow for large area samples, their crystalline quality from the point of view of defects and impurities is not yet at the level of bulk exfoliated samples.

InSe has emerged as a highly promising candidate for advanced electronic and optoelectronic applications. Its appeal lies in ease of fabrication, its relative sability in ambient conditions, the existence of a direct band-gap in few layer samples and the size of the bangap (1.2 eV), which can allow coupling to near infra-red light.

In this section I review the significant advancements in the development of InSe based field-effect transistors (FETs) and photodetectors. By focusing on the electron mobility, device performance, and photoresponsivity enhancements through various experimental techniques, encapsulates the potential of InSe in high-performance electronics and optoelectronics.

In the field of FETs, notably by researchers such as Feng et al., who have improved electron mobility in InSe FETs by introducing a bilayer of polymethyl methacrylate (PMMA) and aluminum oxide (Al_2O_3) as the bottom dielectric layer [**?**], as illustrated in Figure **??**, leading to an enhancement in the room-temperature mobility of multilayer InSe transistors from 64 cm^2/Vs to 1055 cm^2/Vs. This configuration achieved high current on/off ratios of 1×10^8, minimal standby power dissipation, and consistent current saturation across a broad voltage range; Sucharitakul et al. employed various substrates, including PMMA, bare silicon oxide, passivated silicon oxide, and silicon nitride, for fabricating multilayer InSe FET devices [**?**], they extract device field effect mobility and intrinsic Hall mobility through back gating and Hall measurement in a four-probe configuration, across temperatures ranging from 20 to 300 K. The mobilities observed, ranging from 0.1 to

2.0×10^3 cm^2/Vs, are comparable or superior to those of FETs made from widely studied 2D transition metal dichalcogenides, underscoring the considerable potential of InSe for high-performance electronics applications.

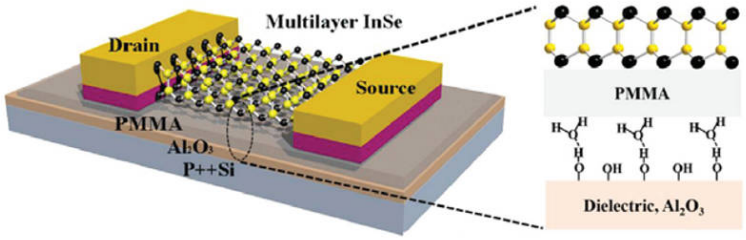

Figure 1.8 – Schematic of a back-gated InSe FET with polymethyl methacrylate (PMMA)/Al_2O_3 bilayer dielectric [?].

The concerted efforts of Feng et al., Luo et al., and Yang et al. have contributed to the advancement of InSe device performance by exploring the effects of various electrode materials. Feng et al. focused on multilayer InSe FETs [?], finding that device performance could be significantly enhanced by selecting metal contacts and optimizing the InSe nanosheet thickness to 33 nm. As can be seen from Figure ??, their investigation revealed a notable increase in electron mobility, from $4.7\,cm^2\,V^{-1}\,s^{-1}$ with aluminum (Al) contacts to $162\,cm^2\,V^{-1}\,s^{-1}$ with indium (In) contacts, alongside on/off ratios between 10^7 and 10^8, with Al demonstrating the lowest performance due to the high resistance of Schottky contact formed ($5.4 \times 10^8\,\Omega\mu m^{-1}$). Luo et al. introduced graphene electrodes in InSe-based photodetectors [?] (as shown in Figure ??), achieving a remarkable improvement in response speed and photoresponsivity, with response times reduced to $120\,\mu s$—about 40 times faster than traditional InSe/metal devices—and a high photoresponsivity of up to 60 A/W, covering a wide spectral range from 400 to 1000 nm. This illustrates the potential of graphene electrodes for high-speed and broad-spectral applications in optoelectronics. Yang et al.'s study on InSe nanoflake photodetectors fabricated via focused ion beam (FIB) showcased extraordinary UV and visible light sensing capabilities [?], achieving a responsivity of up to 1.8×10^7 A W^{-1} and detectivity of up to 1.1×10^{15} Jones, attributed to the high electron mobility (up to $450\,cm^2\,V^{-1}\,s^{-1}$) and the low contact resistance at the platinum (Pt)/InSe interface facilitated by an oxygen-sensitized photoconductivity mechanism (as shown in Figure ??).

The work by Tamalampudi et al. demonstrates the fabrication of high-performance, bendable few-layered InSe photodetectors [?], showcasing their capability for broadband photodetection across the visible to near-infrared spectrum (450 to 785 nm). These devices achieved high photoresponsivities (up to 12.3 A/W at 450 nm on SiO_2 /Si substrates and 3.9 A/W at 633 nm on PET films), outperforming other 2D crystal-based photodetectors such as graphene, MoS_2, GaS, and GaSe. The study highlights the devices' quick response time, long-term stability, and flexibility, indicating potential applications in advanced optoelectronics and 2D heterostructure devices.

The study by Kang et al. introduced a scalable method to prepare high-quality InSe flakes using a surfactant-free, deoxygenated cosolvent mixture of ethanol and water for liquid phase exfoliation [?]. This method minimizes processing residues and avoids chemical degradation, producing InSe flakes and thin films with pristine electronic properties.

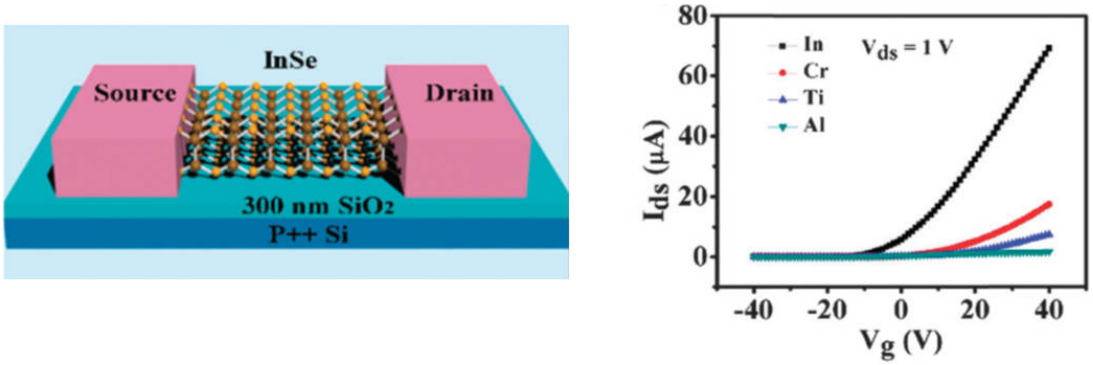

Figure 1.9 – Left: Schematic of a back-gated InSe FET with SiO_2 as the bottom dielectric. Right: Transfer characteristics of a 33 nm thick InSe FET with different metal contacts [?].

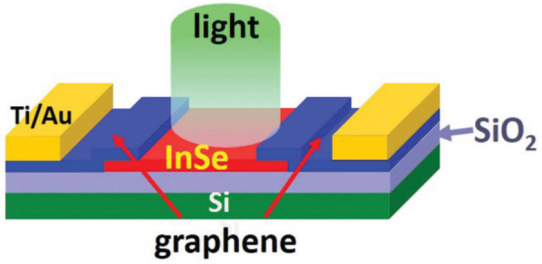

Figure 1.10 – Schematic of an InSe/graphene photodetector [?].

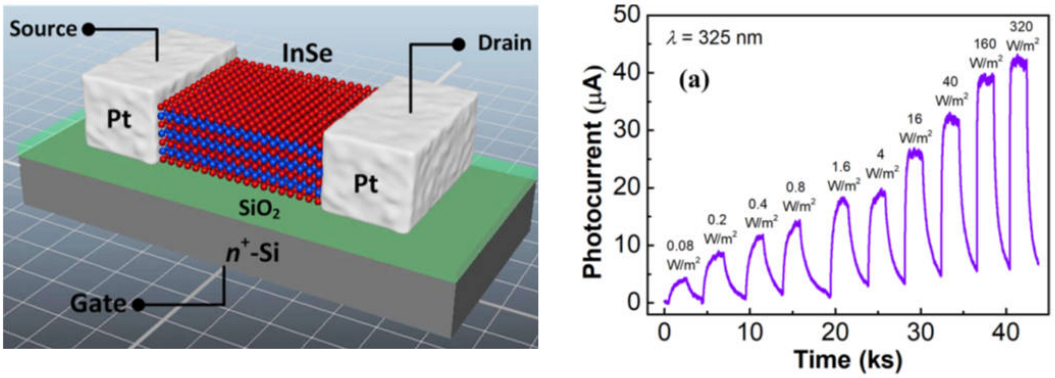

Figure 1.11 – Left: Schematic of a back-gated InSe FET with Pt focused ion beam (FIB) contacts. Right: Photoresponse curves under different excitation intensities at wavelengths (λ) of 325 nm [?].

The photodetectors made from these InSe flakes exhibited exceptional photoresponsivities, around 5×10^7 A W^{-1}.

Chen et al. have made strides in the exploration of heterostructures combining InSe with other materials, showcasing their potential in enhancing optoelectronic device perfor-

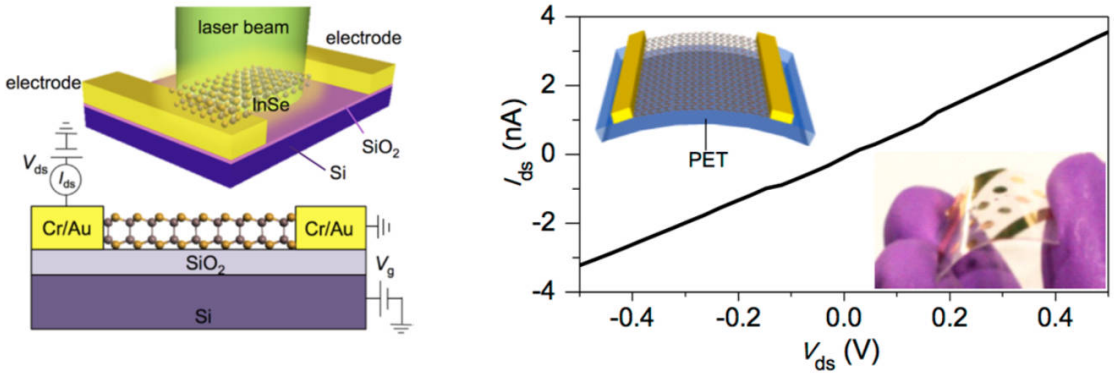

Figure 1.12 – Left: Schematic of an InSe/metal FET under illumination. The metal contacts to the InSe channel are fabricated using a shadow mask. Right: Output curve (I_{ds} vs V_{ds}) of a few-layered InSe photodetector on a flexible polyethylene terephthalate (PET) substrate. Insets show a schematic of an InSe-based flexible photodetector (top) and a digital image of an actual device (bottom) [**?**].

mance. Their work on a photo detector based on a graphene/few-layer InSe heterostructure [**?**] (as shown in Figure **??**)under 532 nm light illumination demonstrated a notable photocurrent variation with source-drain voltage under different illumination powers, with and without a gate voltage, achieving a photoresponsivity of 0.94×10^3 A/W. In another study, they focused on the interaction of light within 2D semiconductor heterostructures like InSe and MoS_2 [**?**](as shown in Figure **??**), employing a 'random transfer' method to create residue-free heterostructures. This study focuses on how the manipulation of layer thicknesses within these heterostructures can significantly enhance their ability to harvest light, For instance, they found that certain thickness combinations of InSe and MoS_2 layers can enhance Raman scattering intensity by up to six times compared to isolated layers. Furthering their research, Chen et al. reported on a novel self-driven photodetector composed of a vertically stacked graphene/InSe/MoS_2 heterostructure [**?**] (as shown in Figure **??**), showcasing rectifying and bipolar behaviors. This device, in self-driven mode, exhibited high photoresponsivity (110 mA W^{-1}), rapid photo-response (less than 1 ms), and high detectivity (over 10^{10} Jones).

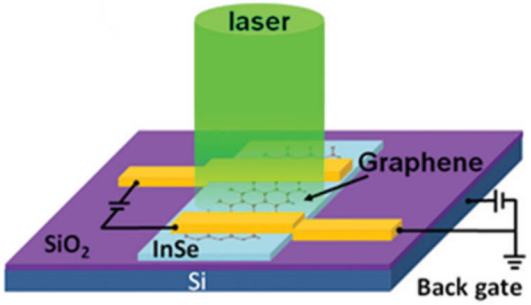

Figure 1.13 – Schematic diagram of the photo-detector based on a graphene/few-layer InSe heterostructure [**?**].

There are also studies delve into the properties and potentials of InSe for optoelectronic applications, elucidating the material's dynamic behaviors and electronic structures

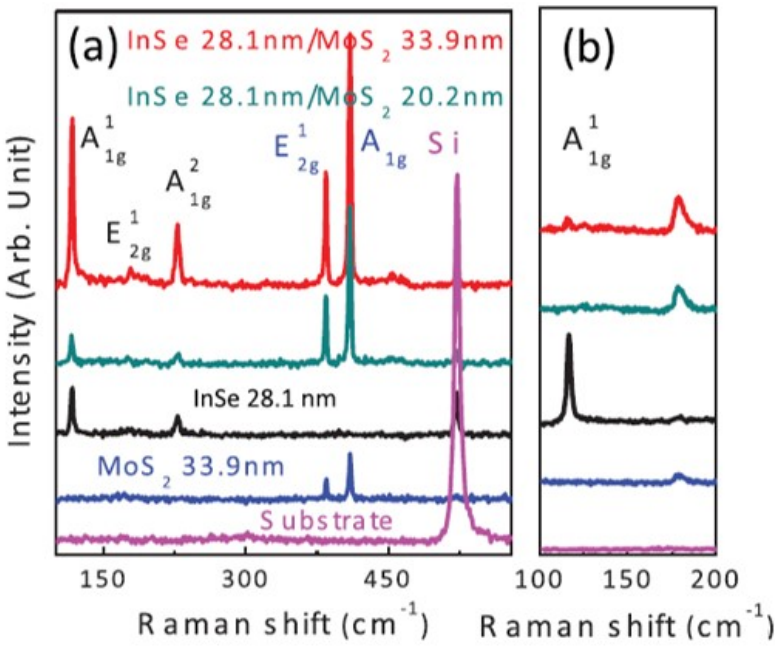

Figure 1.14 – (a) and (b) Raman shift of $InSe/MoS_2$ heterostructure under 532 nm excitation and under 638 nm excitation respectively [**?**].

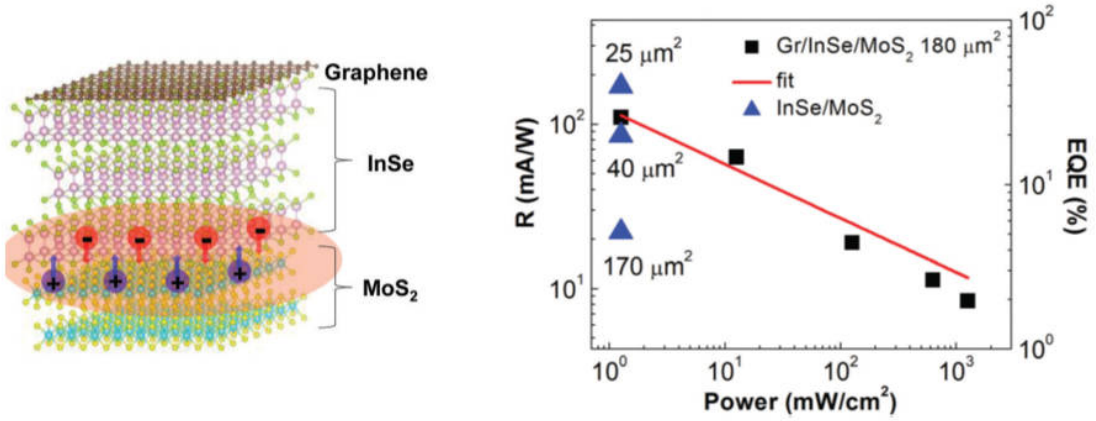

Figure 1.15 – Left: Vertical VDW stacking of the graphene/InSe/MoS_2 heterostructure. Right: The photoresponsivity (R) and external quantum efficiency (EQE) for graphene/InSe/MoS_2 heterostructure photodetectors and compared with different sized devices of InSe/MoS_2 heterostructures, plotted against illumination power density (P). The photoresponsivity is calculated using the equation $R = I_{ph}/(P \times A)$, where I_{ph} represents the photocurrent and A is the device area. The EQE is determined by the formula $EQE = (hcR)/(e\lambda)$, incorporating the constants h (Planck's constant), c (speed of light), e (elementary charge), and λ (wavelength of incident light). The experimental data (symbols) is fitted with a phenomenological power law $R = \alpha P^{\beta-1}/A$, where α and β are empirical fitting parameters [**?**].

through sophisticated experimental techniques. Chen et al.'s use of two-photon photoelectron spectroscopy (2PPE) provided detailed insights into the dynamics of hot carriers in

InSe [?], uncovering that electrons excited to energies of 3.12 eV undergo rapid thermalization to states degenerate with the $\bar{M}$ valley, cooling effectively through Fröhlich coupling with phonons and small momentum transfer. Another study by the same group explored the ultrafast dynamics of hot carriers in a quasi-two-dimensional electron gas (2DEG) on InSe [?], revealing that these carriers, despite the expected screening effects in quasi-2DEGs, still exhibit dynamics heavily influenced by remote coupling with longitudinal optical (LO) phonons, even at high carrier concentrations.

Hugo Henck et al. provided an experimental demonstration that InSe features a direct bandgap of approximately 1.25 eV at the Γ point of the Brillouin zone, indicative of n-type doping potentially caused by intrinsic point defects like vacancies or lattice antisites [?]. Their ARPES analysis revealed the top of the valence band to be poorly dispersive, with a hole effective mass of $m^*/m_0 = -0.95$ in the Γ-K direction and spin-orbit splitting of the deeper-lying bands around 0.35 eV. Zhang et al. observed bandgap renormalization in InSe by approximately 120 meV through controlled in situ surface electron doping using sodium (Na) atoms [?], with ARPES measurements showing a decrease in the bandgap by about 120 meV at a doping level correlating to a carrier concentration of $8.1 \times 10^{12}\text{cm}^{-2}$(as shown in Figure ??). This change underscores the capacity for tuning InSe's bandgap through surface doping, a critical aspect for optimizing its optoelectronic properties.

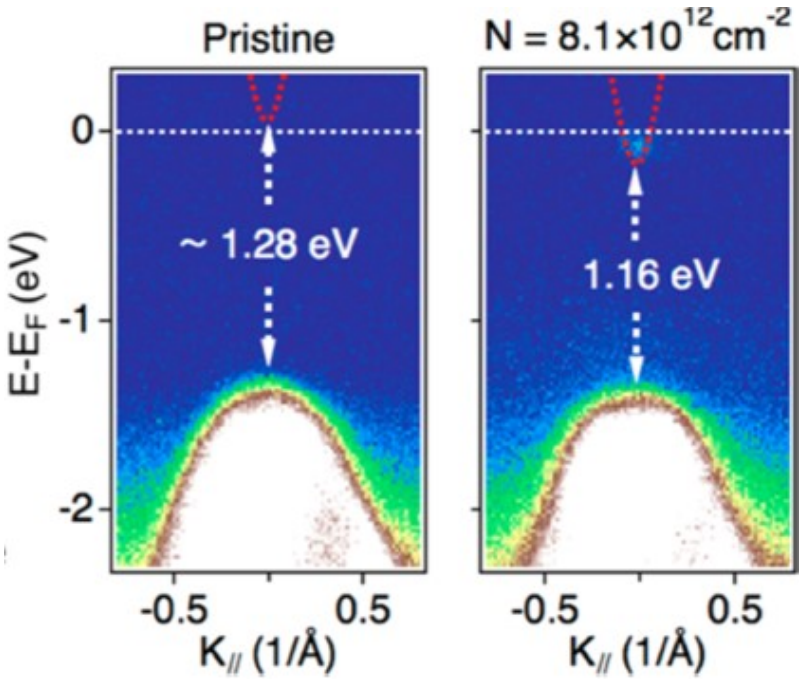

Figure 1.16 – Band structure evolution of InSe as a function of carrier concentration. The zoom-in Angle-Resolved Photoemission Spectroscopy (ARPES) of InSe without Na deposition (left) and with Na deposition (right) for a time of 17 minutes, corresponding to a carrier concentration of $8.1 \times 10^{12}\,\text{cm}^{-2}$ [?].

The potential of InSe is not limited to high mobility and sensitivity, it also demonstrates superior performance in comparison to other 2D materials. The high electron mobility, broad spectral response, and scalability of InSe make it an attractive material for future electronic and optoelectronic devices, promising advancements in high-speed electronics, sensitive photodetectors, and beyond.

1.4 Schottky diodes with 2D materials

Schottky diodes with 2D materials are predominantly recognized for their use in photodetectors, which are devices that convert light into an electrical signal. The unique properties of 2D materials, such as graphene and metal dichalcogenides, contribute to the enhanced performance of these photodetectors [**?**]. These materials offer benefits such as fast response times, high stability, and excellent photo-to-dark current ratios.

Metal chalcogenides, including compounds like SnS_2, In_2S_3, InSe, and GaSe, MoS_2, GaS have received attention due to their efficient photodetection performance and stability. For instance, SnS_2-based detectors are noted for their stability and rapid response [**?**]. WSe_2/SnS_2 photodetectors have shown efficient performance with high photo-to-dark current ratios and specific detectivity [**?**]. A graphene-contacted InSe photodetector has also been highlighted for its excellent photodetection capability [**?**].Ultrabroadband MoS_2 Photodetector with Spectral Response from 445 to 2717 nm [**?**].

The ability to control and synthesize these materials with precision impacts device performance substantially. For example, the controlled synthesis of ultrathin β-In_2S_3 has led to improvements in near-infrared photodetection [**?**]. An InSe/Au Schottky junction device displayed very low dark currents and high photodetection performance, attributed to effective Fermi level pinning at the interface [**?**].

Researchers found that the n-type Schottky contact is formed in the graphene/g-GaSe heterostructure with a Schottky barrier height of 0.86 eV, which can be efficiently modulated by applying the electric field, in-plane strains, and interlayer coupling [**?**]. The I-V characteristics exhibit non-linearity indicating Schottky contact at the GaSe and n-Si interface and this diode can be used as efficient temperature sensor [**?**]. A graphene contacted SnS_2 photodetector exhibited an excellent photodetection capability by charge trapping at the interface and SBH modulation [**?**]. NbS_3 Schottky photodetectors have excellent photoelectric performance, which enables fast photoresponse ($11.6\,\mu s$), low specific noise current ($4.6 \times 10^{-25}\,A^2\,Hz^{-1}$) [**?**]. A 2D $PtTe_2$/Si device showed a high photocurrent at 1-7 mm due to the increased absorption and suppressed photocarrier recombination [**?**]. A $GeSe/MoSe_2$ van der Waals heterojunction shows gate-tunable rectifying behavior and self-powered photovoltaic characteristics [**?**].

The ideal Schottky barrier formed at the interface of a metal and a semiconductor is defined in a straightforward way [**?**], as we shall see in chapter 3. The relevant energy levels for the metal are the Fermi energy and the vacuum level, the difference between the two being the metallic work function. For the semiconductor, we have the energy gap which is the difference between the conduction band energy and the valence band energy, the electron affinity which is the difference between the conduction band and the vacuum level and finally the Fermi energy which lies in the bandgap. The Schottky barrier height (SBH) is determined on contact between the two surfaces which results in charge transfer and polarisation and resulting band bending at the interface.

The SBH (for an n-type semiconductor) is given by the difference between the metal work function and the electron affinity of the semiconductor. In principle, by changing the semiconductor and/or the metal, a wide variety of behaviour can be obtained, ranging from an ohmic contact to a moderate barrier height (a few tenths of eV) to a strong Schottky barrier (1 eV or more). This could in principle allow for the design of a wide variety of metal-semiconductor interfaces tailored for different applications. However the situation is quite different in the real world. As early as the 1960's [**?**], it was noticed that independently of the degree of doping in the semiconductor which can move Fermi levels by the order of 1 eV and the metal work function which can differ by a few eV's,

SBH rarely moved by more than a few tenths of an eV for different semiconductor-metal junctions. V. Heine convincingly argued that this was due to the "pinning" of the Fermi level of the semiconductor by "surface states" in the semiconducting gap. These in fact arise due to the penetration of the tails of metallic wave function into the semiconductor and hence the Fermi energy of the semiconductor is pinned to this "mid-gap" level [**?**].

In few-layer 2D semi-conductors this situation is extremely widespread, amplified by the fact that there is no bulk. Schottky barriers and their lack of tunability due to Fermi level pinning remain a big challenge for future devices of such materials [**?**]. We shall see in chapter 3 that the use of three different contact metals (Au, Ag, Al) with InSe essentially does not the I-V curves of the resulting devices even though metallic work functions change by several tenths of an eV. The only change is observed for the Ag-InSe contact where contact resistance is found to be lowered but the reason as we shall see is an extrinsic one (probable diffusion of Ag ions). One solution to this lack of tunability of the SBH is suggested to be the introduction of an oxide layer between the semiconductor and the metal which can limit the penetration of the metallic wave function into the semiconductor and consequently limit the formation of mid-gap states and the pinning of the Fermi level.

In chapter 4 we will see that another innovative solution exists. We have pioneered the fabrication of a vertical InSe few layers device with metallic Au contacts. With electrostatic space-charge doping we render one of the two contacts ohmic while the other one stays Schottky. The Fermi level is depinned at the InSe-metal contact using a novel doping strategy and this approach leads to a a high current near-ideal Schottky diode like device.

Chapter 2

Experimental Techniques

In this chapter, I will introduce the various techniques employed to prepare, characterize, and fabricate devices, as well as the methods used for device testing. The preparation techniques include mechanical exfoliation and the anodic bonding method. Characterization techniques such as optical microscopy, atomic force microscopy (AFM), Raman spectroscopy, and photoluminescence (PL) spectroscopy are utilized to ensure the samples meet the necessary quality standards for device fabrication in Chapters 3 and 4. The devices fabrication process involves metal evaporation, dry transfer, and wire bonding. Finally, device testing is conducted through electrical measurements and space charge doping.

2.1 Precursors and sample preparation technique

2.1.1 Mechanical exfoliation

As I mentioned in Chapter 1, the synthesis of 2D materials can be broadly categorized into top-down and bottom-up approaches. The top-down method, exemplified by mechanical exfoliation from bulk crystals, is a straightforward technique that yields high-quality, albeit small-area, samples. This method is particularly useful for creating prototype devices and necessitates a single crystal of the layered material. On the other hand, the bottom-up approach involves thin film growth, utilizing a variety of techniques such as Chemical Vapor Deposition (CVD), Physical Vapor Deposition (PVD) on epitaxial substrates (including Molecular Beam Epitaxy [MBE] and Atomic Layer Epitaxy [ALE]), and Pulsed Laser Deposition (PLD). Originating with the landmark isolation of graphene in 2004 [**?**], mechanical exfoliation has become a cornerstone technique in materials science, celebrated for its simplicity and efficacy in synthesizing a wide array of 2D materials.

At its core, mechanical exfoliation transforms bulk crystalline materials into ultrathin layers. Commonly known as the "Scotch tape method", this technique employs adhesive tape to delicately peel layers from the bulk crystal, leveraging the weak van der Waals forces in the material to produce flakes with few nanometers in thickness.

One of the salient advantages of mechanical exfoliation is the preservation of the material's intrinsic properties, a contrast to other fabrication methods that may introduce defects or impurities. This attribute is particularly crucial for 2D InSe, whose electronic and optical properties are highly susceptible to structural imperfections.

In the fabrication of our sample, we employ a mechanical exfoliation process before anodic bonding (a technique that will be elaborated upon subsequently). This sequential methodology is integral for enhancing the effectiveness of the electric field on the sample,

thereby facilitating the formation of larger-sized, two-dimensional materials that exhibit robust adhesion to the glass substrate.

The initial stage of this process is executed using adhesive tape, applied in a series of seven to eight iterative peeling actions to the bulk Si-1%-doped InSe (provided in our lab). As shown in Figure **??**, such systematic application is pivotal for the gradual reduction of the bulk material into progressively thinner layers. Following this, a specific InSe flake is selected with tweezers. The selection is based on stringent criteria, including a flat morphology and minimal thickness, defined by lateral dimensions of approximately 1 millimeter by 1 millimeter and a thickness that is semi-transparent and observable to the naked eye. The chosen sample is then considered as a thin precursor layer apt for the ensuing anodic bonding process. The combined approach of mechanical exfoliation and anodic bonding in our sample preparation is a strategic choice, aimed at optimizing the interaction between the two-dimensional materials and the glass substrate for enhanced performance and application potential.

Figure 2.1 – The stages of mechanical exfoliation as seen through various flake sizes obtained.

2.1.2 Anodic bonding method

Anodic bonding has been a much-employed technique in the silicon industry [**?**] and is still widely used for bonding glass substrates to several 2D semiconductors, metals and superconductors... [**?**] [**?**] [**?**] [**?**], such as GaS, GaSe, InSe [**?**], MoS_2 [**?**], WTe_2 etc [**?**] [**?**], and also plays a pivotal role in microfabrication and microelectromechanical systems (MEMS) production [**?**]. This method, operating at elevated temperatures with an electric field, forges a strong, hermetic bond without necessitating intermediate layers like adhesives. Its relevance is particularly pronounced in applications where high bond strength and stability are imperative.

As shown in Figure **??**, the principle underlying anodic bonding involves the migration of Na^+ ions activated by thermal energy at high temperatures, typically between 180°C and 450°C. When a negative voltage, usually ranging from a few hundred to a thousand volts, is applied to the substrate's back side, Na^+ ions migrate towards it, accumulating at the cathode. This migration leaves behind static oxygen ions, creating a negative

space charge at the glass surface and a corresponding positive charge in the wafer. This phenomenon results in a high electrostatic field at the interface, crucial for bonding thin layer materials to glass.

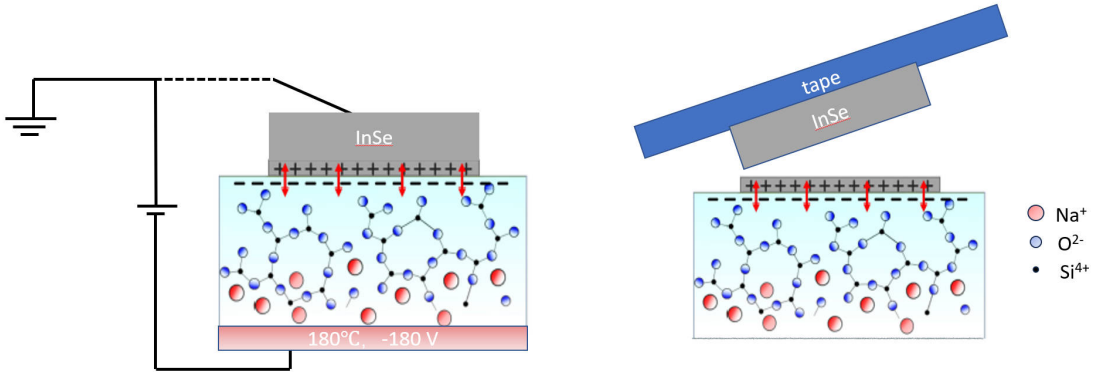

Figure 2.2 – The principle of anodic bonding. Left : Na+ ions migration away from the glass/InSe interface creating a strong electrostatic bond. Right : after bonding, excess layers are removed with adhesive tape.

In this thesis, anodic bonding is employed to fabricate high-quality, large-size InSe layers on borosilicate glass substrates. The process begins with preparing the substrates, which involves cutting them into small squares (approximately 8 mm x 8 mm), followed by cleaning in an ultrasound bath with acetone then ethanol (10 min for both). After drying with nitrogen gas, the substrates are heated on a hot plate at 150 °C. A thin precursor layer, mechanically exfoliated from bulk Si-1%-doped InSe, is then placed atop the glass. The assembly is positioned in an anodic bonding device (as shown in Figure **??**), with the glass heated to 180°C to facilitate Na^+ ion mobility. A negative voltage of -180V is applied, prompting Na^+ ions to drift towards the substrate's back, creating a negative space charge at the glass/InSe interface. This charge induces a positive charge in the InSe sample, leading to an electrostatic field that bonds the InSe to the glass substrate over a 10-minute duration. After bonding, the assembly is cooled to room temperature, and the upper layers of the precursor material are removed by adhesive tape, leaving behind few-layer InSe samples on the glass.

Optical images demonstrate the successful preparation of InSe layers exceeding 100 μm×100 μm in size (as shown in Figure **??**), with a remarkably clean and high-quality surface, as substantiated by Raman shift analyses. The quality of the fabricated samples has been further verified using optical microscopy, atomic force microscopy, and PL spectroscopy, highlighting the efficacy of the anodic bonding method in producing samples free from chemical alterations and suitable for advanced electronic and optoelectronic applications.

2.2 Characterization technique for 2D materials

2.2.1 Optical microscope

After fabricating samples using the anodic bonding method, we employ the optical microscope technique, specifically utilizing the Leica DM2500, as shown in Figure **??**, to

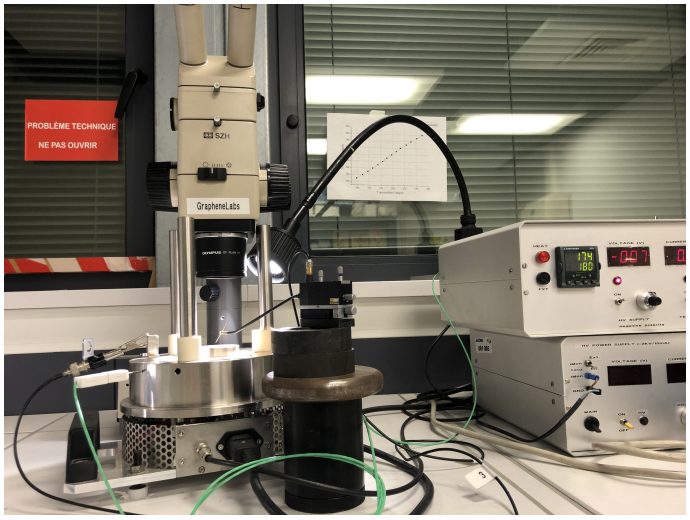

Figure 2.3 – Anodic bonding machine.

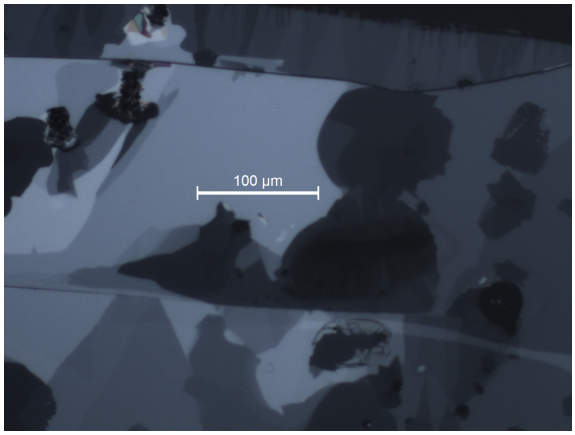

Figure 2.4 – An example of InSe sample gained by anodic bonding method

preliminarily examine their physical properties. This particular microscope is equipped with a range of objectives (5x, 10x, 20x, 50x, 100x) and a charge-coupled device (CCD) camera, enhancing our ability to conduct a detailed inspection and analysis of various material aspects. A key advantage of this technique lies in its capacity to closely observe vital attributes such as size, flatness, and overall uniformity of the materials. These characteristics are crucial in evaluating the quality and appropriateness of materials for specific applications. Furthermore, the differences in optical contrast are instrumental in preliminarily determining material thickness (as shown in Figure **??**).

The Leica DM2500 microscope offers a comprehensive view of the sample, facilitated by the diversity of its objectives. This step is crucial for assessing the quality and reliability of the InSe samples produced via anodic bonding. The findings from this microscopic evaluation will determine the suitability of these samples for subsequent device fabrication.

2.2.2 Atomic force microscopy (AFM)

AFM is a pivotal advancement in the realm of scanning probe microscopies, emerged from the collaborative ingenuity of Binnig, Quate, and Gerber in 1986. This innovative technology heralded a significant leap in surface characterization, allowing researchers

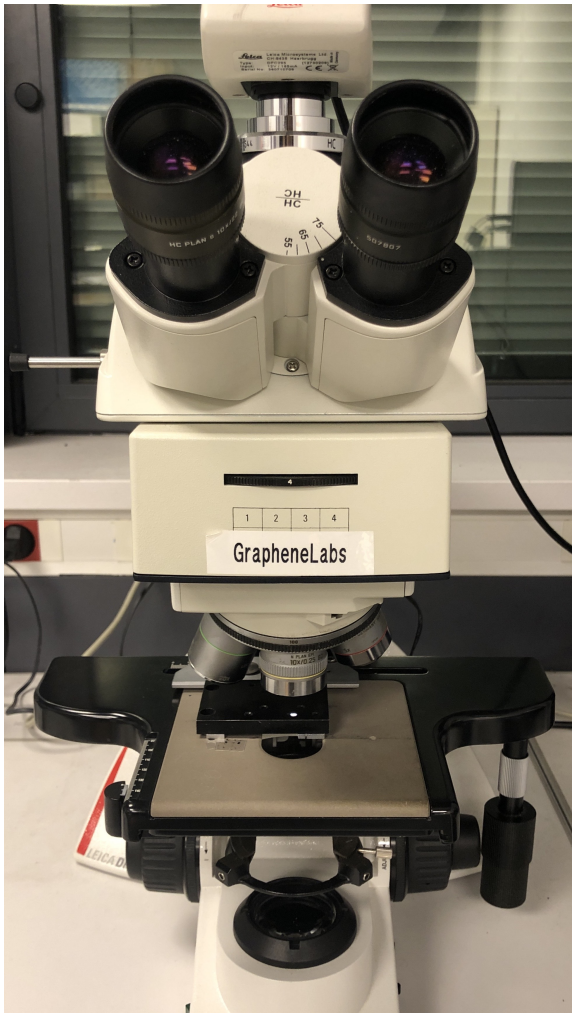

Figure 2.5 – Optical microscope Leica DM2500.

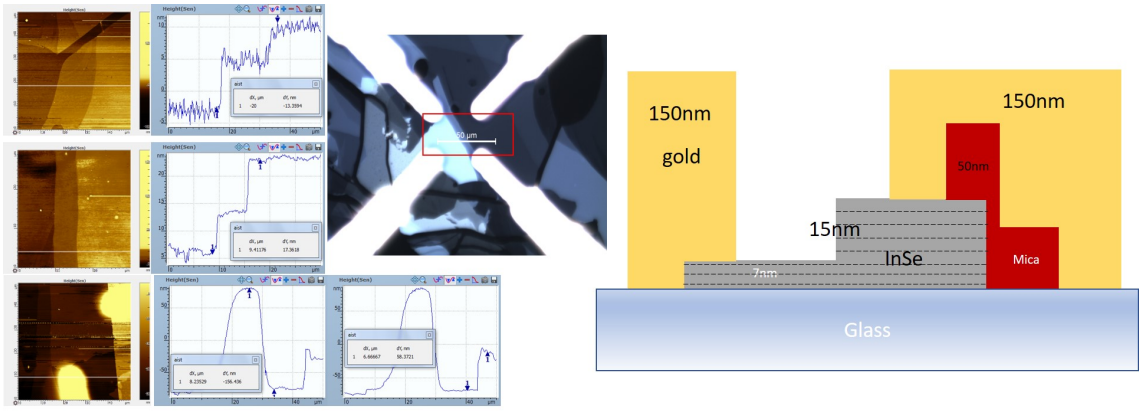

Figure 2.6 – Different thickness of a sample under optical microscope and later tested by AFM, which shows that optical contrast can give indication of thickness (as shown on right).

to visualize surfaces at atomic resolutions [**?**]. Central to the functionality of AFM is its ability to discern surface topography through the detection of forces between a finely pointed probe and the sample surface. This interaction is monitored via the deflection of a cantilever, which is subsequently translated into an electrical signal through a sophisticated laser and photodiode system. This transduction process culminates in a three-dimensional representation of the sample's surface, offering insight into material properties at the nanoscale. This is schematized in Figure **??**.

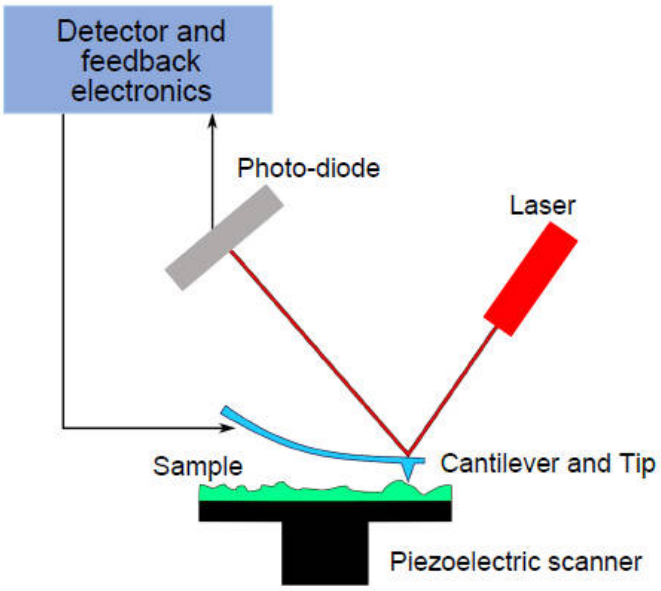

Figure 2.7 – Operating principle of an Atomic Force Microscope. The interaction of the tip with the surface deflects the cantilever, which is detected through the reflection of a laser beam onto a photo-diode. Electronics measure the deflection and control the piezo-scanner with a feedback loop.

The operational versatility of AFM is reflected in its diverse range of modes, each tailored to specific sample characteristics and research objectives:

Contact Mode: In this primary mode of AFM operation, the cantilever, under a consistent force, traverses the sample surface. The interaction between the tip and the sample surface leads to cantilever deflection, proportional to the force exerted during imaging. This deflection alters the position of a laser spot on a position-sensitive photodetector, indicative of surface topographical variations. A feedback loop is employed to adjust the Z scanner, ensuring constant cantilever deflection and thus maintaining a stable imaging force. The Z scanner's displacement is meticulously recorded, enabling the generation of a precise topographical map.

Non-Contact Mode: Characterized by the absence of direct physical contact between the tip and the sample, this mode minimizes potential sample damage. As the tip nears the sample, an attractive force is exerted prior to actual contact. This force is harnessed in non-contact mode to ascertain sample topography. The cantilever, oscillating near its natural resonance frequency, undergoes shifts in frequency and amplitude in response to variations in the tip-sample distance. These shifts, maintained constant through a feedback mechanism, facilitate the acquisition of high-resolution topographic images without jeopardizing the integrity of the tip or the sample.

Tapping Mode: Diverging from the raster scanning approach of the contact and non-contact modes, tapping mode operates through a vertical movement of the AFM probe. This mode is particularly adept at collecting detailed topographical and nanomechanical data. By methodically contacting, applying force, and retracting from specific points on the sample surface, it generates force-distance curves at each point. These curves are insightful, revealing properties such as adhesion, Young's Modulus, and stiffness. The vertical measurement technique of tapping mode is especially advantageous for analyzing sensitive samples and allows for the concurrent assessment of mechanical and electrical properties. Furthermore, The tapping mode in AFM excels in analyzing narrow trenches, overcoming the limitations of contact and non-contact modes in accessing and profiling trench depths with enhanced precision.

Several advanced AFM techniques enhance the understanding of a sample's physical properties, as outlined by Quate (1994) [**?**]. Conductive AFM allows for the electrical analysis of samples by measuring the current between a conductive tip and a biased sample, offering insights into conductivity variations and specific electrical characteristics through I-V spectroscopy. Electrochemical AFM (EC-AFM) integrates AFM with a potentiostat to monitor redox reactions at the sample's surface, providing detailed observations of electrode surface morphology and electrochemical processes through cyclic voltammetry. Scanning Spreading Resistance Microscopy (SSRM) is suited for semiconductor analysis, using a conductive cantilever to assess electrical properties and surface topography under vacuum conditions. Photo-induced Force Microscopy (PiFM) merges infrared spectroscopy with AFM to conduct nanoscale chemical analysis, detecting changes in vibration amplitude of a metal-coated tip induced by molecular dipoles excited by IR light, thus enabling detailed chemical composition analysis.

In this thesis, considering the fragility of 2D layers, non-contact or AC-mode is employed to preserve surface integrity of all samples. The topography map of an InSe device is presented in Figure **??**.

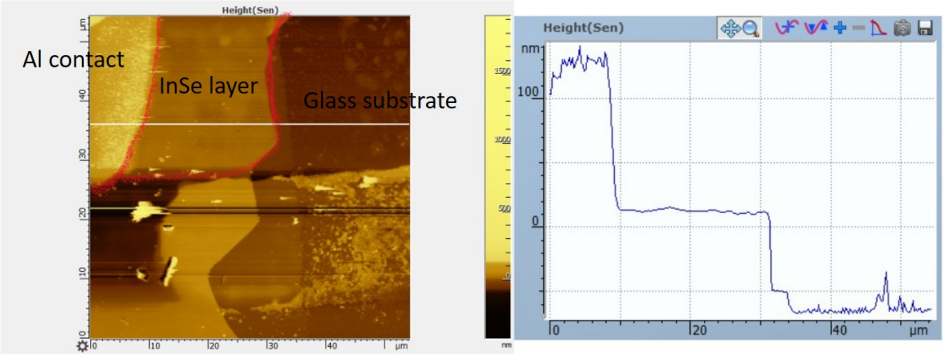

Figure 2.8 – Left: AFM topography map of an InSe device with an evaporated Al contact. The InSe layer border is highlighted in red. Right: height profile along the horizontal white line in left pannel, showing the thickness of InSe layer of about 70 nm, and the Al contact of about 100 nm

2.2.3 Raman microscopy and Photo-luminescence (PL) microscopy

Raman spectroscopy and Photoluminescence (PL) spectroscopy are analytical techniques in materials science, fundamentally based on the interactions of light with matter. These methods provide critical insights into the molecular and electronic structures of various materials. The Raman effect, elucidated by Dr. C.V. Raman in 1928, reveals how light undergoes energy and wavelength shifts due to interactions with molecular vibrations when passing through a transparent medium. This discovery, for which Raman received the Nobel Prize in Physics in 1930, underpins Raman microscopy [**?**] [**?**]. This manifestation of atomic or molecular vibrations, is discernible in the Raman shift, defined by the equation

$$\Delta\lambda = \lambda_{\text{scattered}} - \lambda_{\text{incident}}, \tag{2.1}$$

where $\lambda_{\text{scattered}}$ and $\lambda_{\text{incident}}$ are the wavelengths of the scattered and incident light, respectively.

In Raman spectroscopy, a laser beam (typically 532 nm or 638 nm) illuminates the sample, and the scattered light, after being analysed through a spectrometer, provides insights into molecular structures and excitations, such as phonons. This technique is particularly adept at identifying vibrational, rotational, and other low-frequency modes in a system. The Raman scattered light, identified by its Stokes (energy loss) and Anti-Stokes (energy gain) lines, is differentiated from the more intense Rayleigh scattered light through sophisticated filtering, often utilizing a charge-coupled device (CCD) detector for high sensitivity (see Figure**??**).

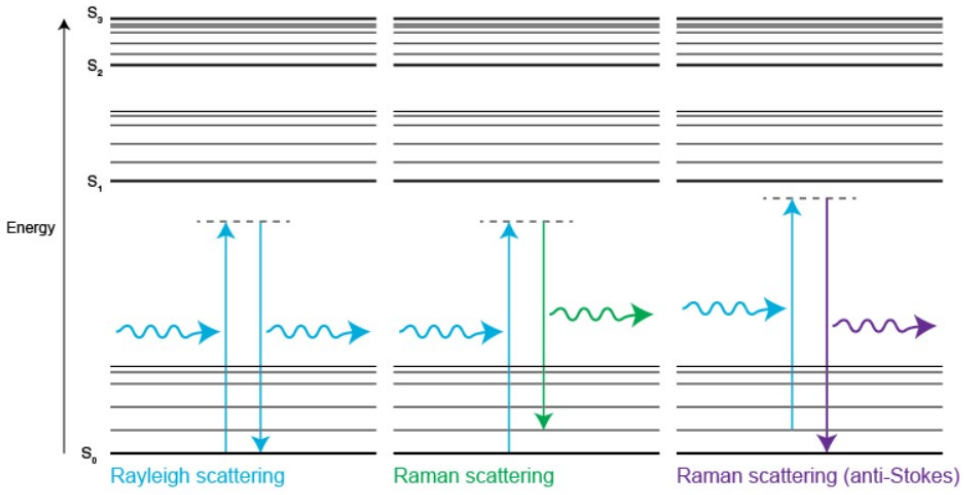

Figure 2.9 – Schematic representation of Rayleigh scattering, Stokes and anti-Stokes Raman scattering from vibrational states. The dashed horizontal lines represent a virtual excited state (copy from https://www.renishaw.com/en/raman-spectroscopy–6150).

For 2D materials or other microscopic to nanoscopic samples, the Raman spectrometer is often coupled to a microscope allowing more efficient light concentration and collection through the miscroscope objective (see Figure**??**). The size of the laser spot (typically 1 micrometer) also allows to take Raman spectra of different parts of the same sample, or even mapping.

As shown in Figure **??**, in PL spectroscopy, photon absorption by a material leads to an excited electronic state, followed by the emission of light as the material reverts to

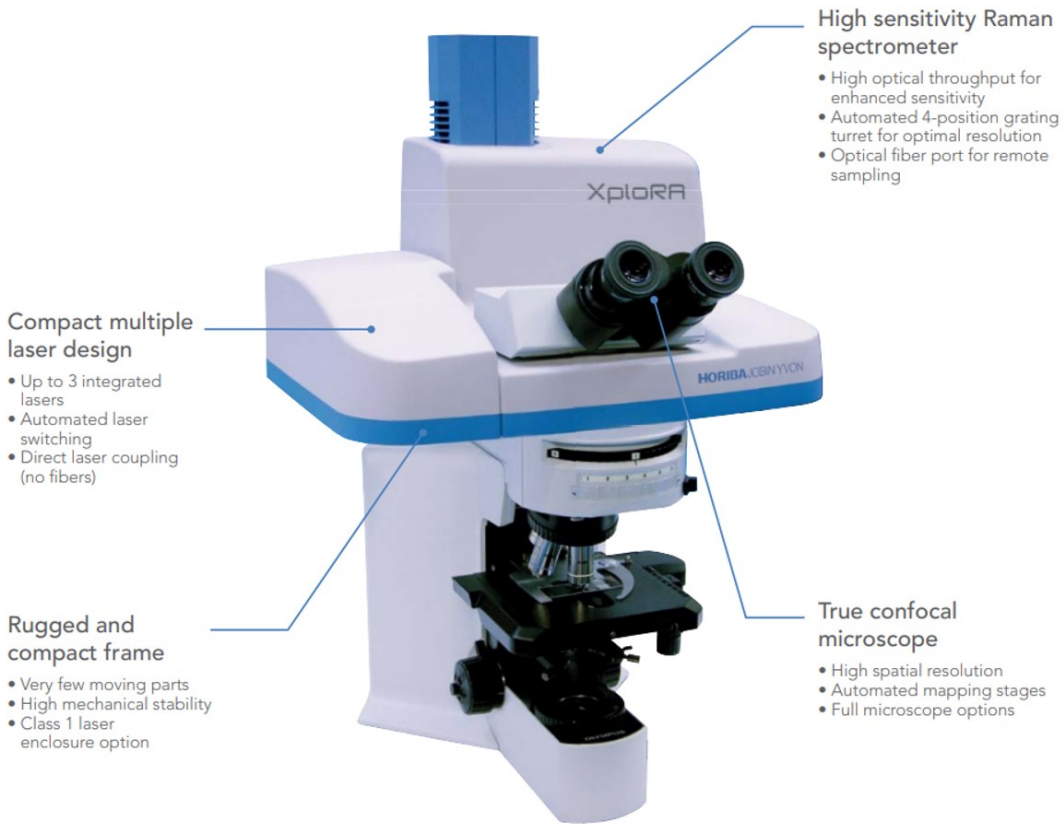

Figure 2.10 – The system of Raman Microscope Xplora from Horiba.

its ground state. This emitted light, encompassing fluorescence and phosphorescence, is rich in information about the material's electronic properties, such as band structure and defects.

2.3 InSe characterization

Raman of InSe

Indium Selenide (InSe) is known to crystallize in various polytypes. Among these, the hexagonal and rhombohedral polytypes are notable. The hexagonal polytypes include β-InSe and ε-InSe, while the γ-InSe represents the rhombohedral polytype [**?**] [**?**]. These polytypes are distinguished by differences in their stacking sequences and c-lattice parameters, although the differences in these parameters can be quite subtle. Each polytype exhibits unique structural and potentially electronic properties due to the variations in atomic arrangement and stacking sequences [**?**].

The table **??** presents information on different polytypes of InSe along with their crystal systems, symmetry class, Schoenflies notations and cell parameters.

The Raman spectroscopic properties of InSe are significantly influenced by both polytype and layer thickness. Different polytypes of InSe exhibit unique Raman shifts, with specific peaks being characteristic of certain polytypes. For example, the ε polytype and γ polytype, typically found in few-layer InSe, displays a distinctive peak around 200 cm^{-1}.

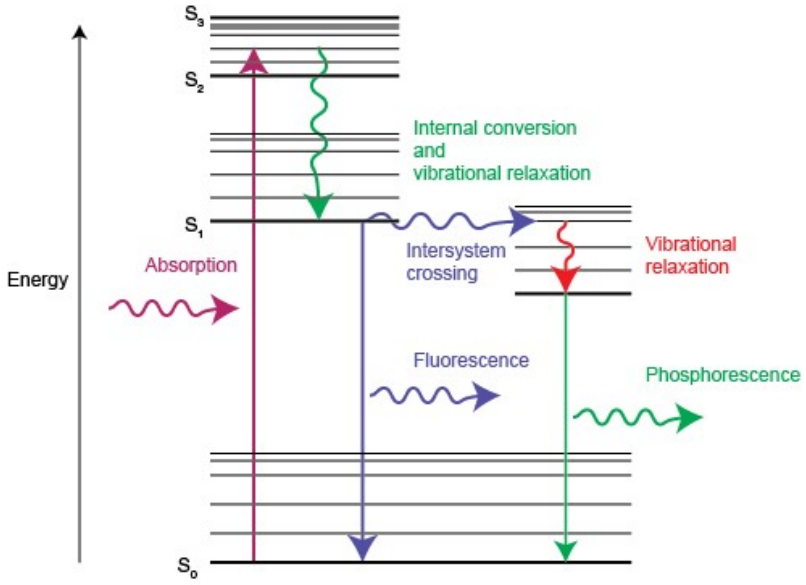

Figure 2.11 – Fundamental principle of Photoluminescence, photoluminescence includes the processes of fluorescence and phosphorescence. copy from https://www.renishaw.fr/fr/spectroscopie-par-photoluminescence-et-fluorescence-expliquees–25809.

Polytype	**Crystal System**	**Symmetry Class**	**Schoenflies Notation**	**Cell Parameters**
γ-InSe	Rhombohedral	Non-Central Symmetry	C_{3v}^5	$a = b = c$, $\alpha = \beta = \gamma \neq 90°$
β-InSe	Hexagonal	Central Symmetry	D_{6h}^4	$a = b \neq c$, $\alpha = \beta = 90°$, $\gamma = 120°$
ϵ-InSe	Hexagonal	Non-Central Symmetry	D_{3h}^1	$a = b \neq c$, $\alpha = \beta = 90°$, $\gamma = 120°$

Table 2.1 – Different polytypes of InSe

In the comparative analysis of Raman spectra for 10 nm and bulk InSe sample gained by anodic bonding method, as shown in Figure **??**, the sharp and intense A_{1g} peak in both samples are indicative of the material's good crystalline quality after the anodic bonding method. The positions of the A_{1g} and E_{2g}^1 peaks are characteristic of the β phase polytype, evidenced by the absence of the $A_1(\Gamma_1^1)$ peak at 196 cm^{-1}.

The literature indicates that the thickness of InSe layers significantly influences the Raman spectrum, with a blue shift in peak frequency observed as layer thickness increases [**?**], likely due to enhanced inter-layer interactions. However, for the Raman spectrum of bulk InSe depicted in figure **??**, no significant blue shift is observed when compared to the 10nm– InSe. Specifically, in the case of the 10 nm InSe layer, the Raman spectrum exhibits broader peaks and altered intensity distribution relative to the bulk sample. These changes can be attributed to the reduced thickness, which potentially enhances surface effects or strain influences on the material.

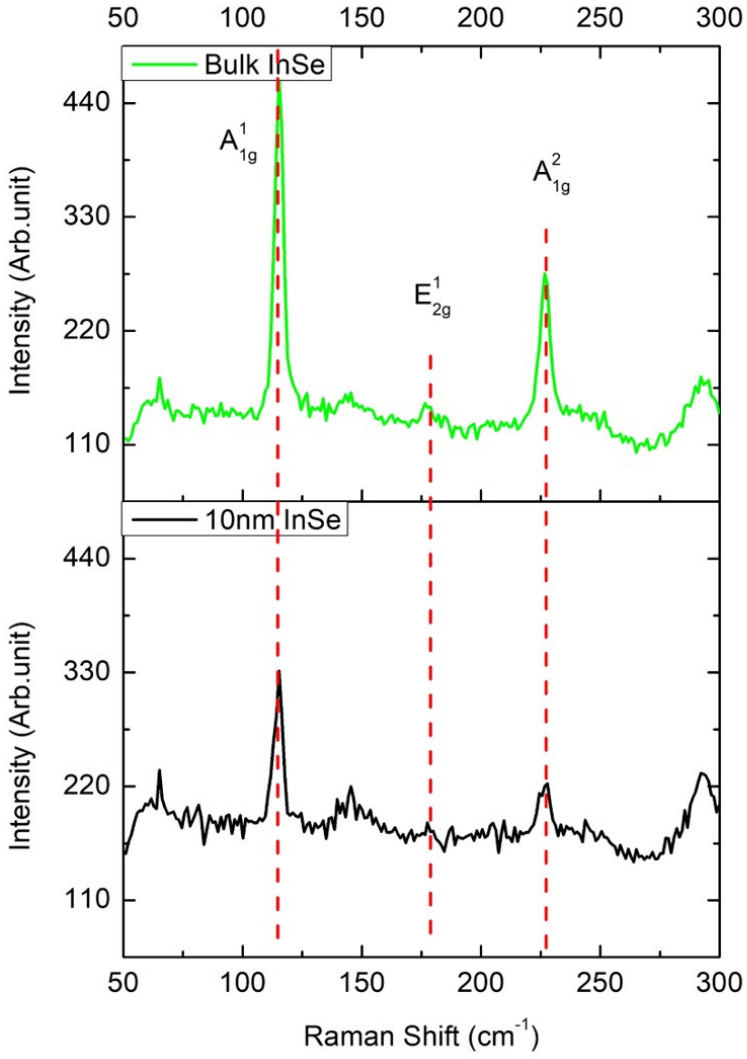

Figure 2.12 – Raman spectra for 10 nm and bulk InSe sample.

Photoluminescence of InSe

In the presented photoluminescence (PL) spectra **??**, the change in intensity can come from the change in thickness of the sample. the shift of energy could come from change in bandgap but also from strain etc. which are higher in thinner samples [**?**]. A discernible blue shift in the PL peak accompanies a rapid decrease in intensity as the InSe layer diminishes in thickness. This variation is concurrent with a band gap shift from 1.26 eV to 1.29 eV. InSe samples exceeding 8 nm in thickness are expected to exhibit pronounced PL emission, attributable to their direct band gap characteristics.

Furthermore, a phenomenon of PL quenching (as shown in Figure **??**) was observed across all InSe samples post-anodic bonding, irrespective of the thickness acquired via this method. This effect is likely a consequence of the samples being heated in open air at 180°C. Contrarily, when samples were heated in a vacuum environment, no PL quenching was observed, underscoring the influence of atmospheric conditions on the process.

Heating InSe in an open-air environment destroys photoluminescence as explained in

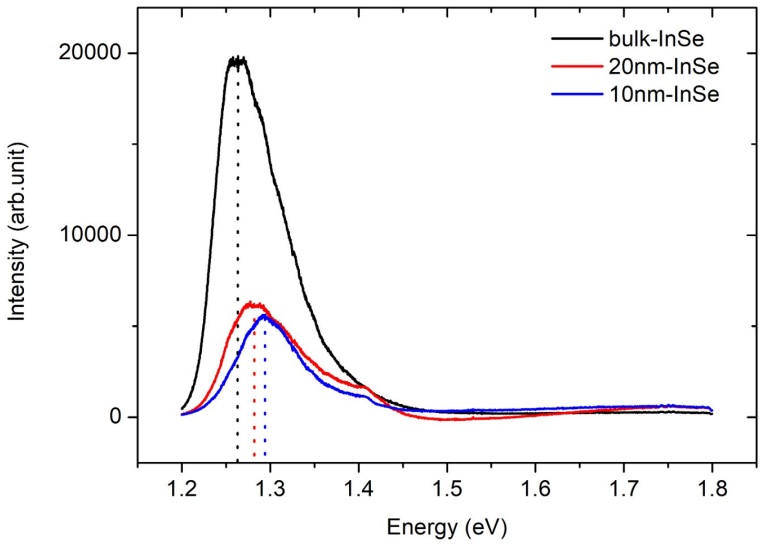

Figure 2.13 – PL spectra of InSe samples with different thicknesses.

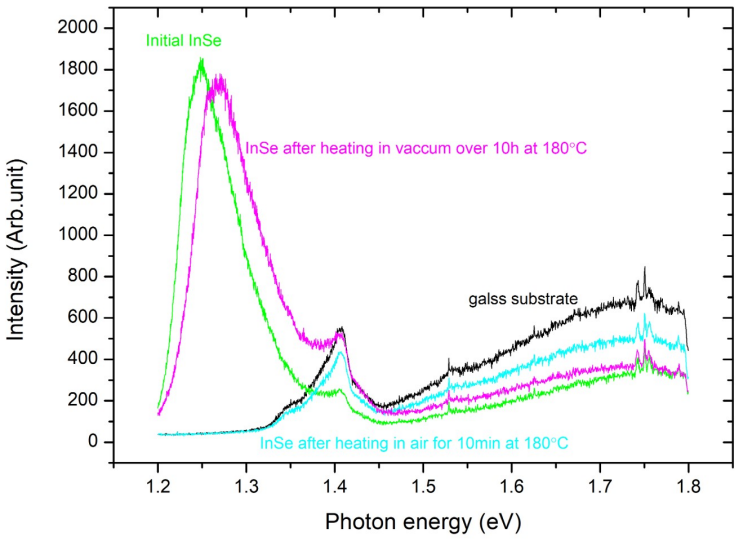

Figure 2.14 – Pl quenching of intrinsic InSe and post-anodic bonding: heat the sample in vacuum doesn't cause Pl quenching, but heat the sample in air does.

the article [**?**], indicative of structural and chemical modifications within the material. The initial decrease in PL intensity primarily stems from the adsorption of oxygen molecules onto the InSe surface, which act as p-type doping agents, thereby altering the PL characteristics of InSe.

As the temperature escalates, InSe undergoes a pivotal chemical transformation. During this stage, oxygen atoms commence intercalating into the InSe lattice, disrupting its intrinsic structure. This intercalation results in the formation of Indium Selenide Oxide

($InSe_{1-x}O_x$) bonds, diminishing the intensity of the original PL peak. Concurrently, a new peak should emerge around 640 nm, attributable to the $InSe_{1-x}O_x$) bonds, signifying the progression of oxidation [**?**]. With further temperature elevation, the oxidation process intensifies. The original PL peak continues its decline, eventually leading to complete quenching. Additionally, the heating process may introduce defects within the InSe layers, which can function as non-radiative recombination centers. In these centers, energy, typically emitted as light in PL, is either dissipated as heat or trapped in defect states, thus result in PL quenching.

2.4 Clean room techniques

To integrate InSe into electronic devices, connecting the material to external apparatus is essential. However, directly attaching copper wire to a 10 nm thick sample is impractical. Instead, it is necessary to define multiple paths for metal deposition on both the sample and the substrate, which then facilitate connections to external circuitry. There are several methods to create the required metal path geometries: lithography and stencil masks.

2.4.1 Lithography

we can use lithography to make precise nanometer scale contacts on a sample but it involves a lot of chemicals, certain semiconductor materials, like InSe, can be sensitive to chemicals used in the lithography process. Photoresists, developers, and etchants might damage or alter the surface properties of the InSe, impacting device performance. The lithographic process, especially if it involves aggressive etching or cleaning steps, could potentially degrade the quality of the InSe surface, which is critical for device functionality.

Therefor all lithography processes were avoided in this thesis. Another technique, free of surface contamination, was used instead: the deposition of metal through a steel stencil mask.

2.4.2 Metal deposition through Stencil Mask

In this thesis, the device fabrication process employs a metal deposition technique on an InSe sample, designed for electronic transport measurements. The method avoids lithography to prevent potential surface contamination that might impair the sample's electrical properties.

The initial step involves using Poly(methyl methacrylate) (PMMA) to affix a custom steel stencil mask onto the 2D InSe sample (Figure**??**). This mask, crucial for creating the desired electronic device geometry, demands precise spatial arrangement of the contacts. The mask's design, featuring strips approximately 10 μm wide near the sample and broadening outward, facilitates wire-bonding.

The steps are as follows:

1. Place the sample (consisting of InSe on a glass substrate) under the microscope. On the computer screen, delineate the anticipated contacts' location on the sample.
2. Secure the stencil mask to the three-axis translation stage, capable of movement in the XYZ directions.
3. Utilizing the microscope, adjust the position of the stencil mask by manipulating the three-axis translation stage to align the mask with the marked contact points.
4. Apply four drops of PMMA to each corner of the glass substrate.

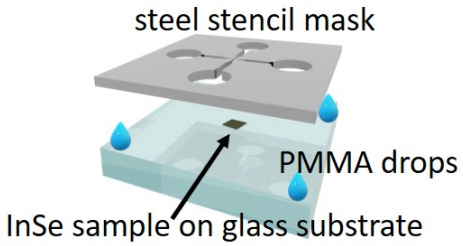

Figure 2.15 – affix a steel stencil mask onto the 2D InSe sample.

5. Elevate the sample stage to bring the glass substrate into contact with the stencil mask.

6. Wait for more than 5 minutes to let the PMMA dry completely.

The metal deposition phase is executed using a Vinci thermal evaporator, which begins the deposition process when the vacuum level of the evaporator reach 10^{-6} mbar. The selected metals for forming contacts with InSe are aluminum (Al), gold (Au), and silver (Ag). Each of these metals will form different types of contacts with InSe, contributing to the diversity of electrical characteristics attainable in the device, which will see in Chapter 3 and Chapter 4.

In the deposition process, the metal is placed in a tungsten crucible within the evaporator and heated to evaporation temperature. The samples, with masks defining contact areas, are strategically placed above the crucible to ensure even deposition. The sample placement in the evaporator is crucial: the mask is 150 μm thick and the strips are as thin as 10 μm. That means an angle of only 4° is enough to completely block the deposition.

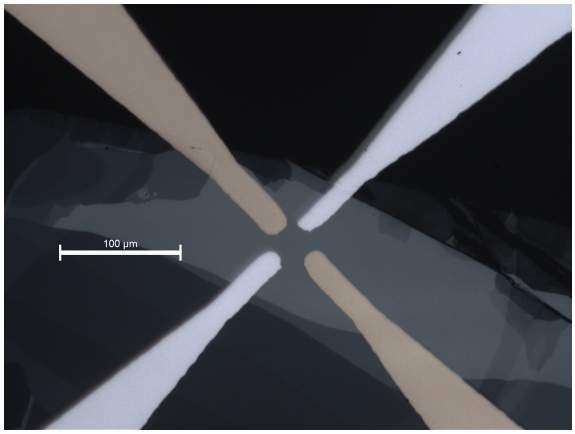

Figure 2.16 – Two pairs of different metal contacts evaporated on an InSe sample in two different metal depositions.

Post-deposition, the samples undergo a precise shaping process using a tungsten needle under an optical microscope. This step ensures conformity to the device geometry layout and eliminates unintended conductive paths.

2.5 Device fabrication

Mica dry transfer

One of the innovative designs in this thesis is the InSe vertical step Schottky diode. This device is distinguished by its unique InSe sample, characterized by a step-like structure. This structure emerges as a natural consequence after the anodic bonding technique, resulting in a configuration where a thick InSe layer naturally combined with a thinner InSe layer. This configuration is not only novel in terms of its physical form but also pivotal in influencing the diode's operational performance.

The construction of this specialized device necessitates meticulous attention, particularly in the placement of two metal contacts, which are integral to the diode's functioning. The placement must adhere to two specific conditions to preserve the device's integrity. Firstly, one contact must exclusively interface with the thin InSe layer. Secondly, the other contact should only interact with the thick InSe. To meet these conditions, a strategic approach is employed involving a thin mica layer. Mica, renowned for its insulating properties, acts as a barrier. It is strategically placed to cover the lateral boundary surface of the thick InSe, where it meets the thin layer, thereby preventing the metal contact from causing a short circuit between these layers - an issue that would impair the diode's functionality. Subsequent to the mica placement, metal deposition is conducted to form the contacts. This procedure ensures that one contact is isolated to the thin layer, while the other is confined to the top of the thick InSe, thus meeting the specific requirements of the InSe vertical step Schottky diode.

To perform the dry transfer method to deposit mica onto an InSe sample, the procedure involved the following steps:

1. The glass slide was thoroughly cleaned using acetone, followed by ultrasonication for 10 minutes. It was then dried using nitrogen gas.
2. A piece of polydimethylsiloxane (PDMS), with dimensions not exceeding 1 cm $\times$ 1 cm, was affixed to the cleaned glass slide. The slide served as a base to ensure the PDMS layer remained flat, which is crucial for the effectiveness of the dry transfer process.
3. The PDMS on the glass slide was heated to approximately 50°C. This heating step is crucial as PDMS becomes less sticky when hot, which facilitates the initial placement and adjustment of the mica piece.
4. A mica piece was mechanically exfoliated using adhesive tape, repeated at least seven times.
5. The tape, containing thin mica sections, was trimmed to dimensions less than 1 cm $\times$ 1 cm.
6. This tape piece, with the exfoliated mica, was placed on top of the PDMS (which was on the glass slide), and allowed to cool down to room temperature. As the PDMS cools, it becomes stickier, thereby securing the mica more effectively for the transfer.
7. After cooling, the tape was peeled off from the PDMS. The PDMS was then examined under a microscope to identify a mica piece of appropriate size and thickness for transfer.
8. Under microscopic guidance, the chosen mica piece was accurately positioned on the InSe sample (the InSe sample was previously bonded to a glass substrate using the anodic bonding method).

9. The PDMS was carefully peeled away from the InSe sample.
10. Precise control of these steps ensured the successful transfer of mica onto the InSe sample, covering the bulk InSe lateral boundary surface.

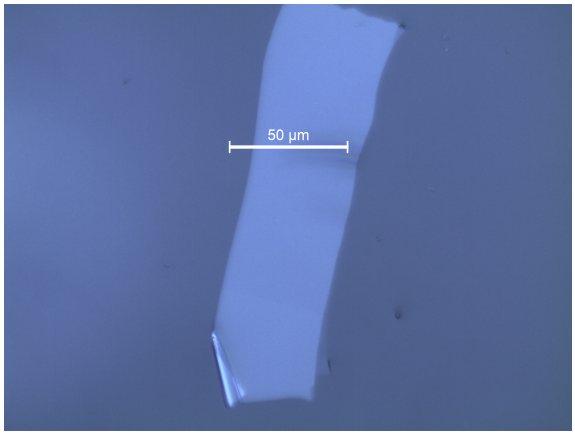

Figure 2.17 – a Mica piece on PDMS under microscope

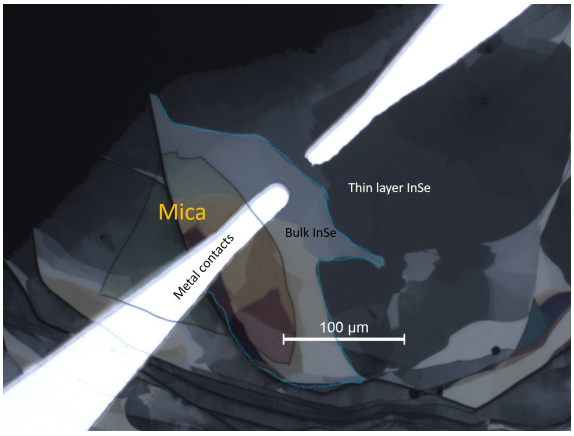

Figure 2.18 – the result of mica dry transfer onto an InSe sample

2.6 Electrical measurements setup

2.6.1 Sample mounting

The Metal-Oxide-Semiconductor Field-Effect Transistor (MOSFET) is traditionally constructed with a silicon-based channel situated between the source and drain regions, formed through chemical doping. The gate, typically composed of metal or polysilicon, is insulated from the channel by a thin silicon dioxide (SiO_2) layer, functioning as the gate insulator. The fundamental operation of a classical MOSFET hinges on modulating the electron flow in the silicon channel via the gate voltage, establishing its role as a crucial component in electronic circuits.

In contrast, the device presented in this thesis exhibits several key deviations from the traditional MOSFET architecture. Primarily, it incorporates a thin-layer InSe for the channel, recognized for its high electron mobility and flexibility. Unlike conventional doping techniques, the source and drain regions in this design are formed through space charge doping in the InSe. This process involves altering the charge distribution within the material using an electric field, allowing for precise control over doping levels and uniformity, consequently enhancing the material quality (Figure**??**).

Diverging from the standard SiO_2 gate insulator, this design utilizes a glass substrate anodically bonded to the InSe channel, ensuring a robust and high-integrity connection. Additionally, the glass substrate back-side is glued with conductive silver paste to an insulated gold electrode acting as the back-gate. Then the assembly is fixed on a sample holder (Figure**??**) and electrical connections are made from the sample holder's pads to the metal contacts of the device and back-gate though wire-bonding, and space charge doping can play a role in modulating the channel conductivity.

Overall, the adoption of an InSe channel, space charge doping for source and drain formation, and a glass substrate for gate insulation distinguish this thesis's device from conventional MOSFETs, representing innovative strides in semiconductor device design.

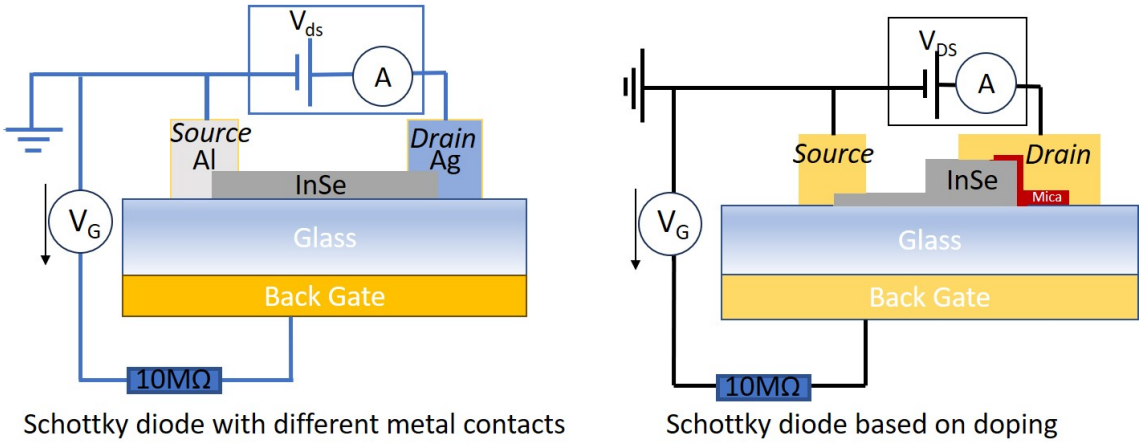

Figure 2.19 – schematic diagram of 2 types of InSe sample

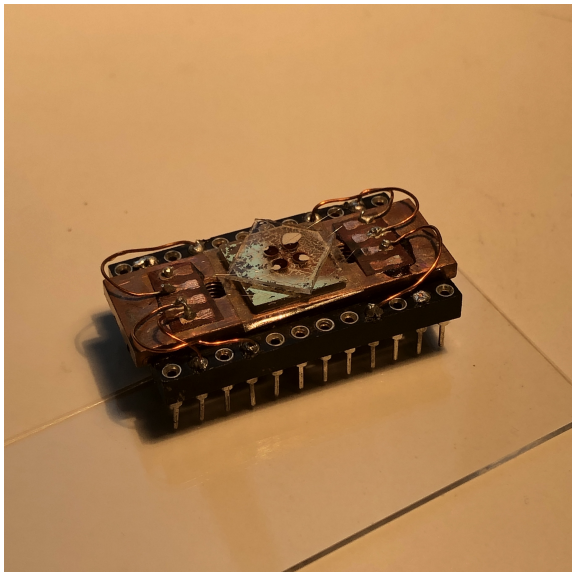

Figure 2.20 – the fabricated device in this thesis

2.6.2 Wire bonding

Wire bonding is a crucial technique in semiconductor device fabrication, employing fine wires to form essential electrical connections between the semiconductor die and its package. This method is fundamental for signal transmission and power supply within the device. Precision, reliability, and adaptability are the keystones of wire bonding, reflecting the dynamic requirements of semiconductor technology.

In this research, the WB-100 wire bonder (as shown in Figure **??**), a versatile machine capable of both wedge and ball bonding, was employed. Its design is characterized by a digital interface with an LCD display, which facilitates a streamlined bonding process. The WB-100's operation hinges on four core parameters: Ultrasonic Generator (USG), Time, Force. Notably, the machine accommodates a broad range of wire diameters, from 17 μm to 50 μm, demonstrating its adaptability. In this study, aluminum (Al) wire is used for all sample devices. Key features of the WB-100 include a motorized Z bond head and wire spool holder, enabling nuanced control over bonding parameters.

The sample preparation for this thesis involved meticulous adjustments of the WB-100 wire bonder's settings to achieve optimal wire bonds. The Ultrasonic Generator (USG) was set at a level of 325, controlling the ultrasonic energy crucial in both ultrasonic and thermosonic bonding. This energy is vital for forming robust, yet non-destructive, bonds between the wire and the substrate. Time was calibrated to 200 milliseconds, determining the bond duration and ensuring optimal adhesion without compromising component integrity. The Force parameter was maintained at 30 grams, balancing sufficient contact with the bonding pad against potential damage to the evaporated metal contacts on the InSe sample. These settings collectively ensured the successful execution of the wire bonding process in the thesis sample devices.

Figure 2.21 – the WB-100 wire bonder

2.6.3 Sheet resistance and van der Pauw measurement

Sheet resistance is one of the most important physical characteristic of 2D materials used in electronic devices. It is defined as the resistance of a square of material, which can be expressed as

$$R_S = \frac{\rho}{t}, \tag{2.2}$$

where ρ is the resistivity and t is the thickness of the material. This definition implies that sheet resistance is independent of the size of the sample but depends on its properties and thickness. The unit of sheet resistance is ohms per square ($\Omega/\square$).

For accurately measuring the sheet resistance of 2D materials like InSe, the van der Pauw method is a well-established technique. This method is particularly suitable for samples that are thin, uniform in thickness, and isotropic [**?**]. The van der Pauw method involves placing four contacts on the perimeter of the sample. In practical scenarios, modifications like the cloverleaf geometry can be employed to optimize contact placement (as shown in Figure **??**), particularly important for materials like InSe where the sample size might be very small or irregular.

To determine the sheet resistance using the van der Pauw method, two key resistance

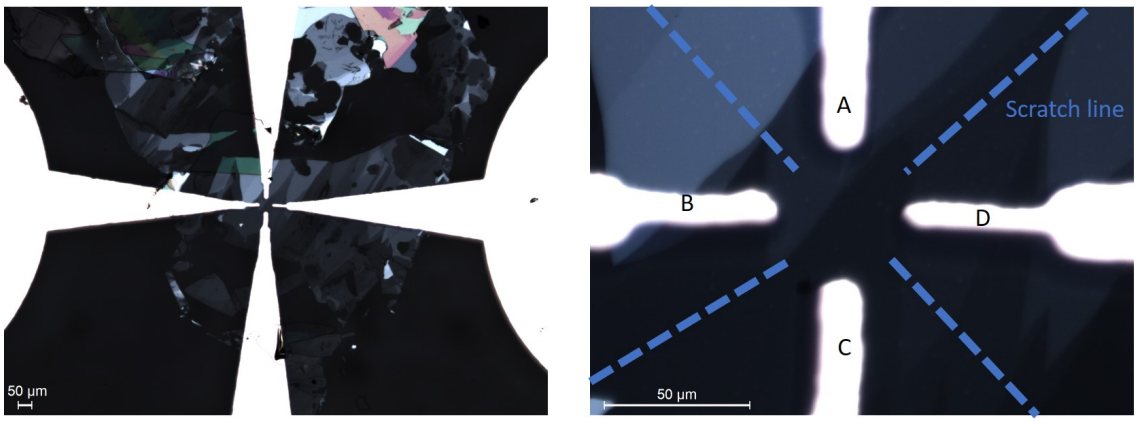

Figure 2.22 – Left: the InSe sample with 4 gold contacts on it and Right: zoom of the sample with the end of the contacts and the cloverleaf cut for van der Pauw measurement.

measurements are made:

$$R_1 = \frac{V_{CD}}{I_{AB}} \tag{2.3}$$

and

$$R_2 = \frac{V_{DA}}{I_{BC}}, \tag{2.4}$$

where V_{CD} and V_{DA} are the voltages measured across different pairs of contacts, and I_{AB} and I_{BC} are the corresponding currents. The sheet resistance R_S is then related to these resistances by the van der Pauw equation:

$$e^{-\frac{\pi R_1}{R_S}} + e^{-\frac{\pi R_2}{R_S}} = 1 \tag{2.5}$$

This equation can be solved numerically to find R_S, however in practice, it is usually reformulated as the following equation:

$$R_S = \frac{R_1 + R_2}{2} \frac{\pi}{\log(2)} f(\frac{R_1}{R_2}) \tag{2.6}$$

where the geometric factor $f(R_1/R_2)$ is introduced to account for the electrical anisotropy of the sample, and has been computed for every possible value, with $f(1) = 1$ for an isotropic sample, and decreasing with anisotropy. Differences between the two measurement directions can appear purely from geometric reason (i.e. the square is not perfectly square, or the cloverleaf is not symmetric), or from intrinsic origin in the material.

As mentionned above, the sheet resistance is an important property of any 2D material and it has been measured extensively in the literature and in previous work from the lab. Therefor these experiments were not repeated in this work.

2.6.4 Electrical measurements apparatus

Electrical measurements of the InSe semiconductor device in this thesis are conducted using the setup depicted in Figure **??**. The device is mounted within a cryostat, which doubles as a vacuum chamber. This design facilitates precise temperature control, essential for annealing the sample or for conducting space charge doping by heating the sample to specific temperatures. The vacuum in the chamber can be maintained at a pressure below 10^{-6} mbar. Temperature regulation, ranging from room temperature to 420 K, is achieved

Figure 2.23 – The InSe device mounted within a cryostat, which doubles as a vacuum chamber

through a resistive heater, ensuring stability and accuracy during the experimentation process.

The apparatus includes two Keithley 2400 source-meters that supply the excitation current to the sample and the gate voltage to the sample/glass substrate's back side, as shown in Figure **??**. These source-meters are instrumental in analysing the output curves, which are crucial for assessing the semiconductor device's performance. These curves illustrate the relationship between the drain-source voltage (Vds) and the drain current (Ids), providing insights into the electrical behavior of InSe.

A significant aspect of this thesis involves the examination of various metal contacts on InSe. This investigation primarily focuses on their distinct characteristics as revealed in the I-V curves. The expected outcomes for different contact types are as follows:

— **Ohmic Contact:** This is characterized by a symmetric I-V curve, indicative of a linear relationship and equal current flow in both the positive and negative voltage directions.

— **Schottky Contact:** This contact type is identified by an asymmetric I-V curve, typically displaying a noticeable threshold voltage. Beyond this threshold, significant current flow is observed in one direction but not the other.

Figure 2.24 – two Keithley 2400 source-meters that supply the excitation current to the sample and the gate voltage to the sample/glass substrate's back side

Another aspect of this thesis is the analysis of the I-V curve of the InSe vertical step Schottky diode device. It provides valuable insights into the diode formation process during the space charge doping method and helps in understanding the device's electrical characteristics, such as its on/off ratio, threshold voltage, and mobility.

2.7 Space charge doping

Space charge doping is an electrostatic doping technique introduced in 2015 for two-dimensional materials [**?**]. This method marks a departure from traditional chemical doping, employing the movement of mobile ionic species, particularly sodium ions (Na^+), in a glass substrate to achieve doping. The technique is renowned for its simplicity, efficiency, and clean approach, as it neither introduces foreign materials into the doped substance nor alters its structural composition.

At the heart of space charge doping is the use of soda-lime glass substrates, which are abundant in mobile Na^+ ions. The process begins at room temperature, where these ions are uniformly distributed within the glass, bound to non-bridging oxygen atoms. The activation of Na^+ ion mobility is achieved by elevating the temperature to between 350 K and 400 K. This heating transforms the soda-lime glass into a negatively charged matrix of SiO_2, teeming with positively charged Na^+ ions.

The application of a negative gate voltage on the glass substrate's underside causes the Na^+ ions to drift towards the bottom, creating a negatively charged space layer. This layer, in turn, induces a mirror positive charge within the sample, resulting in p-doping, or hole doping. Conversely, applying a positive gate voltage pushes the Na^+ ions towards the sample-glass interface, creating a positively charged layer of Na^+ ions that induces n-doping, or electron doping, in the sample, as shown in Figure **??**.

Space charge doping emerges as an alternative to traditional chemical doping methods to circumvent the issues of disorder and structural changes that can adversely affect material properties. Unlike chemical doping, which introduces dopant atoms directly into the crystal lattice of a material causing potential disturbances, space charge doping relies

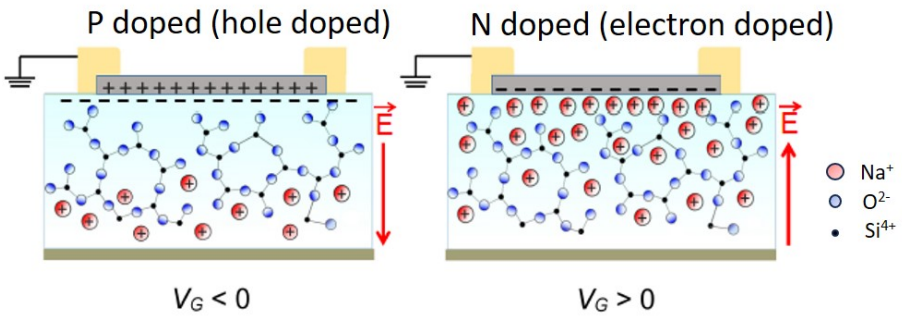

Figure 2.25 – The principle of the space charge doping method.

on applying an external electric field to induce carriers in a material, thereby modulating carrier density without introducing physical dopants. This method has proven effective for high carrier density modulation, up to 10^{15} cm^{-2} [**?**].

Furthermore, the space charge doping process is reversible. Upon cooling the system to room temperature or below, the mobility of the Na^+ ions and the drift current exponentially decrease, effectively "freezing" the Na^+ ions and the doping level within the glass matrix. By annealing the sample it will significantly remove the doping. This feature allows for the repeated use of the same sample without degradation, a notable improvement over irreversible chemical doping methods.

Space charge doping has been used to induce a metal-insulator transition in MoS_2 [**?**], to reveal the superconductor-insulator transition in space charge doped one unit cell $Bi_{2.1}Sr_{1.9}CaCu_2O_{8+x}$ [**?**], and to achieve high-density doping in graphene [**?**]. In this thesis, space charge doping is used to change the Fermi level of different types of InSe, in order to change the contact properties of InSe with several types of metal contacts.

Chapter 3

Planar Symmetric and Asymmetric InSe Devices

This chapter investigates how doping affects the Schottky Barrier Height (SBH) in metal/InSe junctions. The chapter begins by elucidating the formation mechanisms of the Schottky barrier between metals and semiconductors, followed by a review of Schottky devices utilizing 2D materials, with a particular focus on metal/InSe junctions. This section includes a literature survey specific to SBH in metal/InSe configurations.

Subsequent sections detail the experimental setup involving Schottky devices fabricated with InSe and three different metals: gold (Au), aluminum (Al), and silver (Ag). The methodology for calculating the SBH is introduced, including the necessary equations and three fitting models designed to correlate with the current-voltage (I-V) characteristics of the devices developed: the resistance in series model, the back-to-back diodes model, and the 2-way parallel diodes model. Of these, the 2-way parallel diodes model is identified as the most appropriate for the samples studied in this chapter.

The results section presents the analysis of symmetric devices (Au/InSe/Au, Al/InSe/Al, Ag/InSe/Ag) to determine whether the metal/InSe junctions are Schottky or Ohmic types. The chapter also explores asymmetric devices, which include 3 pairs of different asymmetrical metal contacts on InSe (Al/InSe/Ag, Au/InSe/Ag, and Au/InSe/Al). These devices were tested for their I-V characteristics and fitted by 2-way parallel diodes model before and after both N-doping and P-doping.

Finally, the chapter quantifies changes in the Schottky Barrier Height (SBH) resulting from doping. The analysis employs the formula

$$kT \ln\left(\frac{I_{01}}{I_{02}}\right) = \Phi_{b2} - \Phi_{b1}$$

to calculate the variation in SBH after doping. Specific findings include a decrease in SBH by 0.0287 eV in Al/InSe/Ag after N-doping, and an increase by 0.0366 eV after P-doping. Another significant observation is a reduction of 0.073 eV in the SBH in Au/InSe/Ag following N-doping.

3.1 Schottky effect and Schottky devices in 2D materials

3.1.1 Band alignment Model of Metal/Semiconductor junctions

Nearly 150 years ago, experiments reported the presence of rectification at some metal/semiconductor interfaces. These phenomena are explained by the presence of what

would later be called a "Schottky barrier" [?] [?] [?] [?], which plays a critical role in the behavior of these heterostructures. The simplest explanation for the presence of a barrier at metal/semiconductor interfaces comes from the differences in Fermi levels in the metal and the semiconductor (as compared to a theoretical common reference). At the interface, under thermodynamic equilibrium has to be compensated by bending the electronic bands of the semiconductor, leading to the formation of a barrier. This is schematized in Figure ?? and explained in more details in the following. The Figure ?? focusing on the metal in contact with an n-type semiconductor. The principles presented here apply analogously to p-type semiconductors, albeit with modifications for holes and an inverted energy axis.

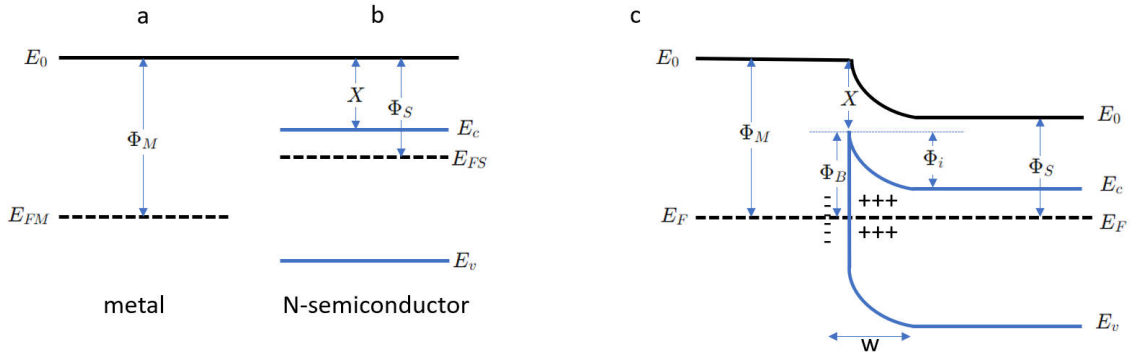

Figure 3.1 – Energy band diagrams illustrating the formation of a Schottky barrier at a metal-semiconductor junction. (a) Shows the work function Φ_M and Fermi energy E_{FM} of the metal. (b) Depicts the work function Φ_S, electron affinity X, and the semiconductor band structure, with a bandgap between E_c and E_v, as well as the Fermi energy E_{FS} for a N- type semiconductor. (c) Presents the idealized equilibrium band diagram for the M/S junction with the charge distribution at the M/S interface is presented, with negative charge gathering at the metal surface and positive charge in the semiconductor consisting of immobile ionized donors spread over a distance W, creating the space charge region. The energy barrier Φ_i hinders electron flow from the semiconductor to the metal, while Φ_B is the Schottky barrier height (SBH) for electron flow in the reverse direction.

Fundamental Concepts and Energies

Fermi Energy: In metals, the Fermi energy (E_F) represents the maximum occupied electron energy state at absolute zero (0 K). In non-degenerate semiconductors, E_F lies in the bandgap, separating occupied and unoccupied states at 0 K. The Fermi-Dirac distribution function, given by

$$f(E) = \frac{1}{1 + e^{(E-E_F)/kT}}$$

describes the probability of electron occupancy in a state at energy E at absolute temperature T, where k is the Boltzmann constant (8.62 x 10^{-5} eV/K).

Vacuum Level and Workfunction: The vacuum level, or free-electron energy (E_0), serves as a reference for energy states, denoting the energy of electrons with zero kinetic energy outside of a material. It is quantified in electron volts (eV). The workfunction (Φ), defined as the difference between E_0 and the Fermi level (E_F), reflects the energy required to move an electron from the Fermi level to the vacuum:

$$\Phi = E_0 - E_F$$

Electron and Hole Densities: The densities of electrons (n) and holes (p) in a semiconductor are governed by the Fermi energy, described by:

$$n = N_c \cdot e^{(E_F - E_C)/kT}$$

$$p = N_v \cdot e^{(E_V - E_F)/kT}$$

Here, N_C and N_V represent the *effective* density of states in the conduction and valence bands, respectively, and are related to the effective masses of electrons and holes [**?**].

Electron Affinity: A fundamental property for characterizing semiconductor materials is the electron affinity (X), representing the energy difference between the vacuum level and the conduction band edge:

$$X = E_0 - E_C$$

Examples include 4.0 eV for Molybdenum Disulphide (MoS_2), 3.6 eV for Gallium Selenide (GaSe), and 4.6 eV for Indium Selenide (InSe).

Charge Transfer and Depletion Layer Formation

When a metal with a workfunction Φ_M contacts a semiconductor with a different workfunction Φ_S, charge transfer ensues until equilibrium is reached, aligning their respective Fermi levels. This transfer results in the formation of a depletion layer at the semiconductor interface, characterized by a lack of free charge carriers. The depletion layer is designated as the space charge region due to its characteristic accumulation of immobile charges. This layer is crucial for establishing a Schottky rectifying junction.

In scenarios where $\Phi_M < \Phi_S$, electron injection from the metal to the semiconductor occurs, leading to an ohmic junction without a depletion layer. Conversely, the contact between a metal and an n-type semiconductor with $\Phi_M > \Phi_S$ results in the formation of a depletion layer, an electric field, and a built-in potential (Φ_i) at the junction, hindering further charge diffusion, as shown in Figure **??**.

Schottky Barrier and Its Significance

The Schottky barrier (Φ_B) emerges as a discontinuity in the allowed energy states at the metal/semiconductor interface, serving as a barrier against electron flow. The Schottky-Mott relation expresses Φ_B in terms of the metal workfunction and semiconductor electron affinity:

$$\Phi_B = \Phi_M - X$$

A similar barrier exists for hole flow in metal/p-type semiconductor junctions:

$$\Phi_B = E_g - |\Phi_M - X|$$

The sum of the Schottky barrier heights (SBH) for electrons and holes is expected to equal the semiconductor's bandgap (E_g). The SBH is a key feature of M/S rectifying junctions, influencing their rectifying characteristics. A larger SBH is usually achieved with elevated workfunction metals on n-type semiconductors or with low workfunction metals on p-type semiconductors. However, experimental data suggests that the Schottky-Mott relations are only qualitatively valid, with SBH often nearly independent of metal workfunction.

3.1.2 The role of interface states and Fermi level pinning

The traditional Schottky-Mott model, an established framework in semiconductor physics, attempts to elucidate the Schottky Barrier Height (SBH) as a function of the metal's work function (Φ_M) and the semiconductor's electron affinity (X). This model, however, has been consistently challenged by experimental findings, particularly when accounting for the role of surface states at metal/semiconductor (M/S) junctions.

J. Bardeen's seminal work in 1947 introduced the concept of surface states, also known as Shockley-Tamm states [**?**]. These states are localized electronic states at the semiconductor's surface, emerging from factors such as incomplete covalent bonds, presence of foreign atoms, and crystal defects. Bardeen's theory proposed that these surface states, with energies within the semiconductor bandgap, can significantly affect the charge distribution at the M/S interface. This insight marked a fundamental shift from the Schottky-Mott model, which assumed a direct relationship between the metal's work function and the SBH, neglecting the dynamic nature of surface states.

As shown in Figure **??**, these surface states are characterized as either acceptor-like or donor-like, impacting the interface's charge distribution based on their occupancy. Acceptor-like states, when occupied by an electron, may become negatively charged, whereas donor-like states can become positively charged when unoccupied. These surface states are related to the charge neutrality level (CNL or Φ_0). The CNL is an energy level where a defect or interface state can capture an electron or hole without creating net charge. The presence and behavior of these states influencing Φ_0, consequently affecting the SBH.

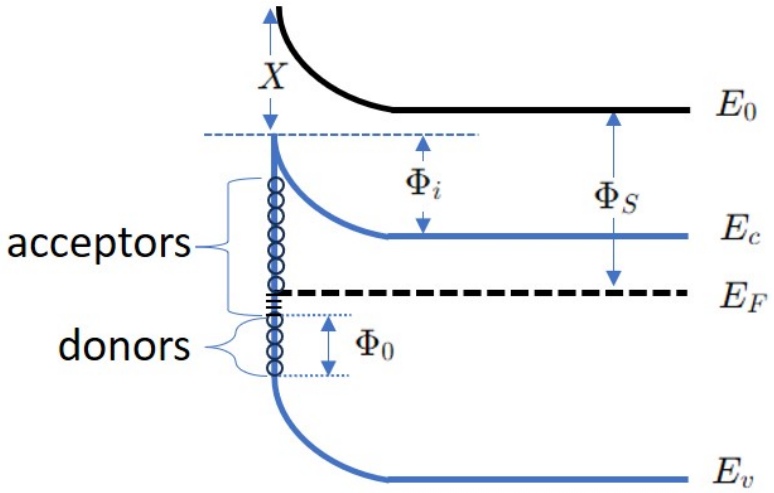

Figure 3.2 – Acceptor-like and donor-like surface states at a semiconductor interface, depicting their effect on charge neutrality level (Φ_0) and Schottky barrier height. Both filled (–) and unfilled (o) surface states are shown.

Moreover, Bardeen emphasized the phenomenon of Fermi level pinning, a process where the surface states can pin the Fermi level at the semiconductor surface. This occurs particularly when there is a high density of surface states near the Fermi level. Even minor variations in the Fermi energy at the semiconductor surface can result in significant charge transfer, underlining the importance of surface states in SBH determination.

In practical scenarios, such as when metal is deposited onto an InSe surface, an additional complexity arises with the formation of an interfacial layer. This layer, often manifesting as a thin oxide layer, is neither entirely metallic nor semiconductor in nature.

It introduces additional interface states and can sustain a voltage drop, thereby altering the junction's properties. The existence of this interfacial layer necessitates considering a physical gap at the interface, essential for the continuity of the vacuum level (E_0) at the interface.

Furthermore, surface states can be categorized as "fast" or "slow" based on their proximity to the bulk semiconductor and their response to voltage bias changes. Fast surface states, in close proximity to the bulk, remain in thermal equilibrium even under rapidly changing voltage conditions. In contrast, slow surface states, being more remote, take longer to reach thermal equilibrium, impacting the junction's response to electrical stimuli.

Given these considerations, it becomes evident that the traditional Schottky-Mott formula is insufficient for accurately determining the SBH in real-world M/S junctions. A more comprehensive approach is required, one that incorporates the intricate interplay of the metal's work function, the semiconductor's electron affinity, the nature of the interfacial layer, and crucially, the density and type of surface states. This holistic approach, as depicted in Figure **??**, is essential for a deeper understanding and accurate prediction of the SBH in these complex junctions.

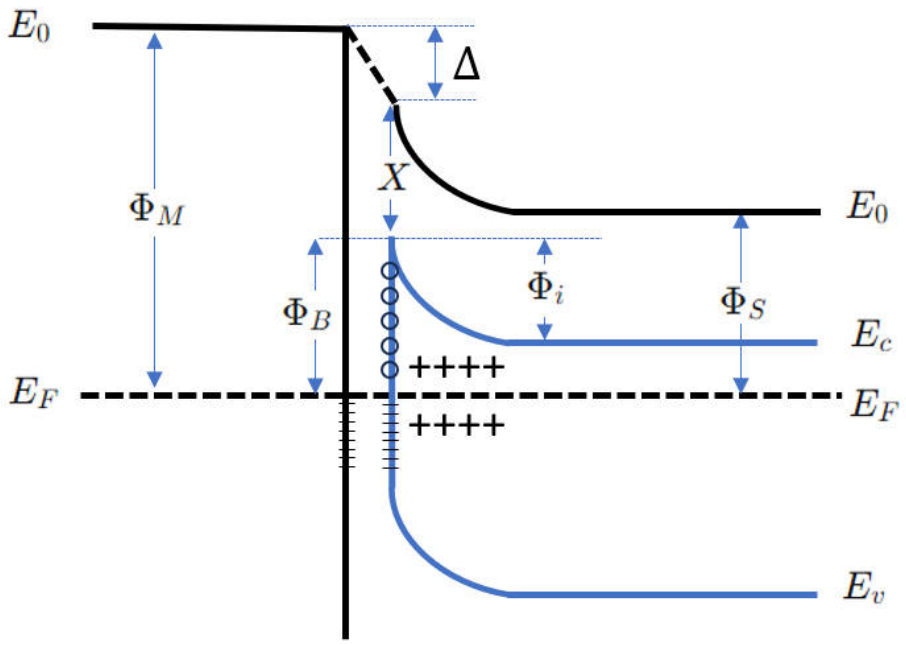

Figure 3.3 – Energy band diagrams of a real metal/semiconductor junction at equilibrium, featuring an electrically transparent thin interfacial layer. This layer ensures the continuity of free electron levels and facilitates electron tunneling, thus sustaining a voltage drop Δ across the junction. The diagram depicts both filled (–) and unfilled (o) acceptor-like surface states, with the Fermi level (E_F) indicating the equilibrium condition. The work function of the metal (Φ_M) and the semiconductor (Φ_S), as well as the electron affinity (X), are also illustrated. Notably, the band bending in the semiconductor and the formation of a Schottky barrier (Φ_B) are key aspects of the junction's electronic properties.

3.1.3 Density of interface states and Schottky barrier height (SBH)

The intricate relationship between the Schottky Barrier Height (SBH), the density of interface states (Dit), and their collective impact on semiconductor properties merits a detailed examination. The formula describing the Schottky Barrier Height at a metal/semiconductor junction is pivotal in this context. It is expressed as

$$\Phi_B = c(\Phi_M - X) + (1 - c)(E_g - \Phi_0), \tag{3.1}$$

where Φ_M is the metal work function, X denotes the electron affinity of the semiconductor, E_g represents the semiconductor bandgap, and Φ_0 is the neutral level in the semiconductor. The constant c, which is influenced by Dit [**?**] [**?**], is a factor that represents the weight of the terms in the SBH and is given by

$$c = \frac{\varepsilon_i}{\varepsilon_i + e^2 \delta Dit}, \tag{3.2}$$

where ε_i is the dielectric constant of the interfacial layer, δ is the thickness of this layer, and e is the elementary charge [**?**].

In scenarios where Dit is exceedingly high, the formula undergoes a simplification. As Dit tends towards infinity, c approaches zero, leading to a simplified Φ_B formula:

$$\Phi_B = E_g - \Phi_0. \tag{3.3}$$

This condition results in the Fermi level at the interface being "pinned" by the surface states at the value Φ_0 above the valence band edge (E_v), rendering the position of the Fermi level fixed relative to the semiconductor's band structure, irrespective of the metal's work function.

Conversely, in situations where Dit is minimal, c tends towards one, reducing the formula to the Schottky-Mott model. This model is mainly dependent on the metal's work function (Φ_M) and the semiconductor's electron affinity (X), and is expressed as

$$\Phi_B = \Phi_M - X. \tag{3.4}$$

This indicates that, with a low Dit, the metal's work function significantly influences Φ_B [**?**].

In summary, the density of interface states (Dit) plays a crucial role in determining the Schottky Barrier Height (Φ_B) at a metal/semiconductor junction. A high Dit results in Fermi level pinning, making Φ_B independent of the metal's work function, whereas a low Dit emphasizes the importance of the metal's work function in determining Φ_B, aligning with the Schottky-Mott model.

3.1.4 Schottky effect and Image charge lowering of the SBH

The Schottky effect is a fundamental phenomenon observed when an electron approaches a metal surface, resulting in a reduction of the material's work function, particularly under strong electric fields as shown in Figure **??**. The work function represents the minimum energy required to extract an electron from the material's surface, and its diminution under a strong electric field enhances electron emission, thereby facilitating efficient electron movement across semiconductor devices like diodes and transistors.

Specifically, in semiconductor physics, the Schottky effect manifests as a reduction in the energy barrier encountered by electrons transitioning from metal to semiconductor. A Schottky diode, characterized by its low forward voltage drop and rapid switching

capabilities, benefits directly from the Schottky effect. The interaction between an electron and its induced positive charge on the metal surface, or the "image charge," along with the influence of external electric fields, modifies the potential energy landscape, effectively lowering the SBH at the metal-semiconductor (M/S) junction.

The potential energy alteration due to the electron-image charge interaction is quantified as

$$-e^2/(16\pi\epsilon_0 x^2), \tag{3.5}$$

where ϵ_0 is the free-space dielectric constant and x is the distance from the metal surface. When considering a semiconductor, the dielectric constant changes to

$$\epsilon_s = \kappa_s \epsilon_0, \tag{3.6}$$

with κ_s being the relative permittivity. The SBH lowering, therefore, becomes

$$\Delta\varphi_B = \sqrt{\frac{e^3|E|_{max}}{4\pi\epsilon_s}}, \tag{3.7}$$

where $|E|_{max}$ represents the maximum electric field at the junction. This field is influenced by an applied voltage V, doping density N, and temperature, as expressed by

$$|E|_{max} = \sqrt{\frac{2eN}{\epsilon_s}(\varphi_i - V - \frac{kT}{e})}, \tag{3.8}$$

linking the SBH lowering directly to the applied voltage, doping density, and temperature. These equations highlight the intricate relationship between the SBH and the maximum electric field, underscoring the ability to fine-tune the SBH through doping. Doping adjusts the semiconductor's electrical properties, offering a method to control the SBH precisely, albeit with less significance in M/S structures than in metal-vacuum systems due to the higher dielectric constant of semiconductors.

3.1.5 Current transport mechanisms in Metal/Semiconductor Schottky junctions

In metal/semiconductor (M/S) Schottky junctions, the primary transport of current is made by majority carriers. In n-type semiconductors, these majority carriers are electrons, in p-type semiconductors, they are holes. This aspect markedly contrasts with the functioning of p-n junctions, where both electrons and holes are crucial for operation. The main transport mechanism in Schottky diodes is Thermionic Emission (TE) [**?**], where thermally excited charge carriers, either electrons in n-type or holes in p-type semiconductors, surmount the potential barrier at the metal-semiconductor interface. This barrier, symbolized as Φ_i, acts as a blockade for the free movement of charge carriers until they acquire sufficient thermal energy to transcend it. This phenomenon underpins the current-voltage (I-V) characteristics observed in Schottky diodes. During forward bias, the potential barrier diminishes, allowing carriers to easily surpass it, resulting in a substantial surge in current. Conversely, in reverse bias, an elevated barrier significantly curtails the current flow.

Additionally, while thermionic emission stands as the predominant conduction mechanism, other processes like thermionic field emission (TFE) and field emission (FE) can also contribute under specific conditions [**?**] [**?**] [**?**]. These alternative mechanisms involve the tunneling of charge carriers through the barrier, rather than their movement over it.

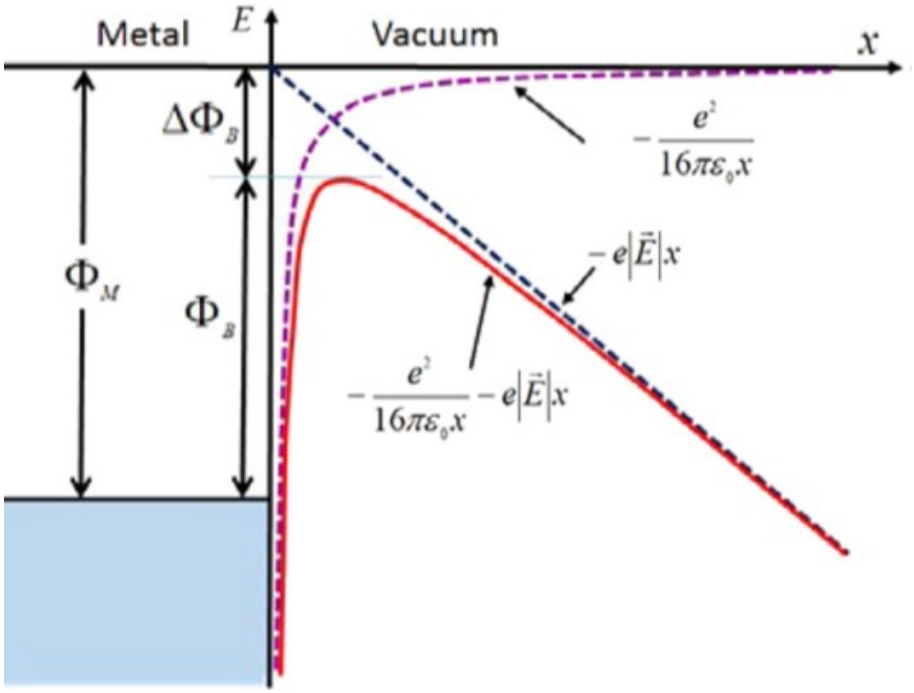

Figure 3.4 – Energy band diagram between a metal surface and vacuum, showing (red continuous line) how the application of an external electric field $\vec{E}$ lowers the effective barrier height by the amount $\Delta\Phi_B$ [**?**].

The dominance of TE, TFE, or FE is contingent upon factors such as the doping level in the semiconductor and the temperature. Typically, at room temperature, TE is the principal mechanism in semiconductors with lower doping levels. In contrast, TFE becomes significant in intermediate doping ranges, and FE predominates at higher doping levels. Furthermore, the current in Schottky diodes is influenced by additional factors including generation/recombination in the space-charge region, electron diffusion in the depletion region, and hole injection from the metal. Additionally, peripheral leakage currents at the metal-contact and currents resulting from interface traps also play a role in determining the overall current behavior in these diodes.

3.1.6 Schottky devices in 2D materials

2D materials employed in Schottky Junction Diodes exhibit unique properties that could be advantageous over traditional p-n junction photodetectors, particularly in terms of reduced junction heating, lower noise levels, and enhanced detectivity.

Graphene-Based Schottky Junctions: due to graphene's exceptional electrical, optical, and mechanical properties, when combined with semiconductors like silicon (Si) [**?**], gallium nitride (GaN) [**?**], gallium arsenide (GaAs) [**?**], zinc oxide (ZnO) [**?**], and tin dioxide (SnO_2) [**?**], graphene forms Schottky junctions that exhibit high on/off ratios, remarkable responsivity, rapid response times, and ultra-low dark current noise. These characteristics make graphene-based photodetectors highly suitable for a broad range of applications, from visible to infrared wavelengths. The synergy between graphene and these semiconductors enhances carrier mobility and light absorption, contributing to the superior performance of the devices.

Transition Metal Dichalcogenide-Based Schottky Junctions: Transition Metal

Dichalcogenides (TMDCs), such as molybdenum disulfide (MoS_2), are another class of 2D materials that have shown great promise in Schottky photodetectors. Devices such as monolayer MoS_2 -based Metal-Semiconductor-Metal (MSM) detectors have demonstrated high photoresponsivity and fast response times [**?**]. Additionally, heterostructures combining graphene and MoS_2 have been reported with high responsivity and detectivity. The exceptional performance of these devices is attributed to the strong light absorption properties of MoS_2, improved photogenerated carrier separation, and rapid charge transportation [**?**] [**?**].

Black Phosphorus-Based Schottky Junction Diodes: Black Phosphorus (BP) has anisotropic crystal structure and tunable bandgap, BP-based Schottky Junction Diodes have exhibited high performance in UV photodetectors, characterized by high specific detectivity and photo-responsivity [**?**] [**?**]. Graphene-BP heterostructure diodes have efficiently operated at NIR wavelengths [**?**]. Additionally, Fabry-Perot cavity enhanced BP/MoS_2 heterojunction diodes have achieved high response speeds in the mid-wave infrared region, demonstrating the versatility of BP in different spectral regions [**?**].

Schottky Junction Diodes with Other 2D Materials: The exploration of Schottky photodetectors has extended to other 2D materials, including various metal chalcogenides like SnS_2, In_2S_3 , InSe, and GaSe. These materials have shown efficient photodetection performance and stability, with some devices demonstrating fast response speeds and high photo-to-dark current ratios [**?**]. Additionally, MXenes, a new class of 2D materials, have attracted attention due to their unique optical and electrical properties [**?**]. For instance, a $Ti_3C_2T_x/GaAs/Ti_3C_2T_x$ detector with Au contacts has exhibited good photodetection properties across a range of visible to NIR wavelengths [**?**]. These developments indicate the vast potential of various 2D materials in enhancing the performance and applicability of Schottky photodetectors.

3.2 Metal-InSe contacts

The interface properties of InSe with various electrode materials have garnered significant attention. This interest stems from the distinct interaction dynamics between InSe and different electrodes, which can influence the electronic and optoelectronic properties of devices.

Di Giulio et al. explored the photovoltaic effect within Au-InSe Schottky barriers, estimating the SBH to be 0.65 eV [**?**]. This determination stemmed from an integrative approach that included analyses of current-voltage (I-V) and capacitance-voltage (C-V) characteristics, alongside the examination of the spectral dependence of the photoemission current.

Chevy and colleagues quantified the microscopic SBH as 0.7 eV [**?**], corroborating findings from I(V) and photovoltage assessments. Their research utilized photoemission spectroscopy to trace the valence band dynamics of InSe as a function of Au deposition thickness. Observations indicated a 0.3 eV valence band elevation at sub-monolayer Au coverage, signifying band bending. The study attributed the emergence of a depletion region and the subsequent rectifying contact to electronic charge redistribution from InSe to Au or to Au-induced gap states. The initial formation of the barrier was hypothesized to result from the primary adatom-substrate interactions rather than the metal's work function or discernible chemical bonds.

Siqi Hu and colleagues proposed an alternative methodology by fabricating a van der Waals (vdW) Schottky junction through the mechanical layering of an Au electrode on a multilayer InSe nanosheet [**?**]. This technique circumvents chemical disorder and defect

states typically present at metal-semiconductor interfaces, thereby mitigating Fermi level pinning, a prevalent challenge in conventional Schottky junctions. The SBH, deduced via the Schottky-Mott rule, was approximated at 0.5 eV. Remarkably, this barrier height remains constant irrespective of the InSe multilayer thickness, provided the semiconductor possesses more than ten layers, as its energy band structure is deemed stable under such conditions.

Qinghua Zhao et al.found the value of the Schottky barrier height of approximately 460 meV for the Au-InSe interface was determined through temperature-dependent electrical measurements of the device kept in the dark [**?**]. This methodology involved studying the current-voltage (I-V) characteristics of the device across a range of temperatures from room temperature (297 K) up to 452 K.

Further theoretical insights into the interface properties of ML InSe are provided in the paper by Bowen Shi [**?**]. Shi and his team found that certain metals, including Ag, Cu, and In, form n-type Ohmic contacts with ML InSe, facilitating efficient electron transport and rendering them suitable for n-type FETs. Remarkably, with ML O-terminated Cr2C electrodes, a lateral p-type Schottky contact is formed despite the high work function of ML InSe, opening up possibilities for p-type device applications. Additionally, the study reveals that scandium (Sc), gold (Au), chromium (Cr), platinum (Pt), palladium (Pd), and graphene form lateral n-type Schottky contacts with ML InSe. This is attributed to the strong Fermi Level Pinning (FLP) caused by Metal-Induced Gap States (MIGS). The MIGS are electronic states within the semiconductor bandgap due to the metal presence. The intensity of FLP is quantified by the pinning factor (S), which describes the change in the electron Schottky Barrier Height (SBH) with the electrode material's work function. For ML InSe, a pinning factor of 0.32 indicates a strong but not complete FLP effect.

3.2.1 Choice of Au,Al,Ag as contacts to InSe

As can be concluded from the previous discussion, the interaction between multilayer indium selenide (InSe), characterized by an electron affinity of approximately 4.6 eV, and metals such as gold (Au), silver (Ag), and aluminum (Al) presents a complex landscape for the formation of Schottky junctions and Ohmic contacts. Atmospheric exposure can also modify the surface properties of these metals, further complicating their interaction with InSe.

Starting from the Schottcky-Mott rule discussed earlier, metals like Au, with a work function of approximately 5.1 eV, tend to form Schottky junctions with InSe, leading to a barrier height of approximately 0.5 eV.

Conversely, metals with work functions closer to or lower than InSe's electron affinity, such as Ag (4.3eV) and Al (4.2eV), may facilitate Ohmic contact formation or minimal Schottky barriers, contingent upon the specifics of their interaction. This alignment allows for more efficient electron transfer, characterized by a linear current-voltage relationship.

In this work we therefore chose to use the three different metals Au, Al and Ag to make our devices, with Au giving probably Schottky contacts and the other two being more Ohmic. Hence, the creation of devices with symetric or asymetric metals as contacts should allow to form different diode-like devices with their own characteristics, and enable the study of their behavior under high space charge doping.

3.3 Schottky diode equations and device models

The formulation for fitting the current-voltage (I-V) curves in this and following sections was derived from the classic diode equation, modified to incorporate the unique characteristics of the devices, especially the asymmetrical contacts involving Al-Ag, Au-Ag and Au-Al. The diode equation serves as a mathematical model delineating the I-V characteristics of a diode. In this scenario, it has been adapted to account for the Schottky diode behavior manifested at the metal-InSe interface.

The general form of the diode equation is expressed as:

$$I = I_0 \left(\exp(\frac{qV}{nkT}) - 1 \right) \tag{3.9}$$

Where:

$$I_0 = AA^*T^2 \exp\left(-\frac{\Phi_b}{kT}\right) \tag{3.10}$$

— I denotes the current through the diode,
— I_0 represents the reverse saturation current, indicative of the current flow through the diode under reverse bias,
— k is the Boltzmann constant,
— T is the absolute temperature,
— A is the area of the Schottky junction,
— A^* is the Richardson constant,
— Φ_b is the barrier height,
— V specifies the voltage across the diode,
— n is the ideality factor, accounting for deviations from ideal thermionic junction behavior.

The ideality factor, n, typically varies from 1 to 2, where a factor of 1 signifies an ideal diode, driven purely by diffusion current mechanisms [**?**]. Diodes in real scenarios often exhibit ideality factors between 1 and 2, attributed to recombination, generation in the depletion region, and other non-ideal phenomena [**?**]. Under certain conditions, especially with materials other than silicon or under high current injection scenarios, n may exceed 2. This factor is generally derived from the slope of the forward bias region of the diode's current-voltage (I-V) characteristic curve, plotted on a semi-logarithmic scale.

Diode Parameter Extraction

The diode equation **??** serves to elucidate the relationship between the diode's current I and variables such as I_0, V, n, and T, with the -1 factor accounting for the negligible reverse saturation current at zero bias.

For conditions where V significantly surpasses $\frac{nkT}{q}$, the equation simplifies to

$$I = I_0 e^{\frac{qV}{nkT}} \tag{3.11}$$

facilitating the extraction of I_0 and n from the I-V curve in the forward bias region. The thermal voltage, $\frac{nkT}{q}$, varies with T and n, with k as Boltzmann's constant ($1.380649 \times 10^{-23}\,\mathrm{J/K}$) and q as the electron charge ($1.602176634 \times 10^{-19}\,\mathrm{C}$).

At room temperature ($T \approx 300\,\mathrm{K}$), and assuming $n = 1$ for simplicity, the thermal voltage, V_T, approximates to $25.85\,\mathrm{mV}$. For $n > 1$, this value increases proportionally, e.g., $51.7\,\mathrm{mV}$ for $n = 2$ at room temperature.

3.3.1 Schottky Diode and Resistance in Series Model

When analysing a device with a perfect Schottky diode at one metal-semiconductor interface and modeling all other electrical resistances as a series resistance R_s, the model adapts to fit asymmetric devices featuring one Schottky and one Ohmic contact. A simplified circuit diagram is shown in Figure **??**. The current flow in this model is described by:

$$I = I_0 \left[e^{\frac{q(V-IR_s)}{nkT}} - 1 \right] \tag{3.12}$$

Inverting this equation to determine V as a function of I yields:

$$V = \left(\frac{nkT}{q} \right) \ln \left(1 + \frac{I}{I_0} \right) + IR_s \tag{3.13}$$

This formulation allows for the determination of corresponding current values for each V, facilitating a comprehensive analysis of the diode's behavior under varying conditions.

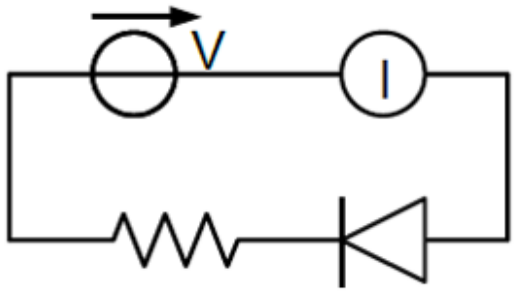

Figure 3.5 – circuit diagram of single-diode and series resistance model.

Note that Dai et al. take the $I \gg I_0$ limit and plot V vs $\ln(I)$ and $\frac{dV}{d\ln(I)}$ vs I to find I_0, n and R_s [**?**]. The result is shown below in Figure **??**, to which I added the result of the model for the whole voltage range. Obviously, the 'model' deviates substantially from the experiment at high positive voltage, however, it is not possible to get a better match for the whole voltage range with this model.

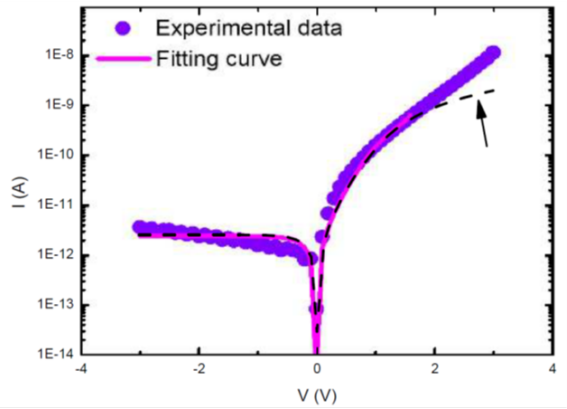

Figure 3.6 – Dai et al.'s fitting result of single-diode and series resistance fitting model.

Frisenda et al. also add a 'short circuit' current term [**?**], to fit curves where the zero

current is offsetted from the zero voltage (for example as a result of photovoltaic effect in their case), as shown in the figure **??**.

$$I(V) = I_0 \left[\exp\left(\frac{q(V - I(V)R_s)}{nkT} \right) - 1 \right] - I_{sc} \tag{3.14}$$

The short circuit current can also be added into the $V(I)$ curve to find the functioning point.

The series resistance represents the total resistance encountered by the current as it flows through the device, including the resistance of the semiconductor material, the contacts, and any other resistive components in the path.

This formula is used to fit the experimental I-V data by adjusting the parameters (I_0, n, R_S, I_{sc}) to closely match the observed behavior of the perfect single-diode curves.

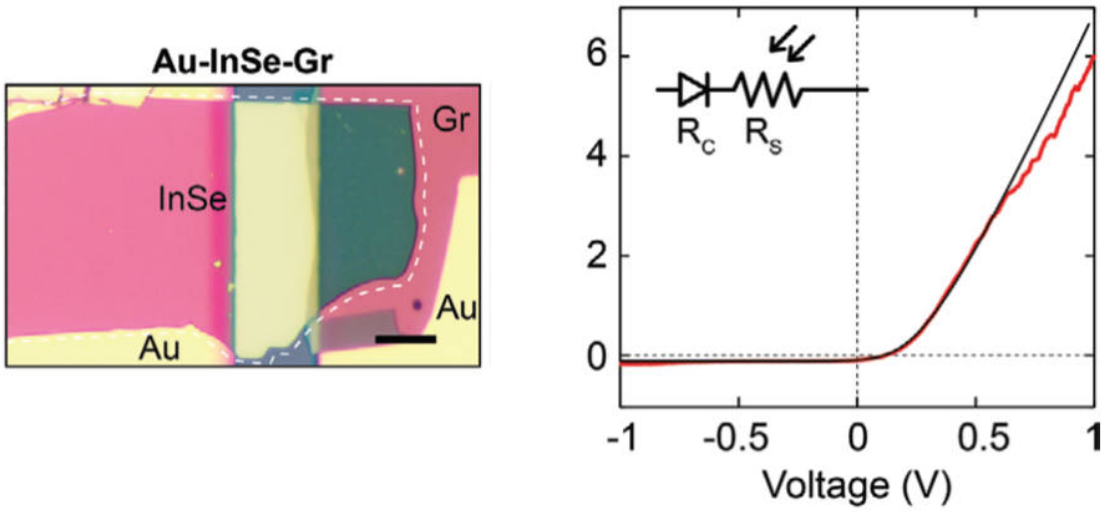

Figure 3.7 – Left: Optical pictures of asymmetric devices based on few-layer InSe with gold (Au) and graphite (Gr) electrodes and Right: experimental I-V curves recorded with the largest illumination density (red curve) and theoretical fit (black curve). the I-V of Au/InSe/Gr is fitted to a Schottky diode with series resistance model.

3.3.2 Back-to-Back Diodes Model

For a symmetric or asymmetric device with a Schottky barrier at both metal/semiconductor interfaces, the previous model cannot represent the whole (I-V) characteristic, even though one may attempt to model each polarity independently. Instead we can make a new model comprising of two Schottky diodes, arranged in a back-to-back configuration with an intervening series resistance (Figure **??**). This model is more general than symmetric Au /Au devices.

In Zhao Qinghua's work, they use the following model to describe a symmetric 2-terminal device with metal/semiconductor Schottky contact on each end and a resistive channel in the middle, representing the resistance of the material [**?**]. This model reflects the symmetrical current behavior with respect to voltage, showing negative curvature and approaching saturation at high bias voltages in both directions.

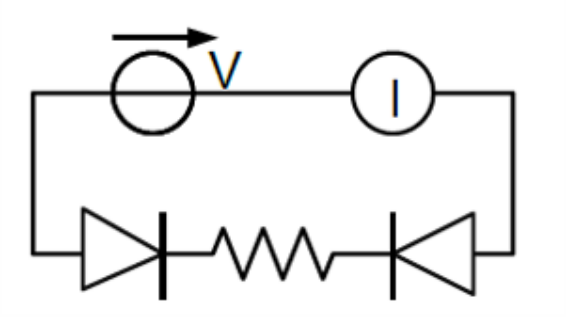

Figure 3.8 – circuit diagram of Back-to-Back Diodes Model.

The voltage drops across the left (V^L) and right (V^R) Schottky diodes are described by the equations:

$$V^L = -\frac{nkT}{q} \ln\left(1 - \frac{I}{I_0^L}\right) \tag{3.15}$$

$$V^R = \frac{nkT}{q} \ln\left(1 + \frac{I}{I_0^R}\right) \tag{3.16}$$

Here, n is the ideality factor of the diodes, T is the absolute temperature, q is the elementary charge, I is the total current, and I_0^L and I_0^R are the reverse saturation currents for the left and right diodes, respectively.

The reverse saturation currents (I_0^L and I_0^R) are linked to the Schottky barrier height (Φ_B) between each metal and InSe by the same relation introduced previously:

$$I_0^{L/R} = AA^*T^2 \exp\left(-\frac{\Phi_B}{kT}\right) \tag{3.17}$$

The total voltage drop (V) across the device is related to V^L, V^R, and the series resistance (R_S) as:

$$V = V^L + V^R + I(V)R_s \tag{3.18}$$

A comprehensive equation is used to express the total current (I) as a function of the applied voltage (V):

$$I(V) = \frac{I_0^L R_0 \exp\left(\frac{q(V - I(V)R_s)}{nkT}\right) - I_0^L R_0}{I_0^L + I_0^R \exp\left(\frac{q(V - I(V)R_s)}{nkT}\right)} \tag{3.19}$$

Obviously in this model the current is limited in both ways and so it **saturates** at positive and negative voltages. Frisenda et al. have used this model (+ some photocurrent) to fit their symmetric Au-InSe-Au devices [**?**], as shown in figure **??**

3.3.3 2-Way Parallel Diodes Model

In layered materials such as InSe, the edges of individual layers are characterized by a significant concentration of dangling bonds. These dangling bonds arise when atoms at the material's edge lack adjacent atoms for bonding, resulting in unpaired electrons [**?**] (as shown in figure **??**). The existence of these dangling bonds can have impact on the electronic properties of the material. Specifically, they increase the chemical reactivity of the edges and can significantly modify the electrical conductivity, among other properties.

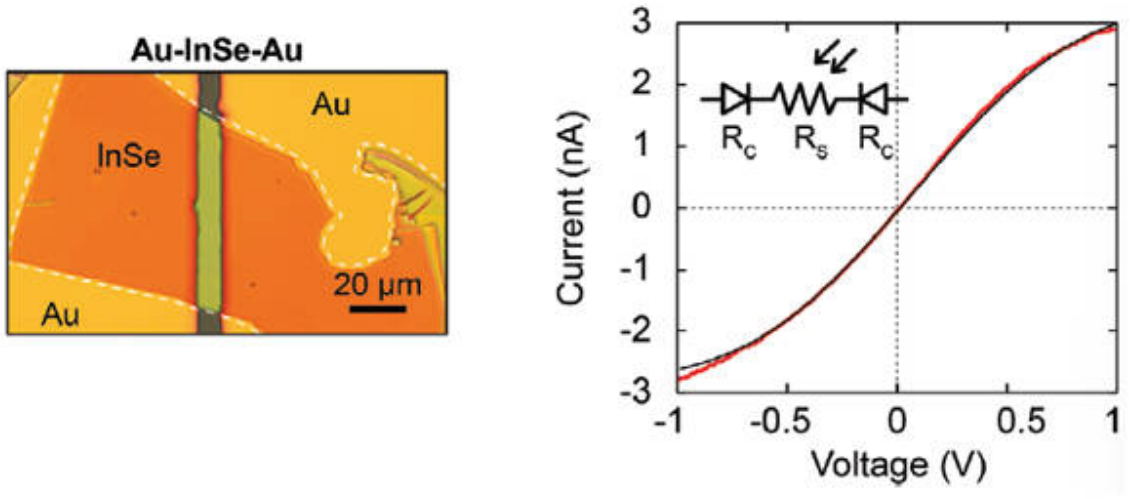

Figure 3.9 – Left: Optical pictures of asymmetric devices based on few-layer InSe with gold (Au) electrodes and Right: experimental I–V curves recorded with the largest illumination density (red curve) and theoretical fit (black curve). the I-V of Au/InSe/Au is is adjusted to the back-to-back Schottky diode model.

Conversely, the surfaces of two-dimensional semiconductors, including the uppermost and lowermost atomic layers, are generally devoid of such dangling bonds. This absence is attributed to the atoms within these layers being in a stable bonding configuration, fully satisfying their valency, noted in metal chalcogenides. Such a configuration minimizes the presence of dangling bonds, ensuring the surfaces are less chemically reactive and maintain consistent electronic properties.

In addition, as explained earlier, in-gap states can arise from defects or impurities. It is well known in the case of 2D materials that adsorbate impurities can dope the semiconductor. This could result in either a highly resistive part (p doping), or on the contrary to a more conductive channel (n doping) since our InSe samples are intrinsically n-doped. Furthermore, metal contacts are deposited by thermal evaporation. The metal atoms have a certain kinetic energy when they land on the InSe surface and this can result in damage or intercalation/penetration of the metal atoms into the InSe layers, altering the ideal interface. In the case of Ag which is known to migrate and intercalate in InSe we have observed this behavior as will be shown later in this chapter. Finally metal induced gap states (MIGS) which represent the tail of the metallic wave function penetrating into the semiconductor can also modify the interface characteristics.

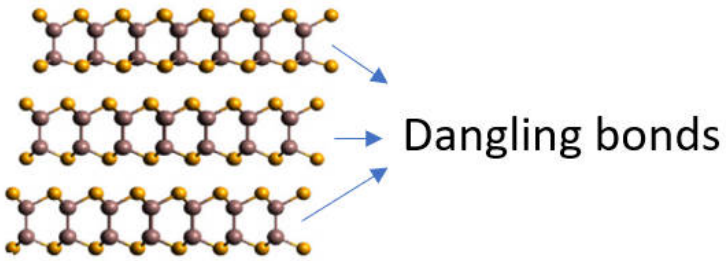

Figure 3.10 – the dangling bonds at the edge of the InSe layers.

In the context of device contacts, the work referenced by Frisenda et al. utilizes van der Waals (vdW) contacts [**?**], which notably do not involve the semiconductor's dangling bonds bonding with metals. This distinction results in an I-V curve that displays saturation at both forward and reverse biases, a characteristic attributable to the dual-diode configuration intrinsic to vdW contact devices. The lack of dangling bonds in vdW contacts is crucial for creating electronically abrupt junctions, enhancing electron tunneling efficiency, and avoiding Schottky-Taam surface states.

However, despite the promising attributes of vdW contact devices, such as their ideal electrical behavior and efficient electron tunneling facilitated by electronically abrupt junctions, their application in industrial settings is currently limited. This limitation stems from challenges related to the stability and scalability of vdW contact devices under industrial manufacturing conditions. In the industry, there is a necessity for device fabrication processes that not only ensure performance efficiency but also manufacturing stability and cost-effectiveness at scale. Consequently, metal evaporation techniques remain prevalent in the industry due to their established reliability and compatibility with existing semiconductor fabrication infrastructures.

Therefore, in my devices, where metal contacts were evaporated directly onto the InSe flakes, this approach was adopted due to its industrial viability. The evaporated metal contacts may interact with the dangling bonds at the edges of the InSe layers, potentially leading to some resistive leaking at the metal/semiconductor contacts, deviating from the idealized Schottky contact behavior. Such deviations are primarily due to the increased interfacial disorder and the augmented interface states and pinning effects typical of conventional metal deposition processes.

So in my devices, the metal/semiconductor contact is not considered a perfect Schottky contact but has some resistive leaking in parallel probably caused by the modifications to an ideal Schottky contact in a "real" metal-InSe interface, as discussed above. For a symmetric or "quasi-symmetric" device, this would lead to the more complex model diagram shown below in Figure **??**.

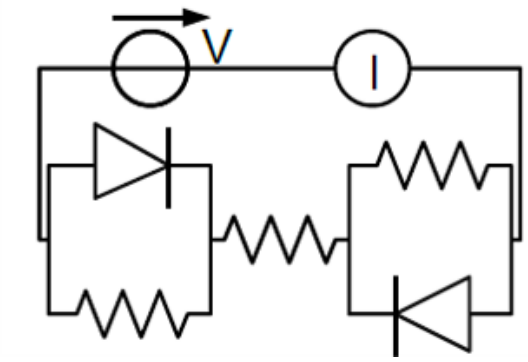

Figure 3.11 – 2-Way Parallel diode model diagram of the metal/semiconductor contact.

The above diagram is equivalent to the following simplified version, with only two (diode + resistor) dipoles in parallel, shown in Figure **??**.

The $I(V)$ characteristic of this model is rather simple to calculate as the currents in both branches just add up. Therefore one can calculate the current in each branch at each V as described earlier for the diode and resistor in series, with one in opposite direction, and add the results. In the most general case, this leads to six independent parameters which can give a wide range of behaviors : (I_{0L} and I_{0R} which indicate the reverse currents of Left/Right direction; R_{sL} and R_{sR} which indicate series resistance of Left/Right direction;

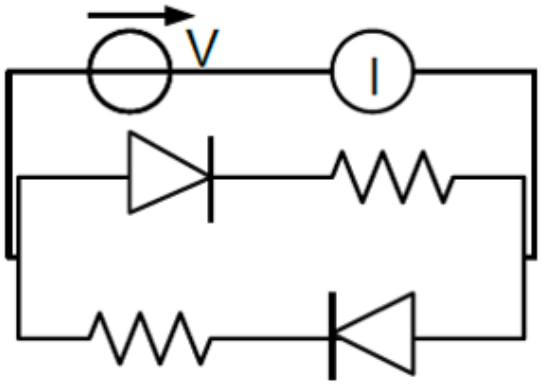

Figure 3.12 – Simplified 2-Way Parallel diode model diagram with diode and resistor in parallel.

α_L and α_R which are inversely proportional to the ideality factors n_{idealL} and n_{idealR} and temperature (*i.e* $\alpha = q/n_{ideal}kT$). However, with so many parameters and non-linear equations, one may expect difficulties to find a unique set of fit parameters, or parameters with a reliably small confidence range.

Note that, importantly, there is no saturation of the current at high voltage in this model.

In the following the fit procedures are performed with **python** and **the curve_fit** function from the **scipy.optimize** package. This allows to get the 'best' fitting parameters and their covariance matrix, whose diagonal parameters gives (in linear approximation) the variance of the fitted parameters. This in turns allows to get 95% confidence intervals as ± two standard deviations.

3.4 Symmetric devices and fitting

3.4.1 Fitting results and discussions

To accurately predict the type of junction, one must consider not only the work functions of the metals and the electron affinity of InSe but also the preparation conditions, interface states, and potential reactions at the metal-semiconductor interface.

To elucidate the characteristics of metal-InSe contacts, I fabricated symmetrical contact devices using three different types of metals in contact with multilayer indium selenide (InSe): Au/InSe/Au, Ag/InSe/Ag, and Al/InSe/Al. where the notation signifies, for a planar few layer device: Drain-Metal contact 1/ few layer InSe / Source-Metal contact 2. The choice of three common metals was made and as will be seen later, the work functions of these vary so that one could expect a variation in the intrinsic nature of the junction. However as we will see later, the intrinsic properties are in general dominated by extrinsic conditions like interface states, defects and impurities. This was a general conclusion all through this work as few layer InSe, though not extremely sensitive to ambient contamination like GaSe or GaS, does suffer from prolonged exposure [**?**]. Thus, though we could prepare our samples and devices in air because of this relative robustness of the material, all measurements are made in vaccuum. Furthermore, variations were seen over a number of devices fabricated, and so all results that are presented have been reproduced at least on two different devices to minimise extrinsic effects. However these are always present as we shall see, and so reproducibility also helps to characterise these in a reliable way.

A symmetrical contact device refers to a configuration where the same metal electrodes serve as the drain and source terminals. The multilayer InSe employed in this research was prepared via anodic bonding from a single crystal of InSe, doped with 1% Si. The metal contacts were applied to the InSe through a process of metal evaporation with the use of a stencil shadow mask as explained in Chapter 2. Microscopic observations, illustrated in Figure **??**, reveal the placement of 2 Au contacts and 2 Ag contacts on a single InSe flake, and similarly, 2 Au and 2 Al contacts on another InSe flake. This methodology enables not only the examination of symmetrical contact behavior on InSe but also the exploration of asymmetrical contact configurations (e.g., Au/InSe/Ag, Al/InSe/Ag, Au/InSe/Al), which will be further discussed in the subsequent section. The schematic diagrams of the InSe devices, showcasing the Au-Au, Ag-Ag, and Al-Al electrode configurations, are depicted in Figure **??**.

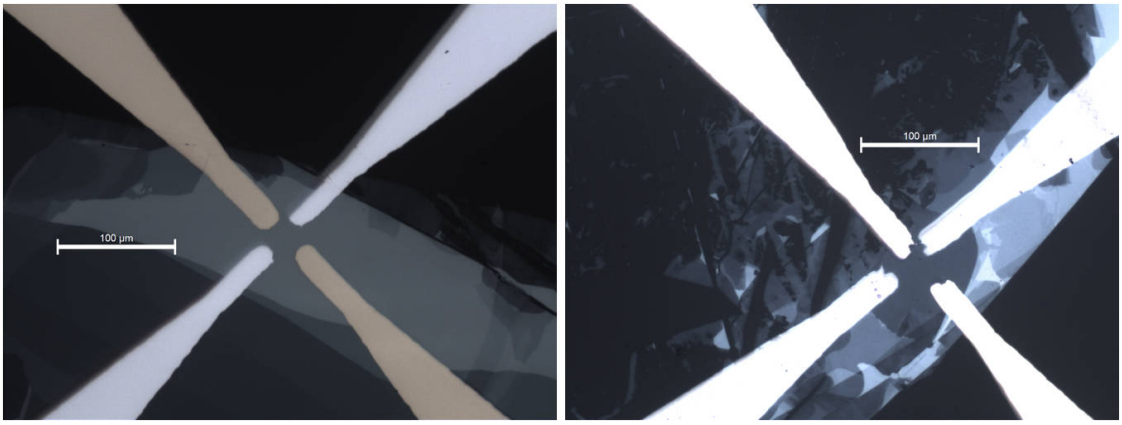

Figure 3.13 – Left: 2 Au contacts and 2 Ag contacts on a single InSe flake and Right: 2 Au and 2 Al contacts on another InSe flake. The InSe Layer thickness in between the contacts is typically around 30 nm.

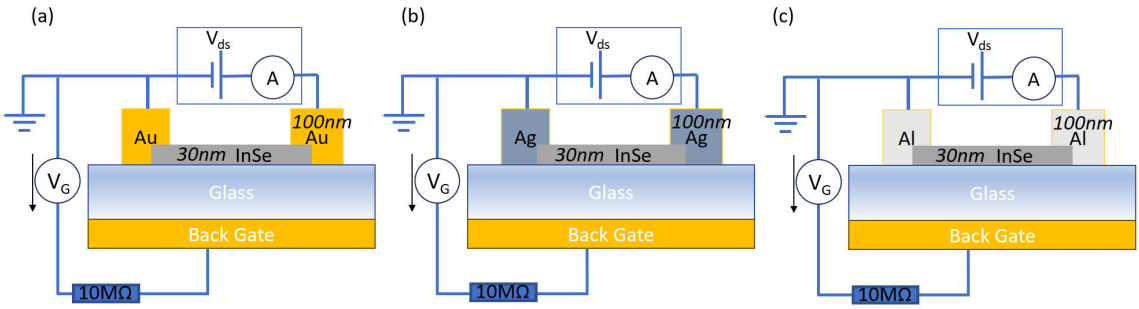

Figure 3.14 – (a) Au-Au, (b)Ag-Ag, and (c)Al-Al electrode configurations on InSe samples.

Typical I-V characteristics of these devices, measured after annealing at a temperature (typically 350 K), well below InSe dissociation, are presented in figure **??** a to c.

None of the I-V curves obtained for symmetric devices were clearly linear. Non-linearity is expected for a symmetric device with a Schottky barrier at each contact, but not with perfectly Ohmic metal/semiconductor contacts. Hence while the non-linearity of the symmetric Au/InSe/Au device is rather unsurprising, the Schottky-Mott model of Ag/InSe and Al/Inse contacts without extrinsic effects would predict Ohmic behavior, in contrast with the experimental results. While both Ag/InSe/Ag and Al/InSe/Al devices are indeed more linear than the Au/InSe/Au, it cannot rule out that a (small) Schottky barrier is formed at the Ag/InSe or Al/InSe interfaces, resulting from interfacial trap states and Fermi level pinning. In addition, while the Al/InSe/Al device appears the most linear here, it also displays the highest resistance, indicating difficult carrier injection into the material. Some hysteretic behavior can be seen in some I-Vs especially the Au/InSe/Au device. This hysteresis is most probably of thermal origin as the device heats up when voltage is rising, and so has lower resistance when the voltage goes back to zero. This chapter will focus on the rising branch of the hysteresis cycle for the purposes of fitting to the model.

While they are not perfectly linear, both Ag/InSe/Ag and Al/InSe/Al device I-V curves are *too* linear to be fitted with the models described before with meaningful parameters. The Au/InSe/Au device clearly does not show saturation at higher voltage that would be characteristic of a back to back diode model, but it shows upturns at both voltage polarities, typical of the 2-way parallel diode model.

Here is the result of the Au/InSe/Au device's current-voltage relationship fitted with the 2-way parallel diode model as shown in Figure **??** and the fitting parameters are summarized as below. Note that the error on the reverse currents ($I_{0L/R}$) are quite substantial (of the same order as the value) and therefore unreliable. Also note that the ideality factors are quite higher than 1.

$$
\begin{aligned}
I_{0L} &= 2.41 \pm 2.39\,\mathrm{nA} \\
I_{0R} &= 1.22 \pm 1.51\,\mathrm{nA} \\
R_{sL} &= 0.04 \pm 0.00\,\mathrm{G\Omega} \\
R_{sR} &= 0.03 \pm 0.00\,\mathrm{G\Omega} \\
\alpha_L &= 5.08 \pm 1.63\,V^{-1} \\
\alpha_R &= 5.12 \pm 1.61\,V^{-1} \\
n_{\mathrm{idealL}} &= 6.02 \pm 1.93\,(\mathrm{at}\ T = 380\,K) \\
n_{\mathrm{idealR}} &= 5.96 \pm 1.88\,(\mathrm{at}\ T = 380\,K)
\end{aligned}
$$

3.4.2 Conclusions from symmetric devices

The experimental findings related to the behavior of various metal contacts on indium selenide (InSe) can be summarized as follows:

1. The gold (Au) contact on InSe does not form an ideal Schottky barrier; instead, it exhibits characteristics of resistive leakage in parallel, indicating a deviation from the expected Schottky behavior due to the presence of additional conductive paths.
2. The aluminum (Al) contact on InSe demonstrates quasi-linear contact behavior; however, it is characterized by a notably high resistance.
3. The silver (Ag) contact on InSe also exhibits quasi-linear contact behavior. Nonetheless, a significant issue arises due to the diffusion of Ag into InSe, which potentially affects the stability and performance of the contact over time.

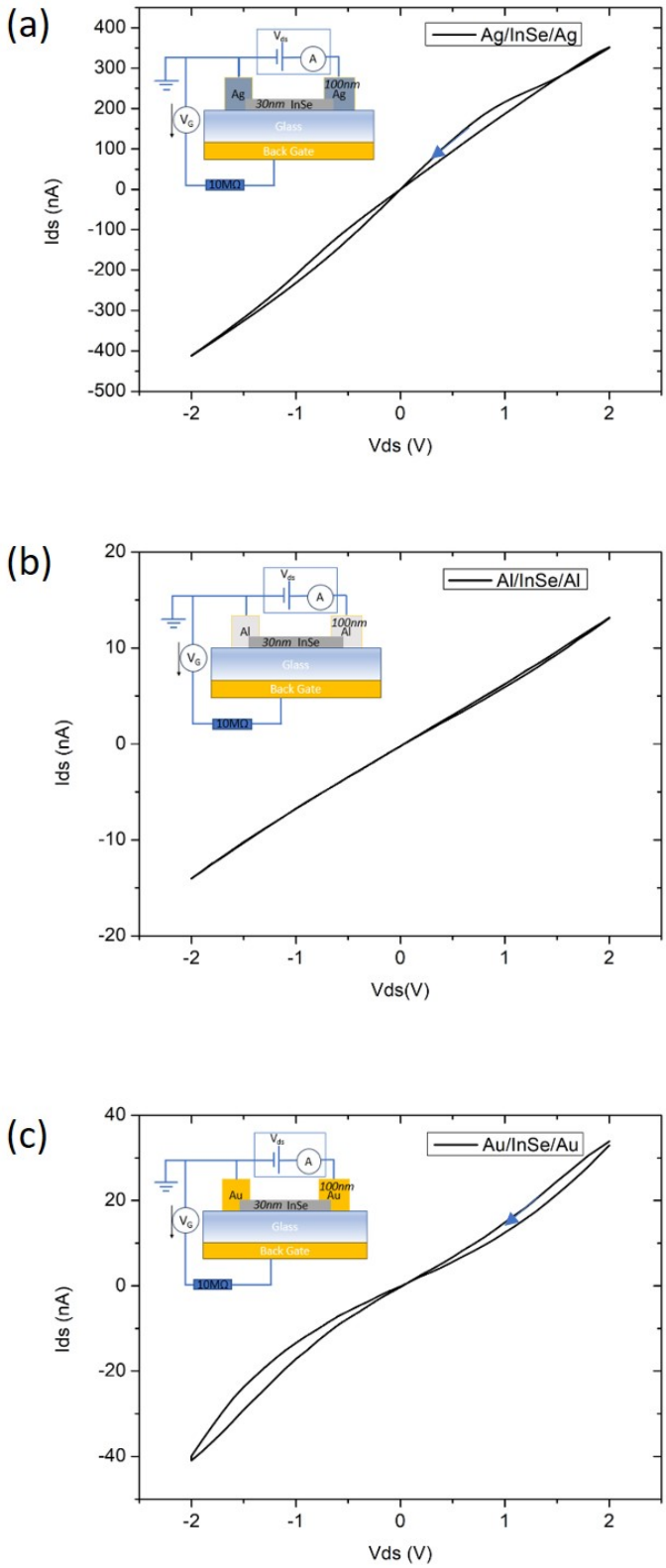

Figure 3.15 – (a) I-V characteristics of InSe device with (a) Ag-Ag electrodes; (b) Al-Al electrodes; (c) Au-Au electrodes.

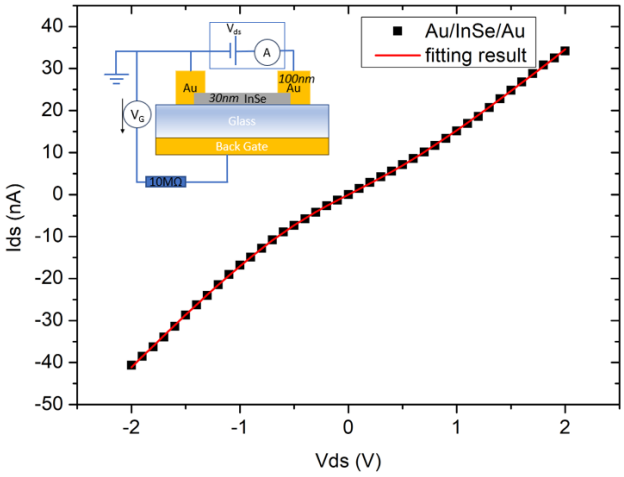

Figure 3.16 – Fitting result of Au/InSe/Au device by 2-Way Parallel diode fitting model.

During the experimental observations, it was noted that silver (Ag) can diffuse into InSe, as evidenced in Figure **??**, in some certain samples where the Ag electrode was evaporated onto InSe. Following the electrical measurements, examination of the samples under an optical microscope revealed the emergence of black dots around the electrode, which were observed to diffuse into the InSe flake.

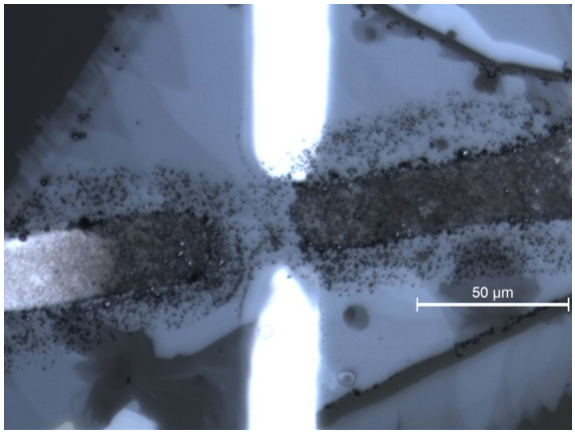

Figure 3.17 – Ag electrodes diffuse into the InSe flake (black dots)after electrical measurement.

To elucidate this phenomenon, the study conducted by Aishani Mazumder provides insight into the intricate dynamics of Ag diffusion within InSe [**?**]. The investigation shows that the initiation of this process is marked by the application of a positive electrical bias, which triggers the oxidation of Ag, subsequently leading to the formation of Ag^+ ions. These ions, once formed, find their migration paths influenced by the structural peculiarities of InSe, notably the vacancies introduced by ambient exposure and the specificities of the fabrication process, such as micromechanical exfoliation. These vacancies, predominantly located at critical junctures near the electrode interfaces and cleaved surfaces of InSe flakes, serve as conduits for the Ag^+ ions, facilitating their movement. Additionally, the study proposes an alternative migration route via the generation of indium interstitials,

suggesting a dual-pathway model for Ag ion diffusion across the semiconductor matrix. Despite the possibility of ohmic contact at an Ag-InSe interface, these observations clearly show that Ag diffusion into the InSe matrix is rampant and could substantially alter the material.

3.5 Asymmetric devices and doping

3.5.1 Fitting results and discussions

In this section, I investigated the rectifying behavior of three pairs of asymmetrical contacts on indium selenide (InSe), fabricating them as three distinct device configurations: Al/InSe/Ag, Au/InSe/Ag, and Au/InSe/Al. The primary objective was to ascertain whether these asymmetrical contacts on InSe could facilitate rectification.

In the Al/InSe/Ag and Au/InSe/Al configuration, it is hypothesized that aluminum (Al) demonstrates the most Ohmic-like behavior when interfaced with InSe (showing the most linear I-V curve). Consequently, the Al electrode was grounded and served as the source, whereas the silver (Ag) and gold (Au) electrode acted as the drain.

For the configurations of Au/InSe/Ag, the measurement of the rectification characteristics of the Au-InSe Schottky junctions necessitates minimizing the influence of electrical transport from the alternative metal contact. This is achieved by selecting an electrode material that forms a contact with low resistance. Consequently, Ag was selected to serve as the source, establishing an Ohmic contact with the InSe channel, due to its ability to fulfil this requirement.

The resuting I-V curves of the InSe devices with Al-Ag; Au-Ag and Au-Al electrode configurations are illustrated in Figure **??** a to c. As noted for the symmetric Au-Au device, some thermal hysteresis can be seen in the measurements, here again focus only the rising branch of the hysteresis cycle for the purposes of fitting to the model.

Doping of the asymmetric devices and inference of change in Schottky barrier height with doping

The influence of doping on the Schottky Barrier Height (SBH) in semiconductors is a critical factor in the performance and efficiency of electronic devices. Doping alters the semiconductor's electronic properties, particularly the built-in potential (Φ_i), which is directly related to the SBH. high-level doping can narrow the energy gap between the semiconductor's Fermi level and its conduction or valence bands, this alteration in the energy landscape results in a diminished barrier height for charge carriers (either electrons or holes) at the metal-semiconductor interface, facilitating their transition across the junction. In n-type doping, the increased electron concentration elevates the Fermi level towards the conduction band. This shift reduces the SBH for electrons, the majority carriers in n-type semiconductors, thereby lowering the energy barrier for electrons moving from the metal into the semiconductor.

Here recall the equation of the reverse saturation current in Schottky diodes:

$$I_0 = AA^*T^2 \exp\left(-\frac{\Phi_b}{kT}\right)$$

As the barrier height Φ_b increases, the exponential term decreases, leading to a decrease in I_0. This relationship is exponential and indicates that even small changes in the barrier height can significantly affect the reverse saturation current.

In our experiments we can effectively change the doping by using the space charge doping method. If the same sample is brought from a certain doping level (1) to another doping level (2), it can result in different barrier heights (Φ_{b1} and Φ_{b2})as the consequence of doping. Hence, we can analyse the relationship between the reverse saturation currents (I_{01} and I_{02}) and the change in barrier height.

$$\frac{I_{01}}{I_{02}} = \exp\left(-\frac{\Phi_{b1} - \Phi_{b2}}{kT}\right)$$

so

$$kT \ln\left(\frac{I_{01}}{I_{02}}\right) = \Phi_{b2} - \Phi_{b1}$$

This equation shows the relationship between the change in barrier height ($\Delta\Phi_b = \Phi_{b1} - \Phi_{b2}$) and the logarithm of the ratio of the reverse saturation currents of the sample at the two doping levels ($\ln(I_{01}/I_{02})$):

- The change in barrier height is directly proportional to $kT \ln(I_{01}/I_{02})$.
- If $\Phi_{b1} > \Phi_{b2}$, then $I_{01} < I_{02}$, indicating that an increase in barrier height leads to a decrease in the reverse saturation current, and vice versa.
- This relationship provides a way to quantify the effect of doping-induced changes in barrier height on the reverse saturation current in semiconductor devices, highlighting how doping levels influence device performance at a given temperature.

In the space charge doping method there are three parameters, which when augmented, increase the amount of doped charge. These are the temperature, the applied gate voltage and the time for which it is applied. The temperature increases the gate current by increasing ionic mobility in glass. The voltage increases the gate current by accelerating ions. The gate current decreases with time for fixed temperature and gate voltage because the built-in electric field hinders the flow of charge, and the built-in electric field strengthens over time. The quantitative evaluation of the effect of doping in terms of carrier concentration was not performed because it needs a different device geometry and

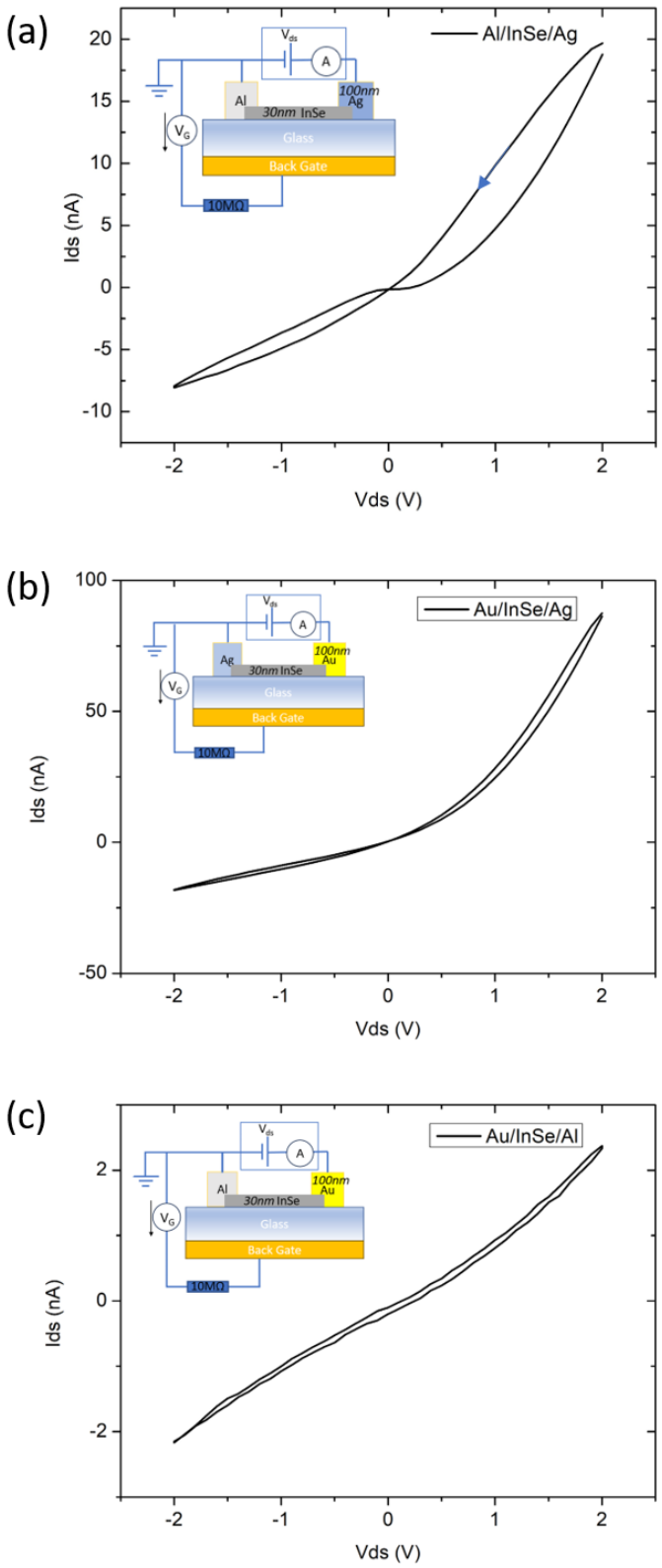

Figure 3.18 – I-V curves of (a) the Al/InSe/Ag devices; (b) the Au/InSe/Ag devices ;(c) the Au/InSe/Al devices with device configuration illustration.

measurement configuration (Hall measurement). However since comparisons are always made for the same device, a qualitative comparison including change of back gate voltage polarity (for n and p doping) and doping time (typically, tens of minutes in this chapter) is sufficient. Furthermore, a numerical value can be extracted to indicate the change in the SBH(eV) which is the quantity directly relevant for this thesis.

Figure **??** a to c represent the result of fitting the measurements on the assymetric contacts for the Al/InSe/Ag device at the temperature of 350 K, with the 2-way parallel diode model. These correspond to the follwing doping conditions: before any doping (a), after electron (N) doping for 20 minutes at a gate voltage of 50 V (b), and after hole (P) doping for 20 minutes at a gate voltage of -50 V (c).

The fitting parameter I_0 in these three conditions has been extracted and is shown below in table **??**.

— $I_0^{\text{undoped}} \approx 0.37\,\text{nA}$
— $I_0^{\text{N-dope}} \approx 0.96\,\text{nA}$
— $I_0^{\text{P-dope}} \approx 0.11\,\text{nA}$

Parameter	undoped	N-dope	P-dope
I_{0L} (nA)	0.37 ± 0.08	0.96 ± 0.11	0.11 ± 0.05
I_{0R} (nA)	0.00 ± 0.00	0.00 ± 0.00	0.00 ± 0.00
R_{sL} (GΩ)	0.04 ± 0.00	0.04 ± 0.01	0.14 ± 0.01
R_{sR} (GΩ)	0.23 ± 0.01	0.74 ± 0.01	0.53 ± 0.02
α_L (V^{-1})	3.32 ± 0.29	4.16 ± 0.24	3.77 ± 0.61
α_R (V^{-1})	33.09 ± 29.86	16.05 ± 2.20	322.64 ± 3116.65
n_{ideal_L} (at $T = 350$ K)	9.99 ± 0.88	7.97 ± 0.46	8.80 ± 1.42
n_{ideal_R} (at $T = 350$ K)	1.00 ± 0.90	2.07 ± 0.28	0.11 ± 0.93

Table 3.1 – Comparison of fitting parameters for samples Al/InSe/Ag before any doping, after N doping and after P doping.

Consequently,

$$\Phi_b^{\text{N-dope}} - \Phi_b^{\text{undoped}} \approx -0.0287\,\text{eV},$$
$$\Phi_b^{\text{P-dope}} - \Phi_b^{\text{undoped}} \approx 0.0366\,\text{eV}.$$

This indicates that for this Al/InSe/Ag device the Schottky barrier height could be decreased by 0.0287 eV due to N doping and increased by 0.0366 eV due to P doping.

Figure **??** a and b present the fitting results for the sample Au/InSe/Ag at a temperature of 380 K, before any doping and after N doping for 1 hour at a gate voltage of 40 V. After P doping, the sample became too resistive to be fitted by the 2-Way parallel diodes model, so it's not showing here.

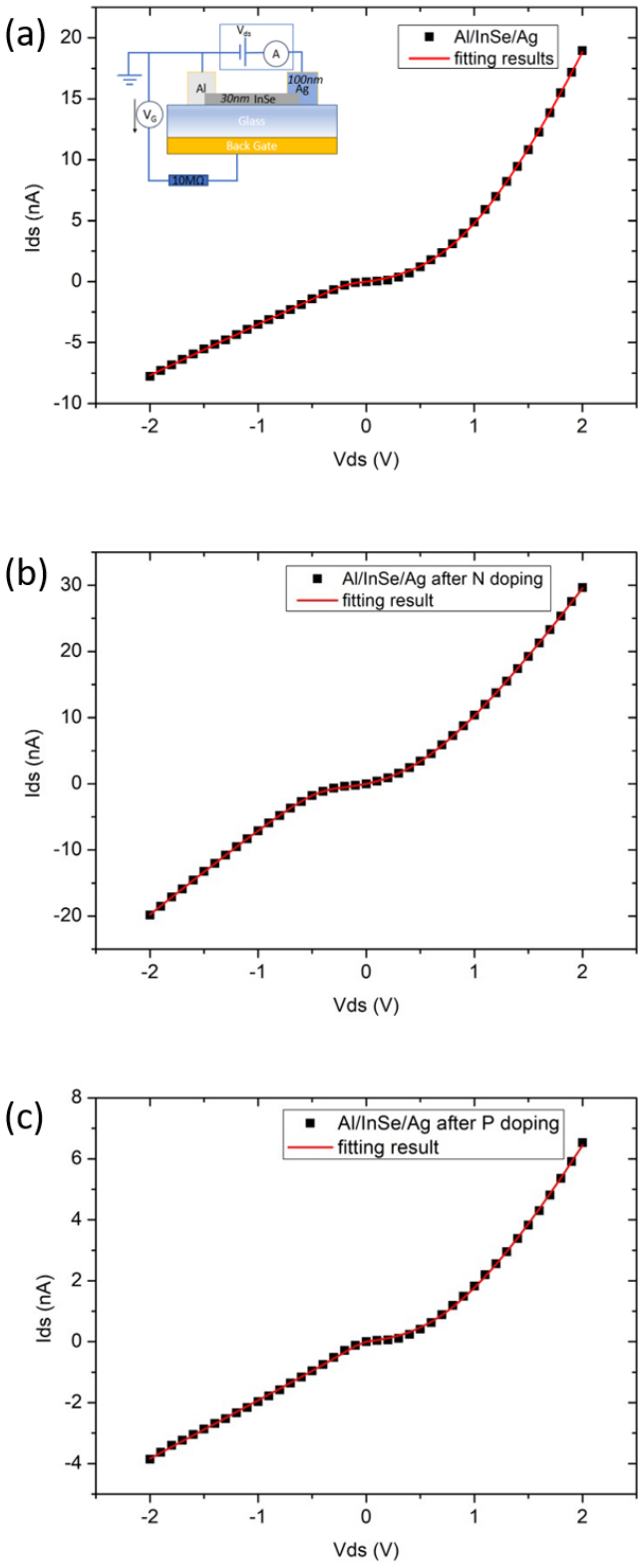

Figure 3.19 – The initial(dots) and fitted (line) I-V curve of the Al/InSe/Ag sample at the temperature of 350 K (a) before any doping; (b) after electrons (N) doping for 20 minutes at a gate voltage of 50 V; (c) after holes (P) doping for 20 minutes at a gate voltage of -50 V.

The fitting parameter I_0 for the undoped condition and after N doping has been extracted and is detailed in the table **??**.

— $I_0^{\text{undoped}} \approx 4.96\,\text{nA}$

— $I_0^{\text{N-dope}} \approx 46.33\,\text{nA}$

Parameter	Undoped	N-dope	P-dope
I_{0L} (nA)	4.96 ± 0.16	46.33 ± 8.54	Not applicable
I_{0R} (nA)	2.86 ± 0.40	23.08 ± 10.10	Not applicable
R_{sL} (GΩ)	0.01 ± 0.00	0.00 ± 0.00	Too insulating to measure
R_{sR} (GΩ)	0.05 ± 0.00	0.00 ± 0.00	Too insulating to measure
α_L (V^{-1})	1.99 ± 0.03	8.70 ± 1.86	Not applicable
α_R (V^{-1})	1.36 ± 0.13	3904.51 ± 14180.80	Not applicable
n_{ideal_L} (at $T = 380$ K)	15.28 ± 0.19	3.51 ± 0.75	Not applicable
n_{ideal_R} (at $T = 380$ K)	22.42 ± 2.18	0.08 ± 0.03	Not applicable

Table 3.2 – Comparison of fitting parameters for sample Au/InSe/Ag before any doping, after N doping, and after P doping. Note that after P-doping the I–V curve of this sample became too insulated to fit.

Consequently,

$$\Phi_b^{\text{N-dope}} - \Phi_b^{\text{undoped}} \approx -0.073\,\text{eV}.$$

This indicates that Au/InSe/Ag device the Schottky barrier height could be decreased by 0.073 eV due to N doping.

Figure **??** presents the fitting results for the sample Au/InSe/Al at a temperature of 350 K, prior to any doping. Note that the I-V curve exhibited minimal rectification characteristics and it's too insulated (as can be seen in the fitting parameters of table **??**), and as such, it was not considered for further fitting and calculation.

Parameter	1.1	1.n	1.p
I_{0L} (nA)	0.18 ± 0.08	0.43 ± 0.38	0.43 ± 0.38
I_{0R} (nA)	0.47 ± 0.26	0.41 ± 0.26	0.41 ± 0.26
R_{sL} (GΩ)	0.43 ± 0.05	0.57 ± 0.53	0.57 ± 0.53
R_{sR} (GΩ)	0.45 ± 0.11	1.48 ± 0.54	1.48 ± 0.54
α_L (V^{-1})	2.24 ± 0.40	0.59 ± 0.38	0.59 ± 0.38
α_R (V^{-1})	1.39 ± 0.56	0.97 ± 0.42	0.97 ± 0.42
n_{ideal_L} (at $T = 350$ K)	14.80 ± 2.66	55.41 ± 35.10	55.41 ± 35.10
n_{ideal_R} (at $T = 350$ K)	23.92 ± 7.74	34.31 ± 14.97	34.31 ± 14.97

Table 3.3 – Comparison of fitting parameters for sample Au/InSe/Al before any doping, after N doping, and after P doping.

3.5.2 Conclusions from asymmetric devices

In this section, I investigated the rectifying behavior of three pairs of asymmetrical contacts on indium selenide (InSe), fabricating them as three distinct device configurations: Al/InSe/Ag, Au/InSe/Ag, and Au/InSe/Al. Post-annealing, these configurations exhibited minimal rectifying behavior and some hysteresis due to heating(the device heats up when voltage is rising and the device has lower resistance when the voltage swapping

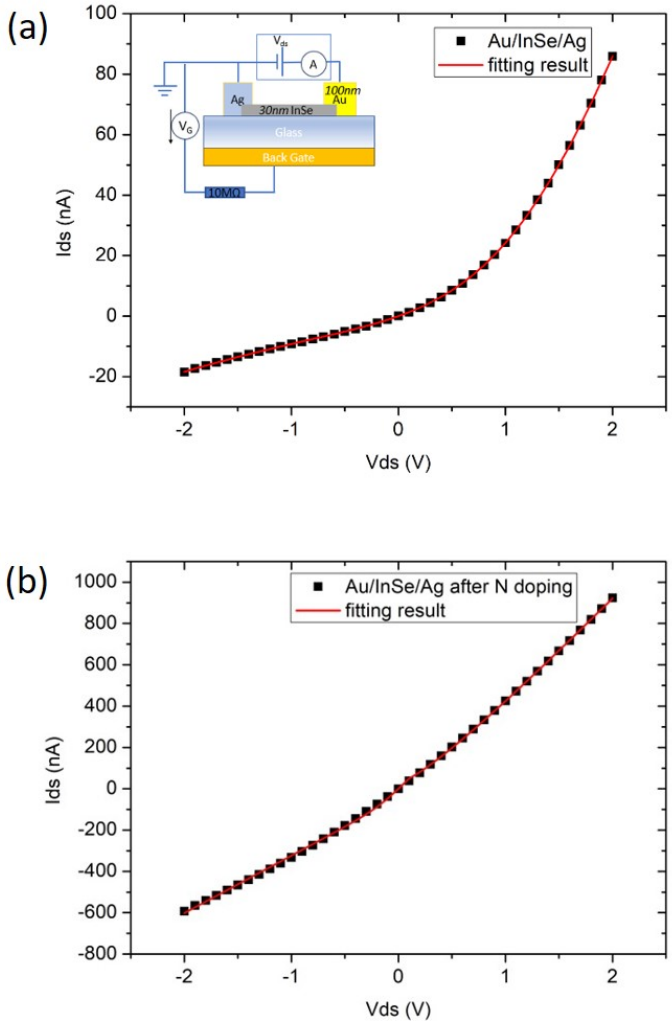

Figure 3.20 – The initial(dots) and fitted (line) I-V curve of the Au/InSe/Ag sample at the temperature of 350 K (a) before any doping and (b) after electrons (N) doping for 1 hour at a gate voltage of 40 V.

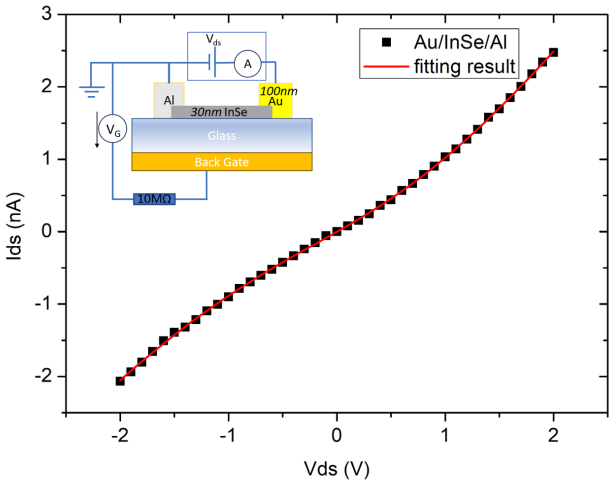

Figure 3.21 – The initial(dots) and fitted (line) I-V curve of the Au/InSe/Al sample at the temperature of 350 K (a) before any doping.

back to zero). However, by applying N-type and P-type doping to these devices, I observed changes in their Schottky barrier heights (SBH).

To better understand how space charge doping modulates the diode behavior, we developed a two-way parallel diode model to fit the electrical curves. This model addresses the non-ideal nature of the metal-semiconductor interface. The fitting results, followed by calculations, yielded the following observations:

— For the Al/InSe/Ag configuration, after N-type doping for 20 minutes at a gate voltage of 50 V, the Schottky barrier height decreased by 0.0287 eV. After P-type doping for 20 minutes at a gate voltage of -50 V, the Schottky barrier height increased by 0.0366 eV.

— For the Au/InSe/Ag configuration, after N-type doping for 1 hour at a gate voltage of 40 V, the Schottky barrier height decreased by 0.073 eV.

The limitation in the SBH change in these samples is likely due to the pinning of the Fermi level by metal-induced gap states (MIGS).

3.6 Conclusions and Perspectives

Several qualitative and quantitative conclusions can be extracted from the work presented in this chapter and will orient the work presented in the next chapter and lead to the principal result of this thesis, that is the modulation of the Schottky barrier height and the experimental fabrication of a metal/ InSe/ metal Schottky diode with the help of electrostatic doping.

From the measurements in this chapter made with devices that changing metal contacts or using asymmetric metal contacts instead of symmetric ones does not substantially change the I-V characteristics. These remain highly resistive and slightly non-linear. Schottky diode behavior is never observed even though, from ideal SBH estimations, the Au contact can be assumed Schottky and the Ag and Al contacts can be assumed to be ohmic. The probable reason for this is the non-ideal nature of the interface which may arise from defects and impurities (defect induced gap states or impurity doping), dangling

bonds from layer edges and metal induced gaps states from the tails of the metallic wave functions which may penetrate into the semiconductor. Another typical materials problem was seen in the case of the Ag - InSe interface where Ag substantial Ag inter-diffusion into InSe is observed. This probably considerably alters InSe properties as seen from the much higher currents in the devices with Ag contacts.

These non-ideal interfaces lead to the use of a model which accounts for the complex metal-semiconductor interface for fitting the measured I-V curves of our devices. Thus each metal-semiconductor contact is considered as a Schottky contact and a further resistive channel is introduced parallel to the Schottky channel. With this 2-way parallel diode model, I succeed in fitting the measured curves and extracting some quantitative parameters. In particular effectively account for the non-saturating behavior of the current at higher voltage in the measured I-V curves.

As showed through a literature survey, whatever the metal contact, the SBH in a metal-InSe device is always estimated to be about 0.5 eV. This clearly points to a SBH determined by Fermi level pinning rather than the difference between the metal Fermi level and the InSe electron affinity. Further proof of Fermi level pinning is provided by the doping experiments on the assymetric devices in this chapter. Those could only alter the SBH by 0.02-0.07 eV while the Fermi level in InSe samples has been measured to be about 0.3 eV below the conduction band minimum [**?**].

Finally three conclusions can be formulated for the aim of fabricating a Schottky diode from a metal-InSe interface:

1. Among the metals tested (Au, Ag, and Al), only gold (Au) demonstrated sufficient stability and Schottky-like behavior to serve as a contact with indium selenide (InSe). However, in a device with dual Au contacts, altering the Schottky barrier height (SBH) at one Au-InSe interface via space charge doping is impractical, as both interfaces will be similarly affected by the doping.
2. The impact of space charge doping on the SBH is notably minimal. To achieve ohmic or near-ohmic behavior at the Au-InSe contact, the Fermi level must be shifted by approximately 0.3 eV [**?**]. Space charge doping, however, produces changes that are an order of magnitude smaller. This limitation is likely due to the pinning of the Fermi level by metal-induced gap states (MIGS) associated with the Au contact.
3. For successful fabrication of a Schottky diode using an Au-InSe-Au structure, it is essential to overcome the issue of Fermi level pinning to enable effective SBH modification through space charge doping. Additionally, it is crucial to selectively dope only one of the two Au-InSe interfaces to achieve ohmic contact and thus create a functional Schottky diode.

Chapter 4

InSe vertical step Schottky diode

In Chapter 3, it was determined that doping planar samples does not enhance diode-like behavior, partly because of the simultaneous doping of both contact interfaces (source and drain). This insight called for an alternative geometry that allows for modification of only one contact interface, thereby motivating the development of the vertical step diode. The samples and experiments described in Chapter 4 embody this innovative approach.

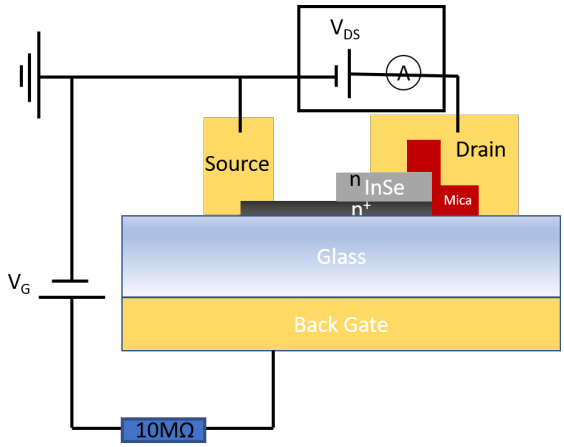

Figure 4.1 – The schematic diagram of the device fabricated in Chapter 4.

4.1 Preamble: Lessons from planar geometry

In the last chapter we reached a few conclusions concerning metal – InSe junctions and how their characteristics can be altered:

1. The model which most accurately describes measured behavior in our planar devices is the one including an ohmic 'leakage' path, that is back to back Schottky diodes with a parallel resistive path. This 2-Way Parallel Diodes Model assumes a 'non-ideal' junction.
2. Regardless of the metal used (Au, Ag, or Al), the I-V characteristics of the metal-InSe junction are similar. This observation suggests that the Schottky Barrier Height (SBH) is, to a certain extent, independent of the metal type. It is also concluded that the SBH varies minimally (on the order of 10 meV) upon electrostatic doping. This minimal change implies pinning of the Fermi level to states within the gap, likely Metal Induced Gap States (MIGS).

3. A Schottky rectifying device requires both an ohmic contact and a Schottky contact. To establish an ohmic contact through electrostatic doping of InSe, the following conditions must be met:
   — The doping must be confined to the InSe corresponding to one junction, while the other junction remains undoped, maintaining a metal–InSe Schottky barrier. This can be achieved using a specific 'step' geometry for the device. Electrostatic space charge doping through the substrate impacts a certain thickness (Debye length) related to the dielectric screening properties of the semiconductor targeted for doping. The Debye length for MoS_2 is calculated to be about 2 nm [**?**]. Given the lower dielectric constant of InSe, an upper limit of a few nanometers is suggested. Therefore, the thickness of the few-layer InSe intended to be doped towards high conductance by electrostatic doping should not exceed roughly 5 nm, corresponding to 6-7 layers. Conversely, the thickness at the junction where electrostatic doping should not change the semiconducting properties of InSe is set to approximately 20 nm or about 30 layers.
   — The device design must ensure a current path through both metal/semiconductor junctions, with current passing vertically from the thin InSe layer at the bottom of the sample to the thicker InSe at the top, as illustrated in figure **??**.
   — It is essential to verify that electrostatic space charge doping of InSe indeed triggers a significant Fermi level shift in the semiconductor beneath the thin contact to achieve an ohmic junction, effectively depinning the Fermi level at this location.

4.2 Vertical step Schottky diode

Here I will describe in detail the alternative geometry that allows modification of only one contact interface.

Following anodic bonding, I selected an InSe sample exhibiting a natural step-like geometry on the glass substrate, as depicted in Figure **??** and Figure **??**. On this figure we can see that the exfoliation process sometimes leaves thin flakes of InSe that are not fully cleaved in the same plane, leaving thicker material in a step shape.

The experimental setup required the placement of two gold contacts on the sample: one in contact with the thin InSe layer and the other exclusively with the thicker portion. To facilitate this configuration, I employed a mica sheet, serving as an insulating barrier, to cover the edge of the thicker InSe section. The mica sheet was carefully exfoliated then transferred onto the edge of the step-shape InSe as described in chapter 2.

Consequently, when gold was evaporated onto the InSe surface, electrical current was directed from the first gold contact (atop the thicker InSe portion) through the thicker and then thinner InSe layers before reaching the second gold contact (atop the thin InSe layer). As measured by AFM (Figure **??**) the thickness of the thin-InSe is about 7 nm; the thickness of thick-InSe is about 25 nm; the thickness of Mica is about 50 nm; and the thickness of the gold electrodes is about 150 nm.

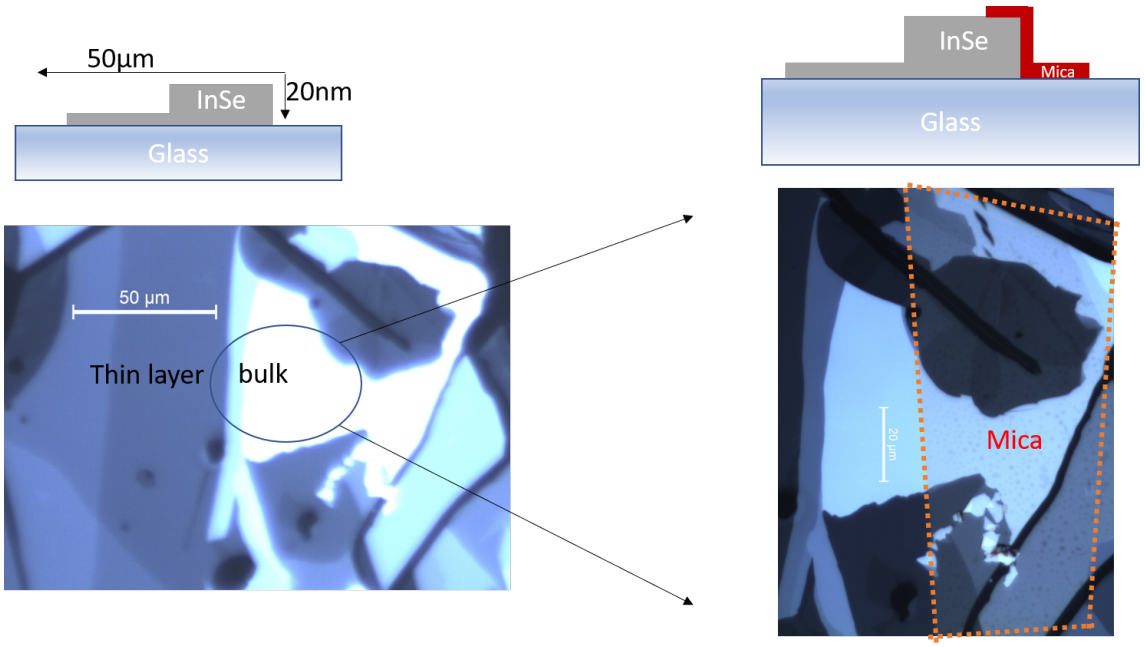

Figure 4.2 – Left: Side view sketch and microscope image of the step-shape InSe sample on the glass substrate after anodic bonding. Right: Side view sketch and the microscope image of InSe sample with a piece of Mica on top to cover the edge of the thicker part.

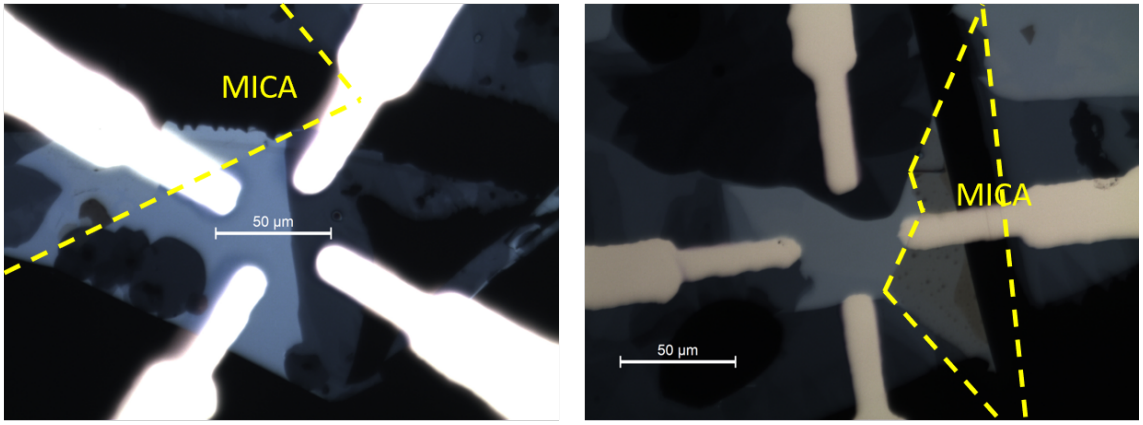

Figure 4.3 – Two different InSe step-shape samples with Mica insulator and gold electrodes, discussed in this chapter.

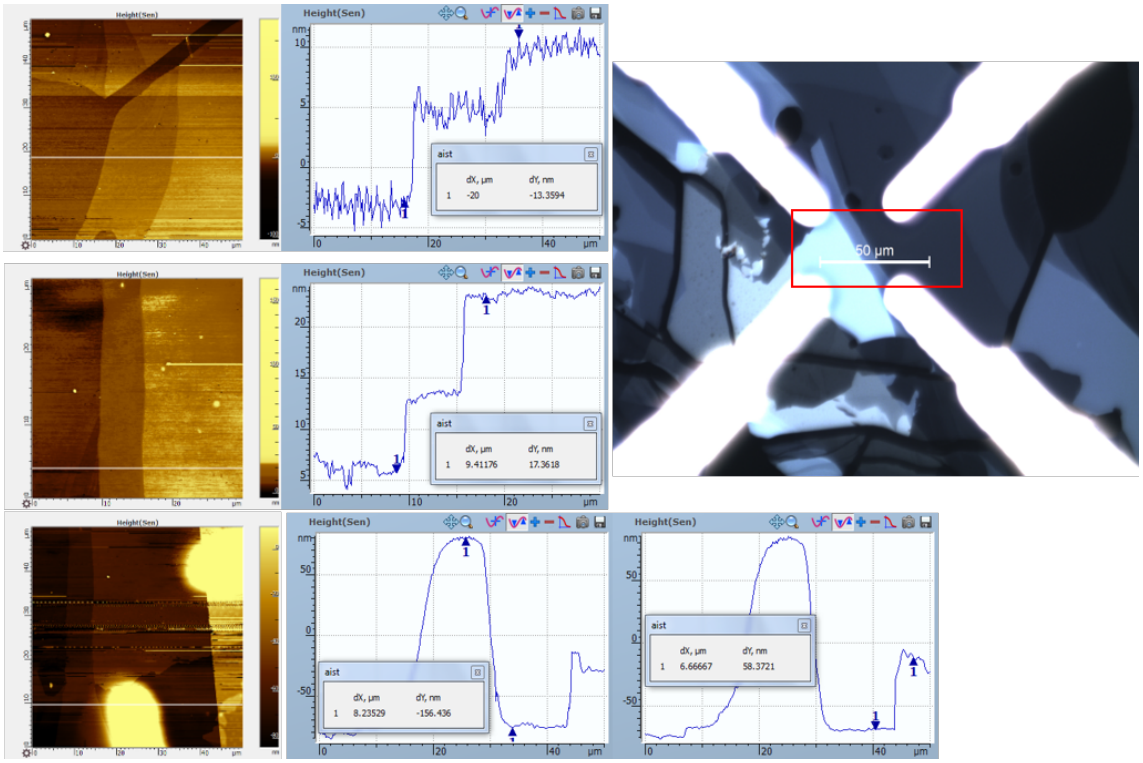

Figure 4.4 – AFM measurement of one step-shape sample with mica insulator and gold contacts.

4.2.1 n-type space charge doping at the thin InSe-metal contact

Several devices were measured in our cryostat under high vacuum. Initial I-V characteristics showed highly resistive and slightly non-linear behavior as expected from our experiments on planar devices.

The following step to try and get rectifying diode-like behavior was to induce electrostatic doping on the thin contact. Indeed, the InSe material used is intrinsically n-doped with a Fermi level approximately 0.3 eV below the conduction band minimum. Ideally, to achieve an ohmic contact we would like the Fermi level to move towards the conduction band minimum and eventually coincide with it as a result of n-type space charge doping. As the top thick part InSe is thicker than the Debye length we don't expect any changes to the metal–InSe interface of the second contact.

In Figure **??** we see the I-V characteristics of two step Schottky devices where n-doping is progressively increased: as space charge doping is a 'slow' process we continuously monitor the I-V characteristic of the device while the space charge is building up below the thin InSe layer. The measured I-V characteristic is essentially the same as those measured in Chapter 3 for planar devices, that is with neither Schottky type rectification nor saturation. With more n-doping the device becomes less resistant as expected but there is no change in the I-V characteristics, in particular no rectifying behavior.

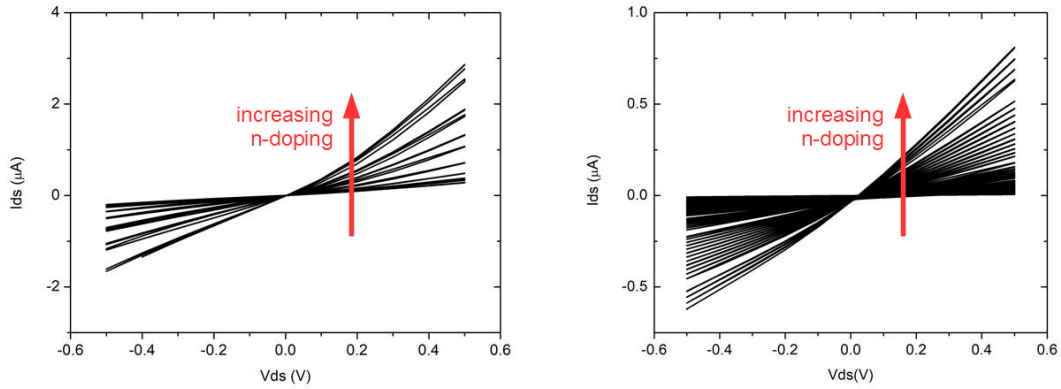

Figure 4.5 – Two step Schottky devices I-V characteristics measured during n-type space charge doping. The red arrow shows the direction of increasing doping. Increasing n-doping does not alter the shape of the I-V characteristic and does not provoke rectifying behavior, although it does lower the internal resistance of the device.

Analysis of some of the curves through the 2-way parallel diode model provides some limited insights into the changes induced by the doping. While the initial curves are not rectifying enough to give reliable result on the diode parameters, the resistance of the sample can be estimated to about 1 MΩ and decreases in the 0.1 MΩ range during doping. Then as the asymmetry gets more pronounced with doping, some diode characteristics can be extracted, albeit with unreliable parameters and large uncertainties, as shown in table **??**.

Nevertheless it appears that the extensive doping process performed here is not sufficient to induce an ohmic contact. This behavior was repeatedly seen in three or four other devices.

Parameter	initial	intermediate	final
I_{0L} (nA)	$*42 \pm 61$	170 ± 140	260 ± 150
I_{0R} (nA)	$*20 \pm 140$	$*36 \pm 66$	$*44 \pm 55$
R_{sL} (MΩ)	1.5 ± 0.45	0.11 ± 0.01	0.098 ± 0.01
R_{sR} (MΩ)	$*0.8 \pm 3.5$	0.35 ± 0.04	0.28 ± 0.02
α_L (V^{-1})	$*16 \pm 25$	12.3 ± 4.6	10.7 ± 3.4
α_R (V^{-1})	$*6 \pm 20$	24 ± 12	30 ± 12
n_{ideal_L} (at $T = 350$ K)	$*2.0 \pm 3.1$	2.7 ± 1.0	3.09 ± 0.97
n_{ideal_R} (at $T = 350$ K)	$*6 \pm 22$	1.36 ± 0.7	1.1 ± 0.43

Table 4.1 – Comparison of fitting parameters for the I-V characteristic of the sample shown in figure **??** (left) before any doping, after some intermediate n-doping and the final curve. Values preceded by a $*$ are considered unreliable due to their large confidence interval.

As we have seen in Chapter 3, Fermi level pinning to MIGS prevents the contact from becoming ohmic, even after substantial doping. Our intuitive conclusion is therefore that 'true' Schottky diode can only be achieved once the Fermi level of the semiconductor is 'depinned' on the thin contact.

4.2.2 Depinning the Fermi level: p-type doping followed by n-type doping

As stated above, the strategy is to modify the Schottky junction between the thin InSe layer and its corresponding gold contact by space charge doping. As elucidated in Chapter 3, n-type doping reduces the Schottky barrier height. Consequently, the device's behavior can be conceptualized as illustrated in Figure **??**. Initially, the device incorporates two back-to-back Schottky diodes as in the planar devices, with inherent resistance leakage and series resistance attributable to the InSe material. Subsequent doping should reduce the Schottky barrier height at the metal-thin InSe contact, eventually leading to an ohmic contact. At this stage, the device's current-voltage characteristics should exhibit rectifying behavior. In the ideal case this means that the top InSe-Au junction remains a Schottky contact while the bottom junction has become ohmic, giving rise to a single Schottky junction and rectification. In practice this situation could be realized to a certain extent, as we shall see in the following.

The question then arises of the strategy to follow to achieve sizeable Fermi level movement with doping (of the order of 0.1-0.3 eV rather than 10 meV obtained until now). This could happen if we could 'depin' the Fermi level so as to achieve ohmic contact with n-type doping at the thin InSe junction.

We derive inspiration from the recurrent observation that an oxide barrier between the semiconductor and the metal is an efficient inhibitor of MIGS in the semiconductor and prevents Fermi level pinning while still allowing charge injection through tunneling [**?**] [**?**]. The reasoning behind this observation is that the oxide barrier reduces the extension of the metal wave-function tail in the semiconductor because of the larger band-gap and smaller dielectric constant.

Although we do not introduce an oxide layer at this junction we can effectively seek to reduce the metal wave-function penetration into the semiconductor and the generation of MIGS. This is done by first p-doping the semiconductor. Indeed, p-type doping reduces the dielectric constant and conductivity, consequently curtailing the penetration of the metallic wave function tail into the semiconductor. This process increases the decay constant

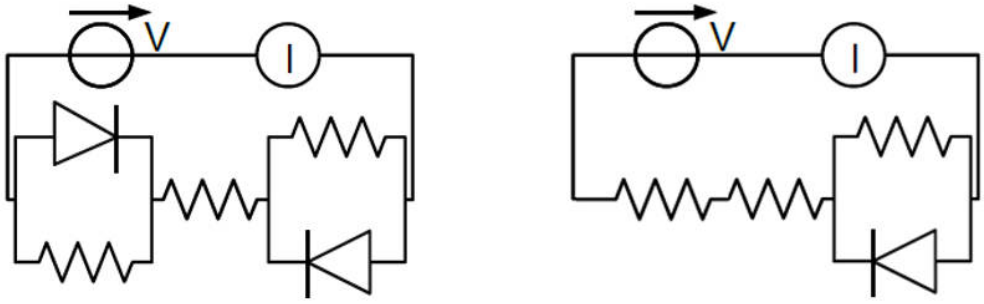

Figure 4.6 – Left: Model for the as-fabricated step shaped InSe sample with gold electrodes. This is the parallel 2-way diode model for two back-to-back Schottky diodes with inherent resistance leakage used in the last chapter. Right: After appropriate doping the thin-InSe/gold contact becomes ohmic.

κ of an electron's wave function. A larger κ indicates that the wave function of the electrons from the metal decays more rapidly into the semiconductor, thereby reducing the metal-induced gap states (MIGS). Subsequently, when n-type doping is undertaken, band bending becomes more efficient compared to the case of Fermi level pinning, leading to a more effective reduction in the Schottky Barrier height.

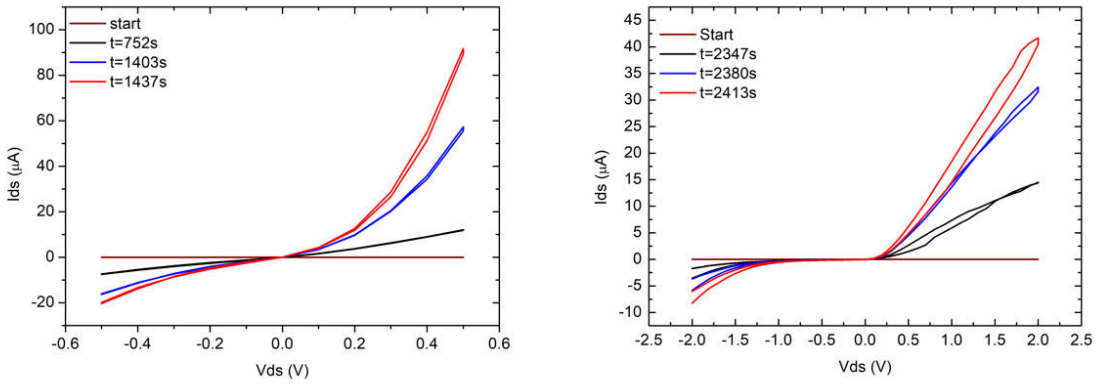

Figure 4.7 – Two step Schottky devices which have first been p-doped and then n-doped to the same levels as the earlier devices. It can be clearly seen that the I-V chracteristic undegoes a marked change, rectifying behavior is obtained and the current obtained in the forward operational regime is one to two orders of magnitude higher than in the simply n-doped case.

In Figure **??** we show the resulting I-V characteristics of two step-shape InSe samples that have been extensively p-doped before n-doping. As can be seen the result is drastically different from just n-doping. After some doping (again we are monitoring the I-V curves while the doping is building up slowly) the initially very insulating sample become rectifying with very high current. This is the first such observation in all our devices:

— This behavior appears rapidly over three or four I-V cycles as n-doping is proceeding.

— Current increases rapidly from a few hundred nA to a few tens of μA, that is two orders of magnitude higher than before.
— The rise in current locally heats the device which explains the hysteresis seen at high voltage. This instantaneously increases charge concentration both by increased space charge doping (increased ion mobility locally in the glass just below the sample due to higher temperature) and due to higher temperature induced free charge in InSe. As it is a positive feedback loop (more current gives more heating, more heating gives more current), it leads to device failure as discussed below.
— The increase in temperature is clearly seen by the hysteresis during the I-V loops.It is so rapid that in both our devices it induced device failure by burning as shown in the photos taken after (Figure **??**)

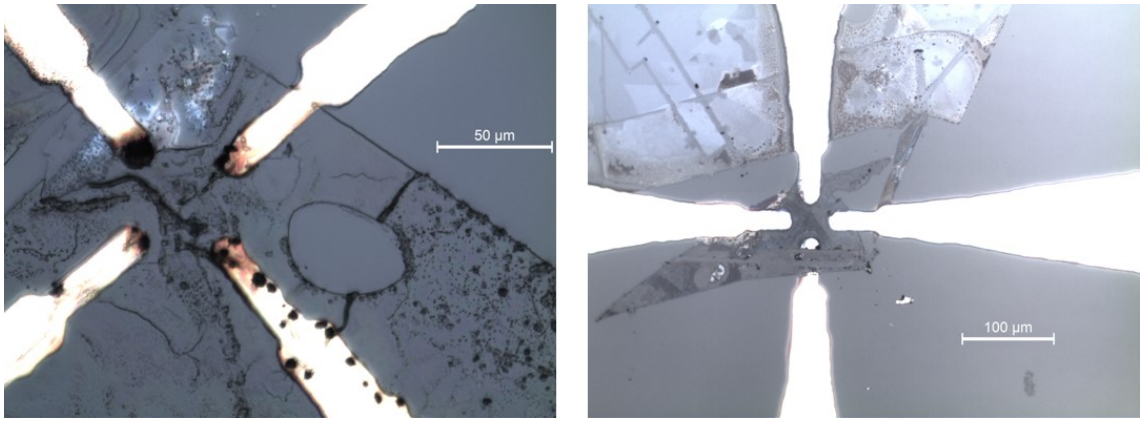

Figure 4.8 – Microscope pictures of the two samples in this chapter after I-V measurement, the samples burned because of large current heating.

4.3 Discussion

Let us attempt some quantitative estimates of the results obtained.

The high current can be attributed to two factors. We attain Schottky rectifying behavior which means a high current in the forward bias direction. As the current direction is vertical in the device, it is the horizontal cross section, or the area of the device which determines effective device resistance rather than the vertical cross section. This is three orders of magnitude larger than the planar cross section. Simultaneously, electronic transport parallel to the c-axis is not efficient (higher resistance) in 2D materials because of the van der Waals bonds between layers. The resultant situation because of these two conflicting tendencies can be gauged by the maximum current obtained through simple n-doping in the devices of Figure **??** which is of the order of 1 μA as compared to 100 nA in the case of our planar diodes of Chapter 3. We gain about one order of magnitude in forward current because of the geometry.

However by comparing the maximum forward current in the directly n-doped devices of **??** and the depinned Fermi level (p-doping followed by n-doping) devices of **??** we see that we have indeed gained between one and two orders of magnitude (1 nA compared to about 50 μA in the best case) by successfully obtaining a near-ohmic contact at the thin InSe-metal junction.

We may however remark that though rectification at low voltage (0.1 V) is obtained in the forward direction, some reverse current is obtained at a few volts in the reverse

direction. This probably does not correspond to a breakdown voltage but rather to some non-ohmic channels in the thin InSe-metal contact. This is why the 2-way parallel diode model is still adapted to our step Schottky geometry.

We have fitted the three latest I-V characteristics before failure of the best device shown in figure **??** (right) with the the 2-way parallel diode model (Figure **??**). Analyzing the resulting parameters in table **??**, the striking difference is the reduction of the internal resistance in both model branches to tens of kΩ level, which can only be achieved with a significant change of the Fermi level towards the conduction band.

Furthermore the diode characteristics from the L branch (*i.e.* the diode at the thick InSe/Gold contact) gives reasonable ideality factors close to unity which indicates that thermionic emission is the dominant process at this Schottky interface. To verify the model validity we also fitted a restricted part of the curves with a single diode and series resistor which gave identical parameters to within the confidence intervals.

There are however un-explained phenomenon in these devices, which would require further investigation:

— Firstly, while the thin contact becomes highly conducting and therefore 'ohmic', the I-V characteristic is still displaying a reversed diode which is well captured by the 2-way parallel diode model. While it is intriguing it may just be a geometric problem as the samples shape are not well defined laterally.

— Secondly, the fitted parameters of the forward diode display an increasing reverse saturation current. With the same arguments stated in Chapter 3 this would require a substantial change in SBH with doping, however it corresponds to the interface with the thicker part, which was assumed far enough from glass to be affected by the doping. This may come from partial screening of the electric field from the space charge, which would result in a barrier lowering similar to the Schottky image force lowering effect.

— Lasty, the complex doping procedure that allowed to achieve this diodes is highly irreversible. Electrostatic doping in itself should intrinsically be reversible as it is just changing the chemical potential. As we argued, p-doping reduces the spreading of the metallic wave-function in the gap by increased screening, but removing p-doping (*i.e* n-doping) should just reverse that process. Hence, the source of irreversibility remains unclear.

Parameter	third to last	second to last	last
I_{0L} (nA)	$*0.4 \pm 1.1$	8.8 ± 4.2	40 ± 21
I_{0R} (nA)	18.5 ± 8.3	15.7 ± 3.5	15.9 ± 5.8
R_{sL} (kΩ)	99.9 ± 36	46.7 ± 0.7	45.4 ± 1.3
R_{sR} (kΩ)	30.9 ± 23	23.5 ± 5	32.8 ± 5.2
α_L (V^{-1})	37.7 ± 14	22.4 ± 2.0	17.0 ± 2.3
α_R (V^{-1})	2.8 ± 0.4	3.18 ± 0.17	3.6 ± 0.29
n_{ideal_L} (at $T = 380$ K)	0.81 ± 0.31	1.36 ± 0.12	1.8 ± 0.3
n_{ideal_R} (at $T = 380$ K)	10.9 ± 1.4	9.6 ± 0.5	8.5 ± 0.7

Table 4.2 – Comparison of fitting parameters for the three latest I-V characteristic of the sample shown in figure **??**. Values preceded by a $*$ are considered unreliable due to their large confidence interval.

In conclusion, we have for the first time successfully depinned the Fermi level in a semiconductor with electrostatic space charge doping. We have succeeded in building a device where Schottky rectifying behavior is obtained by modulating the Fermi level in

the semiconductor on one junction of a metal – semiconductor – metal device so as to create an ohmic junction.

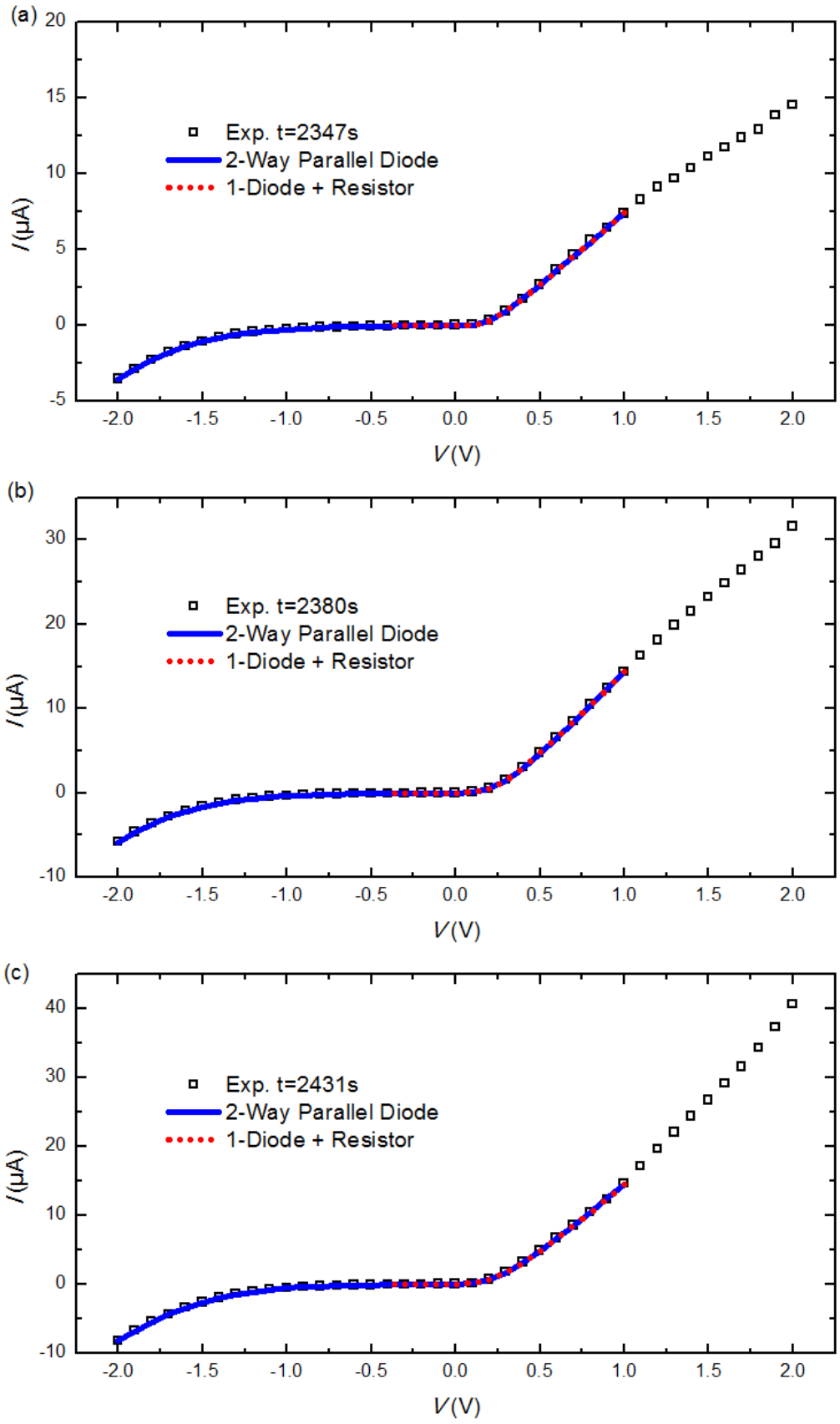

Figure 4.9 – (a), (b) and (c) Three last rectifying I-V characteristics of sample from figure **??** (right) with fits from the 2 way-parallel diode model, and simple diode with series resistor model for comparison. Fits are limited to $V < 1$ V to avoid parts of the curve with heating effects.

Chapter 5

General Conclusions and Perspectives

5.1 General Conclusions

In this thesis, extensive investigative work has been conducted to elucidate the Schottky Barrier Height (SBH) on metal/indium selenide (InSe) contacts and the subsequent changes brought about by electrostatic doping, with an emphasis on modifying the contact characteristics within a Schottky diode framework.

The endeavor began with a focused study on the implications of doping on the SBH within metal/InSe junctions. A suite of devices, incorporating InSe in conjunction with three different metals - gold (Au), aluminum (Al), and silver (Ag) - were fabricated and examined. Through comparing and analysis, the two-way parallel diodes model was concluded to be the most pertinent for the sample devices considered within this body of work. This model proved instrumental in delineating the correlation between the current-voltage (I-V) characteristics of the devices and the fitting model parameters.

Delving deeper, it was ascertained that the Au contacts on InSe failed to make an ideal Schottky barrier. Instead, the I-V characteristics disclosed signs of resistive leakage, hinting at the presence of alternate conductive channels diverging from the traditional Schottky model. Concurrently, the Al contacts showcased quasi-linear contact behavior yet were distinguished by their considerably high resistance. Similarly, the Ag contacts displayed quasi-linear behavior, but their utility was compromised due to Ag's tendency to infiltrate the InSe, potentially undermining the stability and efficacy of the contact over time.

The empirical evidence suggested that altering the metal contacts or employing asymmetric metal configurations did little to significantly shift the I-V characteristics. The I-V results were invariably highly resistive and exhibited a slight non-linearity, deviating from the anticipated Schottky diode behavior. This divergence is potentially attributable to the non-ideal nature of the interface, possibly due to defect-induced gap states, impurity doping, dangling bonds from layer edges, and metal-induced gap states.

Such complexities at the metal-semiconductor interface necessitated the adoption of a nuanced model to fit the measured I-V curves accurately. Consequently, each metal-semiconductor contact was treated as possessing a Schottky contact and an additional resistive pathway. The two-way parallel diode model was adept at fitting the observed I-V curves, allowing for the extraction of significant quantitative parameters, notably accounting for the non-saturating current behavior observed at elevated voltages.

The literature review underscored observation across different metal contacts: the SBH

in metal-InSe devices hovered around the 0.5 eV. This consistency suggests a Fermi level pinning phenomenon that overrides the metal's Fermi level variance and InSe's electron affinity. Doping experiments conducted on asymmetric devices corroborated this, manifesting only minor adjustments in the SBH (ranging from 0.02 to 0.07 eV), despite the Fermi level in InSe samples has been measured to be about 0.3 eV below the conduction band minimum in a device with dual Au contacts [**?**].

In the quest for developing optimal electronic interfaces between metal contacts and InSe, chapter 3 presents a meticulous analysis of the effects of space charge doping on the Schottky Barrier Height (SBH) in metal/InSe junctions. A critical endeavor of this work is the establishment of conditions conducive to ohmic or near-ohmic behavior, particularly at the Au-InSe contact. To realize such conditions, a requisite shift in the Fermi level by approximately 0.3 eV was identified [**?**], which presents challenges due to the comparatively minimal impact of space charge doping. It is posited that the persistence of this challenge stems from the Fermi level's pinning by metal-induced gap states (MIGS) associated with the Au contacts.

To construct a functional Schottky diode using an Au/InSe/Au configuration, it becomes imperative to address the Fermi level pinning phenomenon. Effective SBH modification through space charge doping demands a strategic approach, which includes selectively doping only one interface of the Au-InSe contacts to foster ohmic behavior. The realization of such an approach holds the potential to unlock the full capabilities of Schottky diodes.

The 2-Way Parallel Diodes Model emerges as a robust framework for capturing the complex behavior within the planar devices under study. It underscores the 'non-ideal' nature of the junctions and brings to light a notable observation: the SBH appears to exhibit a degree of metal-type independence. Moreover, the research delineates that electrostatic doping incites only a marginal variation in the SBH, pointing towards the Fermi level's predilection for pinning to MIGS.

For the construction of a Schottky rectifying device, the conditions to establish an ohmic contact through InSe electrostatic doping involve:

1. Doping specificity, wherein only the InSe layer at one junction is doped, while the corresponding layer at the opposing junction remains pristine, maintaining a metal-InSe Schottky barrier. Such specificity can be attained via a 'step' device geometry, leveraging the semiconductor's dielectric screening properties to confine the electrostatic space charge doping within a certain depth.

2. The device design must ensure a current path through both junctions, with current passing vertically through the thin InSe layer at the bottom of the sample and through the thicker InSe at the top.

3. The design and doping must corroborate a significant Fermi level shift within the semiconductor beneath the thin contact. This shift is critical for the de-pinning of the Fermi level and the achievement of an ohmic junction at the intended site.

The insights gleaned from chapter 4 signify advancements in the design and fabrication of InSe Schottky devices, where precise control of contact characteristics is paramount. The work underscores the delicate interplay between doping, device geometry, and material properties in the pursuit of optimizing electronic components. In the devices of Chapter 4, an exploration of doping levels in semiconductor devices has unearthed results concerning the induction of rectifying behavior. A profound increase in current, escalating by two orders of magnitude, has been observed at specific doping thresholds. This considerable enhancement in current results in local heating within the device, leading to a rapid augmentation of charge concentration due to two primary mechanisms: intensified space

charge doping arising from increased ion mobility in glass at higher temperatures, and the generation of free charge carriers within InSe instigated by the thermal elevation.

The occurrence of this positive feedback loop, while indicative of increased device activity, ultimately leads to device failure. This detrimental outcome is evidenced by the manifestation of hysteresis within the I-V measurements and is further substantiated by the physical damage to the devices. The instantaneous nature of the temperature rise, coupled with the significant increase in current, precipitates an overwhelming condition that the device structure cannot withstand, culminating in its burnout.

Despite these challenges, the research presented in this chapter marks a significant achievement: the attainment of true Schottky rectifying behavior. Notably, the device's vertical architecture contributes to a cross-sectional area that is substantially larger-by approximately three orders of magnitude-compared to that of a planar configuration. This structural attribute implies that the horizontal cross-section, rather than the vertical dimension, assumes the role of the effective cross-sectional area within these devices.

This work has successfully accomplished the de-pinning of the Fermi level in a semiconductor through the methodical application of electrostatic space charge doping. The breakthrough lies in the development of a device where true Schottky rectifying behavior is actualized. This is achieved by adeptly modulating the Fermi level at one of the metal-semiconductor junctions, thereby establishing an ohmic junction. The creation of such a device presenting an innovative method to tailor the electronic properties of metal-semiconductor-metal devices and demonstrating the feasibility of Fermi level manipulation through strategic doping processes.

5.2 Perspectives

To further improve performance of InSe-based Schottky devices, there are several perspectives:

1. Investigate the pinning mechanism. This is a challenging proposal as metal-induced gap states (MIGS) are likely very difficult to observe by means other than altering device characteristics. There is no way to observe them via spectroscopy since they are not associated with defect sites. Even defective sites would only produce a very low signal level. However, a detection method could involve using different materials, including both n-doped and p-doped materials, which would require varying doping levels and polarities to counteract the MIGS effect by quenching.
2. Improve control over doping and thermal parameters and prevent device failures. Device failure is a problem to be overcome, but it should not be overly complex to resolve. Control can be achieved through simple modifications to the software that manages doping and I-V measurements to monitor current and hysteresis levels, and to interrupt measurements accordingly when rectifying behavior is achieved. Adding a series current-limiting resistor would also serve as effective protection.
3. Immediate expansion to a different material should focus on transition metal dichalcogenides (TMDs) and MoS_2. Since the initiation of these devices, significant improvements have been made in fabrication techniques, and better devices are likely to be available. An interesting extension would be to use large-area materials obtained by chemical vapor deposition (CVD) to observe the effects of impurities and defects on the pinching of the Fermi level and to evaluate their potential for applications.

Bibliography

[1] Mina Amirmazlaghani, Farshid Raissi, Omid Habibpour, Josip Vukusic, and Jan Stake. Graphene-si schottky ir detector. *IEEE Journal of Quantum electronics*, 49(7):589–594, 2013.

[2] Himani Arora and Artur Erbe. Recent progress in contact, mobility, and encapsulation engineering of inse and gase. *InfoMat*, 3(6):662–693, 2021.

[3] Adrian Balan, Rakesh Kumar, Mohamed Boukhicha, Olivier Beyssac, J C Bouillard, Dario Taverna, William Sacks, Massimiliano Marangolo, Emanuelle Lacaze, Roger Gohler, Walter Escoffier, Jean-Marie Poumirol, and Abhay Shukla. Anodic bonded graphene. *Journal of Physics D*, 43:374013, 2010.

[4] Denis A Bandurin, Anastasia V Tyurnina, Geliang L Yu, Artem Mishchenko, Viktor Zólyomi, Sergey V Morozov, Roshan Krishna Kumar, Roman V Gorbachev, Zakhar R Kudrynskyi, Sergio Pezzini, et al. High electron mobility, quantum hall effect and anomalous optical response in atomically thin inse. *Nature nanotechnology*, 12(3):223–227, 2017.

[5] John Bardeen. Surface states and rectification at a metal semi-conductor contact. *Physical review*, 71(10):717, 1947.

[6] Johan Biscaras, Zhesheng Chen, Andrea Paradisi, and Abhay Shukla. Onset of two-dimensional superconductivity in space charge doped few-layer molybdenum disulfide. *Nature communications*, 6(1):8826, 2015.

[7] Mohamed Boukhicha, Matteo Calandra, Marie-Aude Measson, Ophelie Lancry, and Abhay Shukla. Anharmonic phonons in few-layer mos 2: Raman spectroscopy of ultralow energy compression and shear modes. *Physical Review B*, 87(19):195316, 2013.

[8] L.J. Brillson. The structure and properties of metal-semiconductor interfaces. *Surface Science Reports*, 2(2):123–326, 1982.

[9] Valentin N Brudnyi, S Yu Sarkisov, and Alexey V Kosobutsky. Electronic properties of gase, inse, gas and gate layered semiconductors: charge neutrality level and interface barrier heights. *Semiconductor Science and Technology*, 30(11):115019, 2015.

[10] Thomas Brumme, Matteo Calandra, and Francesco Mauri. First-principles theory of field-effect doping in transition-metal dichalcogenides: Structural properties, electronic structure, hall coefficient, and electrical conductivity. *Physical Review B*, 91(15):155436, 2015.

[11] Han-Ching Chang, Chien-Liang Tu, Kuang-I Lin, Jiang Pu, Taishi Takenobu, Chien-Nan Hsiao, and Chang-Hsiao Chen. Synthesis of large-area inse monolayers by chemical vapor deposition. *Small*, 14(39):1802351, 2018.

[12] Ren-Jie Chang, Haijie Tan, Xiaochen Wang, Benjamin Porter, Tongxin Chen, Yuewen Sheng, Yingqiu Zhou, Hefu Huang, Harish Bhaskaran, and Jamie H. Warner. High-performance all 2d-layered tin disulfide: Graphene photodetecting transistors with thickness-controlled interface dynamics. *ACS Applied Materials & Interfaces*, 10(15):13002–13010, 2018. PMID: 29630341.

[13] Pengfei Chen, Neng Li, Xingzhu Chen, Wee-Jun Ong, and Xiujian Zhao. The rising star of 2d black phosphorus beyond graphene: synthesis, properties and electronic applications. *2D Materials*, 5(1):014002, 2017.

[14] Z. Chen, K. Gacem, M. Boukhicha, J. Biscaras, and A. Shukla. Anodic bonded 2D semiconductors: from synthesis to device fabrication. *Nanotechnology*, 24(41):415708, 2013.

[15] Zhesheng Chen. *Novel two dimensional material devices: from fabrication to photodetection*. PhD thesis, Université Pierre et Marie Curie-Paris VI, 2015.

[16] Zhesheng Chen, Johan Biscaras, and Abhay Shukla. A high performance graphene/few-layer inse photo-detector. *Nanoscale*, 7(14):5981–5986, 2015.

[17] Zhesheng Chen, Johan Biscaras, and Abhay Shukla. Optimal light harvesting in 2d semiconductor heterostructures. *2D Materials*, 4(2):025115, 2017.

[18] Zhesheng Chen, Christine Giorgetti, Jelena Sjakste, Raphael Cabouat, Valérie Véniard, Zailan Zhang, Amina Taleb-Ibrahimi, Evangelos Papalazarou, Marino Marsi, Abhay Shukla, et al. Ultrafast electron dynamics reveal the high potential of inse for hot-carrier optoelectronics. *Physical Review B*, 97(24):241201, 2018.

[19] Zhesheng Chen, Jelena Sjakste, Jingwei Dong, Amina Taleb-Ibrahimi, Jean-Pascal Rueff, Abhay Shukla, Jacques Peretti, Evangelos Papalazarou, Marino Marsi, and Luca Perfetti. Ultrafast dynamics of hot carriers in a quasi–two-dimensional electron gas on inse. *Proceedings of the National Academy of Sciences*, 117(36):21962–21967, 2020.

[20] Zhesheng Chen, Zailan Zhang, Johan Biscaras, and Abhay Shukla. A high performance self-driven photodetector based on a graphene/inse/mos 2 vertical heterostructure. *Journal of Materials Chemistry C*, 6(45):12407–12412, 2018.

[21] Liang Cheng, Jingjing Liu, Xing Gu, Hua Gong, Xiaoze Shi, Teng Liu, Chao Wang, Xiaoyong Wang, Gang Liu, Huaiyong Xing, et al. Pegylated ws2 nanosheets as a multifunctional theranostic agent for in vivo dual-modal ct/photoacoustic imaging guided photothermal therapy. *Advanced materials*, 26(12):1886–1893, 2014.

[22] Manish Chhowalla, Zhongfan Liu, and Hua Zhang. Two-dimensional transition metal dichalcogenide (tmd) nanosheets. *Chemical Society Reviews*, 44(9):2584–2586, 2015.

[23] Manish Chhowalla, Hyeon Suk Shin, Goki Eda, Lain-Jong Li, Kian Ping Loh, and Hua Zhang. The chemistry of two-dimensional layered transition metal dichalcogenide nanosheets. *Nature chemistry*, 5(4):263–275, 2013.

[24] D Chiba, M Yamanouchi, F Matsukura, and H Ohno. Electrical manipulation of magnetization reversal in a ferromagnetic semiconductor. *Science*, 301(5635):943–945, 2003.

[25] A. M. Cowley and S. M. Sze. Surface States and Barrier Height of Metal-Semiconductor Systems. *Journal of Applied Physics*, 36(10):3212–3220, 10 1965.

[26] Nicola Curreli, Michele Serri, Davide Spirito, Emanuele Lago, Elisa Petroni, Beatriz Martín-García, Antonio Politano, Bekir Gürbulak, Songül Duman, Roman Krahne,

et al. Liquid phase exfoliated indium selenide based highly sensitive photodetectors. *Advanced Functional Materials*, 30(13):1908427, 2020.

[27] P Gomes da Costa, RG Dandrea, RF Wallis, and M Balkanski. First-principles study of the electronic structure of γ-inse and β-inse. *Physical Review B*, 48(19):14135, 1993.

[28] Mingjin Dai, Hongyu Chen, Rui Feng, Wei Feng, Yunxia Hu, Huihui Yang, Guangbo Liu, Xiaoshuang Chen, Jia Zhang, Cheng-Yan Xu, and PingAn Hu. A dual-band multilayer inse self-powered photodetector with high performance induced by surface plasmon resonance and asymmetric schottky junction. *ACS Nano*, 12(8):8739–8747, 2018. PMID: 30095888.

[29] Mingjin Dai, Caifang Gao, Qianfan Nie, Qi-Jie Wang, Yen-Fu Lin, Junhao Chu, and Wenwu Li. Properties, synthesis, and device applications of 2d layered inse. *Advanced Materials Technologies*, 7(12):2200321, 2022.

[30] Antonio Di Bartolomeo. Graphene schottky diodes: An experimental review of the rectifying graphene/semiconductor heterojunction. *Physics Reports*, 606:1–58, 2016. Graphene Schottky diodes: An experimental review of the rectifying graphene/semiconductor heterojunction.

[31] Massimo Di Giulio, Gioacchino Micocci, Angelo Rizzo, and Antonio Tepore. Photovoltaic effect in gold-indium selenide schottky barriers. *Journal of applied physics*, 54(10):5839–5843, 1983.

[32] Chengye Dong, Li-Syuan Lu, Yu-Chuan Lin, and Joshua A Robinson. Air-stable, large-area 2d metals and semiconductors. *ACS Nanoscience Au*, 2024.

[33] Masayoshi Esashi. Wafer level packaging of mems. *Journal of Micromechanics and Microengineering*, 18(7):073001, 2008.

[34] Leonid A Falkovsky. Optical properties of graphene. In *Journal of Physics: conference series*, volume 129, page 012004. IOP Publishing, 2008.

[35] Wei Feng, Wei Zheng, Wenwu Cao, and PingAn Hu. Back gated multilayer inse transistors with enhanced carrier mobilities via the suppression of carrier scattering from a dielectric interface. *Advanced materials*, 26(38):6587–6593, 2014.

[36] Wei Feng, Xin Zhou, Wei Quan Tian, Wei Zheng, and PingAn Hu. Performance improvement of multilayer inse transistors with optimized metal contacts. *Physical Chemistry Chemical Physics*, 17(5):3653–3658, 2015.

[37] Karim Gacem, Mohamed Boukhicha, Zhesheng Chen, and Abhay Shukla. High quality 2d crystals made by anodic bonding: a general technique for layered materials. *Nanotechnology*, 23(50):505709, nov 2012.

[38] Chuanhui Gong, Yuxi Zhang, Wei Chen, Junwei Chu, Tianyu Lei, Junru Pu, Liping Dai, Chunyang Wu, Yuhua Cheng, Tianyou Zhai, et al. Electronic and optoelectronic applications based on 2d novel anisotropic transition metal dichalcogenides. *Advanced Science*, 4(12):1700231, 2017.

[39] I Grimaldi, T Gerace, MM Pipita, ID Perrotta, F Ciuchi, H Berger, M Papagno, M Castriota, and D Pacilé. Structural investigation of inse layered semiconductors. *Solid State Communications*, 311:113855, 2020.

[40] Yuzheng Guo and John Robertson. Band structure, band offsets, substitutional doping, and schottky barriers of bulk and monolayer inse. *Physical Review Materials*, 1(4):044004, 2017.

[41] Volker Heine. Theory of surface states. *Phys. Rev.*, 138:A1689–A1696, Jun 1965.

[42] Hugo Henck, Debora Pierucci, Jihene Zribi, Federico Bisti, Evangelos Papalazarou, Jean-Christophe Girard, Julien Chaste, François Bertran, Patrick Le Fèvre, Fausto Sirotti, et al. Evidence of direct electronic band gap in two-dimensional van der waals indium selenide crystals. *Physical Review Materials*, 3(3):034004, 2019.

[43] Ching-Hwa Ho and Yun-Ju Chu. Bending photoluminescence and surface photovoltaic effect on multilayer inse 2d microplate crystals. *Advanced Optical Materials*, 3(12):1750–1758, 2015.

[44] Siqi Hu, Qiao Zhang, Xiaoguang Luo, Xutao Zhang, Tao Wang, Yingchun Cheng, Wanqi Jie, Jianlin Zhao, Ting Mei, and Xuetao Gan. Au–inse van der waals schottky junctions with ultralow reverse current and high photosensitivity. *Nanoscale*, 12(6):4094–4100, 2020.

[45] Yonghong Hu, Shengli Zhang, Shaofa Sun, Meiqiu Xie, Bo Cai, and Haibo Zeng. Gese monolayer semiconductor with tunable direct band gap and small carrier effective mass. *Applied Physics Letters*, 107(12), 2015.

[46] Zi-Yu Hu, Kai-Yue Li, Yong Lu, Yan Huang, and Xiao-Hong Shao. High thermoelectric performances of monolayer snse allotropes. *Nanoscale*, 9(41):16093–16100, 2017.

[47] Shengxi Huang and Xi Ling. Black phosphorus: optical characterization, properties and applications. *Small*, 13(38):1700823, 2017.

[48] Wenjuan Huang, Lin Gan, Haotian Yang, Nan Zhou, Renyan Wang, Wanhui Wu, Huiqiao Li, Ying Ma, Haibo Zeng, and Tianyou Zhai. Controlled synthesis of ultrathin 2d β-in2s3 with broadband photoresponse by chemical vapor deposition. *Advanced Functional Materials*, 27(36):1702448, 2017.

[49] Xiao Huang, Zhiyuan Zeng, and Hua Zhang. Metal dichalcogenide nanosheets: preparation, properties and applications. *Chemical Society Reviews*, 42(5):1934–1946, 2013.

[50] Muhammad Hussain, Syed Hassan Abbas Jaffery, Asif Ali, Cong Dinh Nguyen, Sikandar Aftab, Muhammad Riaz, Sohail Abbas, Sajjad Hussain, Yongho Seo, and Jongwan Jung. NIR self-powered photodetection and gate tunable rectification behavior in 2d GeSe/MoSe2 heterojunction diode. 11.

[51] T Ikari, S Shigetomi, and K Hashimoto. Crystal structure and raman spectra of inse. *physica status solidi (b)*, 111(2):477–481, 1982.

[52] Raisul Islam, Gautam Shine, and Krishna C Saraswat. Schottky barrier height reduction for holes by fermi level depinning using metal/nickel oxide/silicon contacts. *Applied Physics Letters*, 105(18), 2014.

[53] Hamad Rahman Jappor. Electronic structure of novel gas/gase heterostructures based on gas and gase monolayers. *Physica. B, Condensed Matter*, 524:109–117, 2017.

[54] Jianfeng Jiang, Lin Xu, Chenguang Qiu, and Lian-Mao Peng. Ballistic two-dimensional inse transistors. *Nature*, 616(7957):470–475, 2023.

[55] Joohoon Kang, Spencer A Wells, Vinod K Sangwan, David Lam, Xiaolong Liu, Jan Luxa, Zdeněk Sofer, and Mark C Hersam. Solution-based processing of optoelectronically active indium selenide. *Advanced Materials*, 30(38):1802990, 2018.

[56] Sudiksha Khadka, Thushan E Wickramasinghe, Miles Lindquist, Ruhi Thorat, Shrouq H Aleithan, Martin E Kordesch, and Eric Stinaff. As-grown two-dimensional mos2 based photodetectors with naturally formed contacts. *Applied Physics Letters*, 110(26), 2017.

[57] Changsik Kim, Inyong Moon, Daeyeong Lee, Min Sup Choi, Faisal Ahmed, Seunggeol Nam, Yeonchoo Cho, Hyeon-Jin Shin, Seongjun Park, and Won Jong Yoo. Fermi level pinning at electrical metal contacts of monolayer molybdenum dichalcogenides. *ACS nano*, 11(2):1588–1596, 2017.

[58] AA Klyukanov, PA Gashin, and R Scurtu. Ideality factor in transport theory of schottky barrier diodes. *arXiv preprint arXiv:1204.0335*, 2012.

[59] Summayya Kouser, Anagha Thannikoth, Uttam Gupta, Umesh V Waghmare, and CNR Rao. 2d-gas as a photocatalyst for water splitting to produce h2. *Small*, 11(36):4723–4730, 2015.

[60] Hai Li, Gang Lu, Yanlong Wang, Zongyou Yin, Chunxiao Cong, Qiyuan He, Lu Wang, Feng Ding, Ting Yu, and Hua Zhang. Mechanical exfoliation and characterization of single-and few-layer nanosheets of wse2, tas2, and tase2. *small*, 9(11):1974–1981, 2013.

[61] Zhong Lin, Amber McCreary, Natalie Briggs, Shruti Subramanian, Kehao Zhang, Yifan Sun, Xufan Li, Nicholas J Borys, Hongtao Yuan, Susan K Fullerton-Shirey, et al. 2d materials advances: from large scale synthesis and controlled heterostructures to improved characterization techniques, defects and applications. *2D Materials*, 3(4):042001, 2016.

[62] Teng Liu, Chao Wang, Xing Gu, Hua Gong, Liang Cheng, Xiaoze Shi, Liangzhu Feng, Baoquan Sun, and Zhuang Liu. Drug delivery with pegylated mos2 nanosheets for combined photothermal and chemotherapy of cancer. *Advanced Materials (Deerfield Beach, Fla.)*, 26(21):3433–3440, 2014.

[63] Xiaochi Liu, Min Sup Choi, Euyheon Hwang, Won Jong Yoo, and Jian Sun. Fermi level pinning dependent 2d semiconductor devices: Challenges and prospects. *Advanced Materials*, 34(15):2108425, 2022.

[64] Yuan Liu, Jian Guo, Enbo Zhu, Lei Liao, Sung-Joon Lee, Mengning Ding, Imran Shakir, Vincent Gambin, Yu Huang, and Xiangfeng Duan. Approaching the schottky–mott limit in van der waals metal–semiconductor junctions. *Nature*, 557(7707):696–700, 2018.

[65] Wengang Luo, Yufei Cao, Pingan Hu, Kaiming Cai, Qi Feng, Faguang Yan, Tengfei Yan, Xinhui Zhang, and Kaiyou Wang. Gate tuning of high-performance inse-based photodetectors using graphene electrodes. *Advanced Optical Materials*, 3(10):1418–1423, 2015.

[66] L Andrew Lyon, Christine D Keating, Audrey P Fox, Bonnie E Baker, Lin He, Sheila R Nicewarner, Shawn P Mulvaney, and Michael J Natan. Raman spectroscopy. *Analytical Chemistry*, 70(12):341–362, 1998.

[67] Yandong Ma, Ying Dai, Meng Guo, Lin Yu, and Baibiao Huang. Tunable electronic and dielectric behavior of gas and gase monolayers. *Physical Chemistry Chemical Physics*, 15(19):7098–7105, 2013.

[68] Waleed E. Mahmoud, A.A. Al-Ghamdi, W. Shirbeeny, F.S. Al-Hazmi, and Shamshad A. Khan. Electrochemical growth of gase nanostructures and their schottky barrier characteristics. *Superlattices and Microstructures*, 63:162–167, 2013.

[69] C Malavika, R Anu Roshini, RS Surya Kanthi, and ES Kannan. Single crystal flake parameters of mos2 and mose2 exfoliated using anodic bonding technique and its potential in rapid prototyping. *Journal of Physics Communications*, 4(10):105015, 2020.

[70] R Mamy, X Zaoui, J Barrau, and A Chevy. Au/inse schottky barrier height determination. *Revue de physique appliquée*, 25(9):947–950, 1990.

[71] ED Marshall, M Murakami, and LJ Brillson. Contacts to semiconductors, 1993.

[72] Aishani Mazumder, Taimur Ahmed, Edwin Mayes, Sherif Abdulkader Tawfik, Salvy P Russo, Mei Xian Low, Abhishek Ranjan, Sivacarendran Balendhran, and Sumeet Walia. Nonvolatile resistive switching in layered inse via electrochemical cation diffusion. *Advanced Electronic Materials*, 8(4):2100999, 2022.

[73] F Molitor, J Güttinger, C Stampfer, S Dröscher, A Jacobsen, T Ihn, and K Ensslin. Electronic properties of graphene nanostructures. *Journal of Physics: Condensed Matter*, 23(24):243201, may 2011.

[74] Winfried Mönch. On the present understanding of schottky contacts. *Festkörperprobleme 26: Plenary Lectures of the Divisions "Semiconductor Physics" "Dynamics and Statistical Mechanics" "Low Temperature Physics" "Magnetism" "Metal Physics" "Thin Films" "Surface Physics" "Vacuum Technology" of the German Physical Society (DPG) Freudenstadt, April 7... 11, 1986*, pages 67–88, 1986.

[75] Kiana Montazeri, Marc Currie, Louisiane Verger, Pouya Dianat, Michel W Barsoum, and Bahram Nabet. Beyond gold: Spin-coated ti3c2-based mxene photodetectors. *Advanced Materials*, 31(43):1903271, 2019.

[76] Shawn P Mulvaney and Christine D Keating. Raman spectroscopy. *Analytical Chemistry*, 72(12):145–158, 2000.

[77] Michael Naguib, Vadym N Mochalin, Michel W Barsoum, and Yury Gogotsi. Two-dimensional materials: 25th anniversary article: Mxenes: a new family of two-dimensional materials (adv. mater. 7/2014). *Advanced Materials*, 26(7):982–982, 2014.

[78] Rahul Raveendran Nair, Peter Blake, Alexander N Grigorenko, Konstantin S Novoselov, Tim J Booth, Tobias Stauber, Nuno MR Peres, and Andre K Geim. Fine structure constant defines visual transparency of graphene. *science*, 320(5881):1308–1308, 2008.

[79] Dipali Nayak and R Thangavel. A density functional theory study on the strain modulated electronic and photocatalytic properties of a gase monolayer for photocatalytic water splitting and artificial photosynthesis. *New Journal of Chemistry*, 46(23):11447–11461, 2022.

[80] K. S. Novoselov, A. K. Geim, S. V. Morozov, D. Jiang, Y. Zhang, S. V. Dubonos, I. V. Grigorieva, and A. A. Firsov. Electric field effect in atomically thin carbon films. *Science*, 306(5696):666–669, 2004.

[81] Jong Sik Oh, Kyong Nam Kim, and Geun Young Yeom. Graphene doping methods and device applications. *Journal of nanoscience and nanotechnology*, 14(2):1120–1133, 2014.

[82] F.A. Padovani and R. Stratton. Field and thermionic-field emission in schottky barriers. *Solid-State Electronics*, 9(7):695–707, 1966.

[83] Andrea Paradisi, Johan Biscaras, and Abhay Shukla. Space charge induced electrostatic doping of two-dimensional materials: graphene as a case study. *Applied Physics Letters*, 107(14), 2015.

[84] Martin Parenteau and Cosmo Carlone. Influence of temperature and pressure on the electronic transitions in sns and snse semiconductors. *Physical Review B*, 41(8):5227, 1990.

[85] Soohyung Park, Thorsten Schultz, Dongguen Shin, Niklas Mutz, Areej Aljarb, Hee Seong Kang, Chul-Ho Lee, Lain-Jong Li, Xiaomin Xu, Vincent Tung, et al. The schottky–mott rule expanded for two-dimensional semiconductors: Influence of substrate dielectric screening. *ACS nano*, 15(9):14794–14803, 2021.

[86] Qiong Peng, Rui Xiong, Baisheng Sa, Jian Zhou, Cuilian Wen, Bo Wu, Masakazu Anpo, and Zhimei Sun. Computational mining of photocatalysts for water splitting hydrogen production: two-dimensional inse-family monolayers. *Catalysis Science & Technology*, 7(13):2744–2752, 2017.

[87] Elisa Petroni, Emanuele Lago, Sebastiano Bellani, Danil W Boukhvalov, Antonio Politano, Bekir Gürbulak, Songül Duman, Mirko Prato, Silvia Gentiluomo, Reinier Oropesa-Nuñez, et al. Liquid-phase exfoliated indium–selenide flakes and their application in hydrogen evolution reaction. *Small*, 14(26):1800749, 2018.

[88] Huynh V Phuc, Victor V Ilyasov, Nguyen N Hieu, Bin Amin, and Chuong V Nguyen. Van der waals graphene/g-gase heterostructure: Tuning the electronic properties and schottky barrier by interlayer coupling, biaxial strain, and electric gating. *Journal of Alloys and Compounds*, 750:765–773, 2018.

[89] CF Quate. The afm as a tool for surface imaging. *Surface Science*, 299:980–995, 1994.

[90] Arne Quellmalz, Xiaojing Wang, Simon Sawallich, Burkay Uzlu, Martin Otto, Stefan Wagner, Zhenxing Wang, Maximilian Prechtl, Oliver Hartwig, Siwei Luo, et al. Large-area integration of two-dimensional materials and their heterostructures by wafer bonding. *Nature communications*, 12(1):917, 2021.

[91] Altaf Ur Rahman, Juliana M Morbec, Gul Rahman, and Peter Kratzer. Commensurate versus incommensurate heterostructures of group-iii monochalcogenides. *Physical Review Materials*, 2(9):094002, 2018.

[92] Ahmed A Ramadan, Robert D Gould, and Ahmed Ashour. On the van der pauw method of resistivity measurements. *Thin solid films*, 239(2):272–275, 1994.

[93] Emlyn Huw Rhoderick and Richard H Williams. *Metal-semiconductor contacts*, volume 129. Clarendon press Oxford, 1988.

[94] Christopher R Ryder, Joshua D Wood, Spencer A Wells, and Mark C Hersam. Chemically tailoring semiconducting two-dimensional transition metal dichalcogenides and black phosphorus. *ACS nano*, 10(4):3900–3917, 2016.

[95] Nihit Saigal. *Aspects of electronic structure of bulk and monolayer MoS2 studied using optical spectroscopy*. PhD thesis, Master's thesis, Tata Institute of Fundamental Research, 2016.

[96] Otto F Sankey, Roland E Allen, Shang-Fen Ren, and John D Dow. Dangling bonds and schottky barriers. *Journal of Vacuum Science & Technology B: Microelectronics Processing and Phenomena*, 3(4):1162–1166, 1985.

[97] R Schlaf, S Tiefenbacher, O Lang, C Pettenkofer, and W Jaegermann. Van der waals epitaxy of thin inse films on mote2. *Surface science*, 303(1-2):L343–L347, 1994.

[98] Dieter K Schroder. *Semiconductor material and device characterization*. John Wiley & Sons, 2015.

[99] A Segura, JP Guesdon, JM Besson, and A Chevy. Photovoltaic effect in inse-application to solar energy conversion. *Revue de Physique Appliquée*, 14(1):253–257, 1979.

[100] Mashiyat Sumaiya Shawkat, Shihab Bin Hafiz, Molla Manjurul Islam, Sohrab Alex Mofid, Mohammad M. Al Mahfuz, Aritra Biswas, Hee-Suk Chung, Emmanuel Okogbue, Tae-Jun Ko, Debashis Chanda, Tania Roy, Dong-Kyun Ko, and Yeonwoong Jung. Scalable van der waals two-dimensional ptte2 layers integrated onto silicon for efficient near-to-mid infrared photodetection. *ACS Applied Materials & Interfaces*, 13(13):15542–15550, 2021. PMID: 33755434.

[101] Bowen Shi, Yangyang Wang, Jingzhen Li, Xiuying Zhang, Jiahuan Yan, Shiqi Liu, Jie Yang, Yuanyuan Pan, Han Zhang, Jinbo Yang, et al. n-type ohmic contact and p-type schottky contact of monolayer inse transistors. *Physical Chemistry Chemical Physics*, 20(38):24641–24651, 2018.

[102] Yumeng Shi, Jing-Kai Huang, Limin Jin, Yu-Te Hsu, Siu Fung Yu, Lain-Jong Li, and Hui Ying Yang. Selective decoration of au nanoparticles on monolayer mos2 single crystals. *Scientific reports*, 3(1):1839, 2013.

[103] Dong Hee Shin and Suk-Ho Choi. Graphene-based semiconductor heterostructures for photodetectors. *Micromachines*, 9(7):350, 2018.

[104] Edoardo Sterpetti, Johan Biscaras, Andreas Erb, and Abhay Shukla. Comprehensive phase diagram of two-dimensional space charge doped bi2sr2cacu2o8+ x. *Nature communications*, 8(1):2060, 2017.

[105] Guoxiong Su, Viktor G Hadjiev, Phillip E Loya, Jing Zhang, Sidong Lei, Surendra Maharjan, Pei Dong, Pulickel M. Ajayan, Jun Lou, and Haibing Peng. Chemical vapor deposition of thin crystals of layered semiconductor sns2 for fast photodetection application. *Nano letters*, 15(1):506–513, 2015.

[106] Sukrit Sucharitakul, Nicholas J Goble, U Rajesh Kumar, Raman Sankar, Zachary A Bogorad, Fang-Cheng Chou, Yit-Tsong Chen, and Xuan PA Gao. Intrinsic electron mobility exceeding 103 cm2/(v s) in multilayer inse fets. *Nano letters*, 15(6):3815–3819, 2015.

[107] Yuanhui Sun, Shulin Luo, Xin-Gang Zhao, Koushik Biswas, Song-Lin Li, and Lijun Zhang. Inse: a two-dimensional material with strong interlayer coupling. *Nanoscale*, 10(17):7991–7998, 2018.

[108] Simon M Sze, Yiming Li, and Kwok K Ng. *Physics of semiconductor devices*. John wiley & sons, 2021.

[109] Srinivasa Reddy Tamalampudi, Yi-Ying Lu, Rajesh Kumar U, Raman Sankar, Chun-Da Liao, Che-Hsuan Cheng, Fang Cheng Chou, and Yit-Tsong Chen. High performance and bendable few-layered inse photodetectors with broad spectral response. *Nano letters*, 14(5):2800–2806, 2014.

[110] Chaoliang Tan and Hua Zhang. Two-dimensional transition metal dichalcogenide nanosheet-based composites. *Chemical Society Reviews*, 44(9):2713–2731, 2015.

[111] Jakub Tworzydło, Björn Trauzettel, Misha Titov, Adam Rycerz, and Carlo WJ Beenakker. Sub-poissonian shot noise in graphene. *Physical review letters*, 96(24):246802, 2006.

[112] George Wallis and Daniel I Pomerantz. Field assisted glass-metal sealing. *Journal of applied physics*, 40(10):3946–3949, 1969.

[113] Fang Wang, Johan Biscaras, Andreas Erb, and Abhay Shukla. Superconductor-insulator transition in space charge doped one unit cell bi2. 1sr1. 9cacu2o8+ x. *Nature Communications*, 12(1):2926, 2021.

[114] Feng Wang, Zhenxing Wang, Lei Yin, Ruiqing Cheng, Junjun Wang, Yao Wen, Tofik Ahmed Shifa, Fengmei Wang, Yu Zhang, Xueying Zhan, et al. 2d library beyond graphene and transition metal dichalcogenides: a focus on photodetection. *Chemical Society Reviews*, 47(16):6296–6341, 2018.

[115] Xiaoya Wang, Haiyan Nan, Wei Dai, Qin Lin, Zheng Liu, Xiaofeng Gu, Zhenhua Ni, and Shaoqing Xiao. Optical studies of the thermal stability of inse nanosheets. *Applied Surface Science*, 467-468:860–867, 2019.

[116] Yang Wang, Peisong Wu, Zhen Wang, Man Luo, Fang Zhong, Xun Ge, Kun Zhang, Meng Peng, Yan Ye, Qing Li, Haonan Ge, Jiafu Ye, Ting He, Yunfeng Chen, Tengfei Xu, Chenhui Yu, Yueming Wang, Zhigao Hu, Xiaohao Zhou, Chongxin Shan, Mingsheng Long, Peng Wang, Peng Zhou, and Weida Hu. Air-stable low-symmetry narrow-bandgap 2d sulfide niobium for polarization photodetection. *Advanced Materials*, 32(45):2005037, 2020.

[117] Wei Wei, Ying Dai, Chengwang Niu, Xiao Li, Yandong Ma, and Baibiao Huang. Electronic properties of two-dimensional van der waals gas/gase heterostructures. *Journal of Materials Chemistry C*, 3(43):11548–11554, 2015.

[118] Jing Wu, Gavin Kok Wai Koon, Du Xiang, Cheng Han, Chee Tat Toh, Eeshan S Kulkarni, Ivan Verzhbitskiy, Alexandra Carvalho, Aleksandr S Rodin, Steven P Koenig, et al. Colossal ultraviolet photoresponsivity of few-layer black phosphorus. *ACS nano*, 9(8):8070–8077, 2015.

[119] Wanhui Wu, Qi Zhang, Xing Zhou, Liang Li, Jianwei Su, Fakun Wang, and Tianyou Zhai. Self-powered photovoltaic photodetector established on lateral monolayer mos2-ws2 heterostructures. *Nano Energy*, 51:45–53, 2018.

[120] Yao Wu, Xin Yan, Xia Zhang, and Xiaomin Ren. A monolayer graphene/gaas nanowire array schottky junction self-powered photodetector. *Applied Physics Letters*, 109(18), 2016.

[121] Ying Xie, Bo Zhang, Shuxian Wang, Dong Wang, Aizhu Wang, Zeyan Wang, Haohai Yu, Huaijin Zhang, Yanxue Chen, Mingwen Zhao, et al. Ultrabroadband mos2 photodetector with spectral response from 445 to 2717 nm. *Advanced Materials*, 29(17):1605972, 2017.

[122] Chen Xu, Shengjie Peng, Chaoliang Tan, Huixiang Ang, Huiteng Tan, Hua Zhang, and Qingyu Yan. Ultrathin s-doped mose 2 nanosheets for efficient hydrogen evolution. *Journal of Materials Chemistry A*, 2(16):5597–5601, 2014.

[123] Kun Xu, Chen Xu, Yiyang Xie, Jun Deng, Yanxu Zhu, Weiling Guo, Meng Xun, Kenneth BK Teo, Hongda Chen, and Jie Sun. Graphene gan-based schottky ultraviolet detectors. *IEEE Transactions on Electron Devices*, 62(9):2802–2808, 2015.

[124] Wei Yan, Vivek Raj Shresha, Quentin Jeangros, Nima Sefidmooye Azar, Sivacarendran Balendhran, Christophe Ballif, Kenneth Crozier, and James Bullock. Spectrally selective mid-wave infrared detection using fabry-pérot cavity enhanced black phosphorus 2d photodiodes. *ACS nano*, 14(10):13645–13651, 2020.

[125] Hung-Wei Yang, Ho-Feng Hsieh, Ruei-San Chen, Ching-Hwa Ho, Kuei-Yi Lee, and Liang-Chiun Chao. Ultraefficient ultraviolet and visible light sensing and ohmic contacts in high-mobility inse nanoflake photodetectors fabricated by the focused ion beam technique. *ACS applied materials & interfaces*, 10(6):5740–5749, 2018.

[126] Jieun Yang, Damien Voiry, Seong Joon Ahn, Dongwoo Kang, Ah Young Kim, Manish Chhowalla, and Hyeon Suk Shin. Two-dimensional hybrid nanosheets of tungsten

disulfide and reduced graphene oxide as catalysts for enhanced hydrogen evolution. *Angew. Chem. Int. Ed*, 52(51):13751–13754, 2013.

[127] Shengxue Yang, Yan Li, Xiaozhou Wang, Nengjie Huo, Jian-Bai Xia, Shu-Shen Li, and Jingbo Li. High performance few-layer gas photodetector and its unique photoresponse in different gas environments. *Nanoscale*, 6(5):2582–2587, 2014.

[128] Zhibin Yang, Wenjing Jie, Chun-Hin Mak, Shenghuang Lin, Huihong Lin, Xianfeng Yang, Feng Yan, Shu Ping Lau, and Jianhua Hao. Wafer-scale synthesis of high-quality semiconducting two-dimensional layered inse with broadband photoresponse. *ACS nano*, 11(4):4225–4236, 2017.

[129] Xinmao Yin, Chi Sin Tang, Yue Zheng, Jing Gao, Jing Wu, Hua Zhang, Manish Chhowalla, Wei Chen, and Andrew TS Wee. Recent developments in 2d transition metal dichalcogenides: phase transition and applications of the (quasi-) metallic phases. *Chemical Society Reviews*, 50(18):10087–10115, 2021.

[130] Zongyou Yin, Xiao Zhang, Yongqing Cai, Junze Chen, Jen It Wong, Yee-Yan Tay, Jianwei Chai, Jumiati Wu, Zhiyuan Zeng, Bing Zheng, et al. Preparation of mos2–moo3 hybrid nanomaterials for light-emitting diodes. *Angewandte Chemie International Edition*, 53(46):12560–12565, 2014.

[131] Young-Jun Yu, Yue Zhao, Sunmin Ryu, Louis E Brus, Kwang S Kim, and Philip Kim. Tuning the graphene work function by electric field effect. *Nano letters*, 9(10):3430–3434, 2009.

[132] Zhiyuan Zeng, Chaoliang Tan, Xiao Huang, Shuyu Bao, and Hua Zhang. Growth of noble metal nanoparticles on single-layer tis 2 and tas 2 nanosheets for hydrogen evolution reaction. *Energy & Environmental Science*, 7(2):797–803, 2014.

[133] Hang Zhang, Junxiang Huang, Yongwei Wang, Rui Liu, Xiulan Huai, Jingjing Jiang, and Chantelle Anfuso. Atomic force microscopy for two-dimensional materials: A tutorial review. *Optics Communications*, 406:3–17, 2018.

[134] Shengli Zhang, Ning Wang, Shangguo Liu, Shiping Huang, Wenhan Zhou, Bo Cai, Meiqiu Xie, Qun Yang, Xianping Chen, and Haibo Zeng. Two-dimensional ges with tunable electronic properties via external electric field and strain. *Nanotechnology*, 27(27):274001, 2016.

[135] Songqing Zhang, Junliang Liu, Maxwell Merle Kirchner, Han Wang, Yongling Ren, and Wen Lei. Two-dimensional heterostructures and their device applications: progress, challenges and opportunities. *Journal of Physics D: Applied Physics*, 54(43):433001, 2021.

[136] YI Zhang, Luyao Zhang, and Chongwu Zhou. Review of chemical vapor deposition of graphene and related applications. *Accounts of chemical research*, 46(10):2329–2339, 2013.

[137] Zailan Zhang, Zhesheng Chen, Meryem Bouaziz, Christine Giorgetti, Hemian Yi, Jose Avila, Bingbing Tian, Abhay Shukla, Luca Perfetti, Dianyuan Fan, et al. Direct observation of band gap renormalization in layered indium selenide. *ACS nano*, 13(11):13486–13491, 2019.

[138] Qinghua Zhao, Wanqi Jie, Tao Wang, Andres Castellanos-Gomez, and Riccardo Frisenda. Inse schottky diodes based on van der waals contacts. *Advanced Functional Materials*, 30(24):2001307, 2020.

[139] Zhaoqiang Zheng, Jiandong Yao, Lianfeng Zhu, Wei Jiang, Bing Wang, Guowei Yang, and Jingbo Li. Tin dioxide quantum dots coupled with graphene for high-

performance bulk-silicon schottky photodetector. *Materials Horizons*, 5(4):727–737, 2018.

[140] Jiadong Zhou, Jia Shi, Qingsheng Zeng, Yu Chen, Lin Niu, Fucai Liu, Ting Yu, Kazu Suenaga, Xinfeng Liu, Junhao Lin, et al. Inse monolayer: synthesis, structure and ultra-high second-harmonic generation. *2D Materials*, 5(2):025019, 2018.

[141] Xing Zhou, Xiaozong Hu, Shasha Zhou, Hongyue Song, Qi Zhang, Lejing Pi, Liang Li, Huiqiao Li, Jingtao Lü, and Tianyou Zhai. Tunneling diode based on wse2/sns2 heterostructure incorporating high detectivity and responsivity. *Advanced Materials*, 30(7):1703286, 2018.

[142] Xiaona Zhu, Ran Ding, Zegao Wang, Yin Wang, Xudong Guo, Zhengxun Song, Zuobin Wang, and Mingdong Dong. Recent advances in synthesis and biosensors of two-dimensional mos2. *Nanotechnology*, 30(50):502004, 2019.

[143] You Zi, Jun Zhu, Lanping Hu, Mengke Wang, and Weichun Huang. Nanoengineering of tin monosulfide (sns)-based structures for emerging applications. *Small Science*, 2(3):2100098, 2022.